HERITABILITY ESTIMATION OF RELIABLE CONNECTOME FEATURES

A Thesis

Submitted to the Faculty

of

Purdue University

by

Linhui Xie

In Partial Fulfillment of the

Requirements for the Degree

of

Master of Science in Electrical and Computer Engineering

August 2018

Purdue University

Indianapolis, Indiana

THE PURDUE UNIVERSITY GRADUATE SCHOOL
STATEMENT OF COMMITTEE APPROVAL

Dr. Paul Salama, Co-chair

Department of Electrical and Computer Engineering, IUPUI

Dr. Li Shen, Co-chair

The Perelman School of Medicine, University of Pennsylvania

Dr. Jingwen Yan

Department of BioHealth Informatics, IUPUI

Dr. Maher Rizkalla

Department of Electrical and Computer Engineering, IUPUI

Dr. Zina Ben Miled

Department of Electrical and Computer Engineering, IUPUI

Approved by:

Dr. Brian King

Head of the Graduate Program

ACKNOWLEDGMENTS

I would like to express my sincere gratitude to Professor Li Shen, Professor Jingwen Yan, and Professor Paul Salama for their guidance and support.

I would like to also thank Professor Maher Rizkalla for his guidance.

I wish to thank the other member of my committee, Professor Zina Ben Miled for her advice on programming issues.

Finally, I would like to thank my family for their commitment and continued support.

TABLE OF CONTENTS

Page

LIST OF TABLES

LIST OF FIGURES

Figure Page

Figure Page

Figure Page

Figure Page

Figure Page

Figure Page

Figure Page

ABBREVIATIONS

HCP	Human Connectome Project
SOLAR	Sequential Oligogenic Linkage Analysis Routines Measure
sMRI	Structural Magnetic Resonance Imaging
dMRI	Diffusion Magnetic Resonance Imaging
DWI	Diffusion Weighted Magnetic Resonance Imaging
WM	White Matter
GM	Gray Matter
CSF	Cerebrospinal fluid
FA	Fractional Anisotropy
FL	Fiber Length
FN	Fiber Number
ROI	Regions of Interest
ICC	Intraclass Correlation Coefficients
AHBA	Allen Human Brain Atlas
SIFT	Spherical-deconvolution Informed Filtering
DMN	Default Mode Network

ABSTRACT

Xie, Linhui. M.S.E.C.E., Purdue University, August 2018. Heritability Estimation of Reliable Connectome Features. Major Professors: Paul Salama and Li Shen.

Brain imaging genetics is an emerging research field aimed at studying the underlying genetic architecture of brain structure and function by utilizing different imaging modalities. However, not all the changes in the brain are a direct result of genetic effect. Furthermore, the imaging phenotypes are promising for genetic analyses are usually unknown. In this thesis, we focus on identifying highly heritable measures of structural brain networks derived from Diffusion Weighted Magnetic Resonance imaging data. Using data for twins that is made available by the Human Connectome Project (HCP), the reliability of edge-level measures, namely fractional anisotropy, fiber length, and fiber number in the structural connectome as well as seven network-level measures, specifically assortativity coefficient, local efficiency, modularity, transitivity, cluster coefficient, global efficiency, and characteristic path length were evaluated using intraclass correlation coefficients. In addition, estimates of the heritability of the reliable measures were also obtained. It was observed that across all $64,620$ network edges between 360 brain regions in the Glasser parcellation, approximately 5% were significantly high heritability based on fractional anisotropy, fiber length, or fiber number. Moreover, all tested network level measures, that capture network integrity, segregation, or resilience, were found to be highly heritable, having a variance ranging from 59% to 77% that is attributable to an additive genetic effect.

1. INTRODUCTION

Brain imaging genetics is an emerging research field that integrates genotyping and neuroimaging data to explore the underlying genetic architecture of brain structure and function. Genetic analysis of imaging measures not only allows the detection of risk variants associated with diseases, but also provides insights into the underlying biological mechanism of brain changes before patient being diagnosed. However, not all the changes in the brain are a consequential result of genetic effect. Moreover, it is not usually known which imaging phenotypes are promising for genetic analyses. Therefore, prior to that, it is important to quantify the degree to which brain imaging phenotypes can be attributed to genetic effect using heritability estimation. The broad meaning of heritability is to quantify a phenotype with a value on how is the trait variation due to the genetic variation among samples.

1.1 Genetic Effect on Brain Connectivity

Recently, substantial attention has been drawn to the genetic influence on structural brain connectivity, which appeared to be altered in heritable diseases (e.g. Alzheimer's disease [1]). One widely utilized measure is fractional anisotropy (FA) [2], which is a measure of fiber integrity and is very sensitive to the white matter changes in various diseases [3]. Brain-wide, regional and voxel level FA measures have all been found to be highly and significantly heritable (p value significant after string Bonferroni correction) [3,4]. Other features that have been investigated include white matter fiber tract shapes [5], white matter volume, network level characteristic path length and clustering coefficient [4], and fiber orientation distribution [6]. However, these studies mostly focus on the heritability of tracts (i.e. white matter ROIs) themselves, but not on the resulting anatomical connections of the human brain (i.e. connec-

tome). To this end, the heritability of brain connectomic edge-level features (i.e. FA) remains largely unknown. The heritability of brain connectomic topological features are to be investigated.

1.2 Heritability of Brain Connectivity

To bridge this gap, we propose to perform a comprehensive heritability analysis of anatomical brain networks using the twin data from the Human Connectome Project (HCP) [7]. We employ a new brain parcellation (partition on brain surface) with 360 brain regions of interest (ROIs) [8] to generate brain networks with improved anatomical precision. These brain regions are defined based on functional MRI (fMRI), which allows us to examine the genetic influence on the structural coordination within/between functional brain circuits. Using three sessions of diffusion weighted imaging (DWI) scans for each individual, we first evaluate the reliability of three edge-level measures, including fractional anisotropy, fiber length and fiber number, and seven network-level measures using intraclass correlation coefficients (ICC) [9]. The heritability of these reliable network measures were then estimated using Sequential Oligogenic Linkage Analysis Routines (SOLAR)-Eclipse software. Across all 64,620 edges between 360 ROIs, approximately 5% of them show significantly high heritability in fractional anisotropy, fiber length or fiber number. Top functional brain circuits connected by these heritable edges include visual and default mode network (DMN). Brain regions in DMN are later found to have similar gene expression patterns in the Allen Human Brain Atlas (AHBA). All the tested network level measures, capturing the integrity, segregation or resilience of brain networks, are highly heritable with variance explained by the additive genetic effect ranging from 59% to 77%.

This thesis is arranged as follow, Chapter 2 provides a review of research related to connectome and heritability studies. The approaches used in this study are given in Chapter 3, in addition to the results of reliability test and heritability estimation of

connectome features based on the cohorts of several different twin groups. Chapter 4 summarizes the work and the contribution of this thesis. Future work is also discussed in chapter 4.

2. LITERATURE REVIEW

2.1 Connectomics

One of the most sophisticated systems in the human body is the brain, which consists of 86.1 +/- 8.1 billion neurons and their neuronal interactions, giving rise to a total of approximately 10^{15} synaptic connections [10, 11]. Finding the structural connections among neurons (including electrical and chemical connections between axons and dendrites) is essential for understanding brain functions. More and more neuro-scientists have recently realized the importance of constructing human brain connectivity networks to reveal brain functionalities.

To investigate the underlying brain anatomical connections, Sporn [12] and Hagmann [13] independently proposed the concept the "Human Connectome" whose purpose is to depict brain networks and reveal the connection rules of brain network. The Connectome can be seen as a complex of cross-connected neurons and neuron clusters, as well as interconnected cortical areas. Given that neighboring neurons are more likely to connect with each other, densely connected adjacent neurons lead to "small-world" properties for many anatomical or functional differentiated cortical areas [14–18]. The relatively few long-distance connections are a result of economical selection of both short and long axons inside the brain to achieve material and energy efficiency [19, 20]. In this way, the brain is able to achieve an economical working pattern that is both globally collaborative and locally focused [19, 21]. Since it is unrealistic and infeasible to construct massive connections for each single neuron at the microscale level ($\sim 10^{-6}$m), on the basis of functionally or anatomically distinct cortical areas, it thus more practical to assemble the Human Connectome at mesoscale level ($\sim 10^{-4}$m) [12]. The brain is no longer treated as a group of discrete anatomical units or a collection of chemical substances, rather it can be viewed as a complex unity

of neuron clusters. Using brain connectivity networks, it is possible to reveal topological properties inside the brain and consequently the internal working mechanism of the brain can be explored.

The idea of the Connectome can be traced back to the first description of brain neuronal connectivity of 302 neurons inside a tiny Caenorhabditis elegans nervous system that was carried out by Brenner in 1986 [22]. In 1991, Felleman was able to depict all 305 synaptic connections among visually related cortical areas in a macaque monkey and show the hierarchical structures in its brain [23]. Around the same time, Young reported approximately same number of visual cortical areas and their interconnections in a macaque monkey, showing the economical work pattern [24]. Young then investigated the same network connections in a cat by using non-metric multidimensional scaling methods and revealed the local densely connected and global sparsely interconnected topological organization [25]. However, there has been few work done to obtain the network of structural connections of a human brain through physiological anatomy. This is mainly due to the fact that the invasive method of obtaining human brain structural connectivity cannot be performed on a living person. On the other hand, can we make assumption that the human structural brain network is similar to that brain connectivity for the macaque hence can be inferred based on the connection patterns of macaque brains [26]? Nonetheless, such an inference is inappropriate since human brains and mammalian brains have distinct structure and relatively less functional similarities [26]. Hence, using non-invasive methods to construct human brain connectivity networks have emerged as a promising area.

Recent developments in Magnetic Resonance Imaging (MRI) techniques, namely Diffusion Tensor Imaging (DTI) and Diffusion Spectrum Imaging (DSI) have enabled the visualization of axonal tracts inside the brain as well as fiber orientation due to the water molecular mainly move along the direction of fiber bundle [27,28]. By using these tools, the characteristics and mechanics of brain structure and brain function are more easily found when compared to previous methods [20]. Both DTI and

DSI attempt to quantify diffusion, which is the random microscopic movement of water molecules from high concentration to low concentration. In a uniform media, molecules can diffuse freely in all possible directions. Thus their movement is isotropic and is consequently represented by a spherical tensor inside a voxel (a minimum unit of 3D MRI scan) [28]. Examples of this phenomenon are exhibited by the Cerebrospinal Fluid (CSF) and cerebral gray matter, where there are less obstacles and hence the diffusion of molecules is approximately isotropic [29]. However, in the brain's white matter, diffusive anisotropy exists due to weak perpendicular diffusion and strong parallel diffusion on the direction of traveling along a nerve fiber, resulting in an ellipsoidal tensor [29–31]. Therefore, the diffusion coefficient of water molecules along the direction of nerve fibers is greater than that along the perpendicular direction. Based on this principle, DTI can effectively observe and track white matter fiber bundles by measuring the diffusion rates of water molecules in such nerve fibers structures [27].

The DTI is a new magnetic resonance imaging technique developed on the basis of Diffusion Weighted Imaging (DWI) technology. A commonly used DWI technique is to apply two diffusion sensitizing gradient magnetic fields (same magnitude and direction) symmetrically to both sides of a 180° pulse in a spin echo (SE) sequence [32]. In the case of stationary water molecules, the first gradient pulse causes all proton spins, resulting in a phase change. Meantime, the latter gradient pulse re-aggregate the phase. The signal will be decreased if the phase dispersion does not completely accumulated [33]. Therefore, the diffusion motion will make the signal collected by the above sequence decrease, thereby the specific diffusion direction could be observed [33]. However, DWI imaging only applies sensitive gradients in the three principal directions of X, Y and Z axes. It is lack of precision to evaluate the diffusion of different tissues in three-dimensional space. The degree of tissue anisotropy is often underestimated. To address this issue, DTI is introduced and can be used to quantitatively analyze the diffusion characteristics of water molecules in tissues in three-dimensional space.

From the neuroscience perspective, there are various types of nerve fiber tracts in the brain's white matter. Since water molecules in these fiber bundles mainly move along the direction of the fiber bundles, this enables DTI and DSI to obtain diffusion coefficients in multiple different spatial directions to achieve the reconstruction of these neuron fiber bundles [34]. In addition, DTI and DSI can determine the connections between hundreds of distinct functional brain regions, although they are unable to distinguish the direction between neurons [35]. Nonetheless, single synaptic connections and multiple synaptic connections can be distinguished by DTI and DSI. This indicates that functional brain connections can be predicted by the corresponding structural connections, but it is difficult to predict structural connections based on functional network [35]. Some direct functional connections exist but there are no such direct structural connections.

2.2 Brain Connectivity Construction

The analysis of DTI or DSI brain networks describes the brain as a network of nodes and edges. A node in a structural brain network can be defined as a single neuron, a local neuronal circuits, or cortical areas with specific functions. The defined cortical areas can form a local subnetwork as a node in or as a part of a brain network at a higher-scale. [36–38]. In many current research works, each node in the network represents a different brain region divided by a priori template [36–38]. Edges represent white matter fiber bundles connected between brain regions, also known as brain region of interest (ROI). Thus, a brain network is a multi-scale complex network with a hierarchical structure.

The study of neuroimaging brain networks focuses mainly on mesoscale and large-scale regions since current clinical neuroimaging collection accuracy is at the millimeter level. Common division templates include, the structural atlas such as the Brodmann Altas [39], the Harvard Oxford Atlas (HOA) [40], the Anatomical Automated Labeling (AAL) Altas [41], the LONI Probabilistic Brain Atlas (LPBA40) [42], the

John Hopkins Atlas [43], and functional atlases such as Yeo 7 [44], Yeo 17 [44], Shen Atlas [45], and Glasser Atlas [8]. In diffusion tensor imaging tractography fiber bundles tracking algorithms can either be deterministic or probabilistic [46]. Although probabilistic algorithms tend to have higher accuracy, yet in real network analyses deterministic algorithms are usually used as they incur a lesser amount of computation [47].

In general, DTI is used in conjunction with spatial normalization to obtain the diagonalized diffusion tensor matrix, in which three eigenvalues and associated eigenvectors (representing principal directions) are obtained [48]. Fractional Anisotropy (FA), which is a measure of mean diffusivity, is then found using the three eigenvalues. An FA value of 0 of represents isotropic diffusion while a value of 1 indicates maximum anisotropy. This measure however does not show the direction of diffusion. In addition, to constructing brain connectivity, it is necessary to define connectivity strengths, usually in the form of connection weights. Using the method of fiber assignment that is based on continuous tracking of white matter anatomy [49], the termination condition for a fiber either a fractional anisotropy (FA) value less than 0.2 or a bending rate (angle between two neighbor tensor) greater than 45° [2, 50]. Current streamline tractography algorithm called spherical-deconvolution informed filtering of tractograms (SIFT), constructs connectivity weights in proportion to the corresponding quantitative density of the underlying white matter fibers [51]. Instead of removing streamlines, an updated version of SIFT, SIFT2, provides a computationally efficient cross-sectional streamline determination method [51].

2.3 Analysis of Brain Connectivity in Alzheimer's Disease

Although the genome for humans can be determined at birth, yet brain connectivity networks are constantly changing throughout their lives. The study of various brain associated diseases from the perspective of the network appears to be a good way to unravel the nature of these diseases and to explore the underlying changes to

cerebral nervous system. Based on recent fMRI based research on Alzheimers disease (AD), AD patients' functional brain networks experiences degradation compared to normal patients. This degradation exhibits high specificity and sensitivity which is also an important objective index for clinical diagnosis [52]. It is common for brain network disorder to cause many mental or neurological diseases [53–55]. In addition, complex brain networks studies have been extended to brain cognitive studies [56]. Patients' brains with neurological or psychiatric disorders display functional variance with structural damage and variance. However, the relationship between this type of brain structural variation and brain functional variation remains unknown. Moreover, what mechanisms and relationships exist between network plasticity and brain structure to development, aging, or specific training still warrant further investigation?

The next chapter introduce the test re-test reliability for the multiple datasets. Intra Class Correlation (ICC) is employed to set a threshold to keep reliable features. Ploygenic model for SOLAR-Eclipse genetic tools is discussed and String Bonferroni Correction is applied to set a threshold for keeping significant heritable connectomic features.

3. METHOD AND RESULTS

The mapping of brain cortical regions for data obtained from human connectome was carried out initially to construct brain network connectivity. The steps required in this construction of structural data are addressed in this chapter. Given that sessions of Diffusion Weighted Imaging were performed for every subject, test-retest reliability was analyzed for each connectomic features. A polygenic model was applied to estimate heritability. The theory behind the polygenic model as utilized in this work is introduced and the results are discussed in this chapter.

3.1 Human Connectome Project Data

To conduct heretibility analysis we downloaded high spatial resolution Diffusion Weighted Imaging (DWI) data from the Human Connectome Project (HCP) [7]. In total, there were 179 twin pairs, with an age range of 29.1 ± 3.68, including 136 mono-zygotic females, 98 mono-zygotic males, 68 di-zygotic females and 56 di-zygotic males. DWI data was processed following the MRtrix3 guidelines [57]. More specifically, we generate anatomical image based on brain T1 image and tissue segmentation, and used it to constrain the streamline propagation in fiber tractography [58]. Given different b-value, sample water movement formed varied radius spherical shell (in Q-space) [59]. The white matter fiber orientation information was then extracted by multi-shell, multi-tissue constrained spherical deconvolution from different tissue type (WM/GM/CSF) in DWI [60]. Fiber orientation distribution function could be estimated and apparent fiber density were exploited to produce reliable WM/GM/CSF volume maps [60,61]. Subsequently, random seeds on the basis of the voxel are selected to generate initial tractogram for 10 million streamlines following two conditions with maximum fiber tract length at 250 mm and FA larger than 0.06. Instead of filter-

ing out the unsatisfied streamlines, the updated Spherical-Deconvolution Informed Filtering of Tractograms (SIFT2) technqiue making use of complete streamlines, is applied to generate more biologically accurate brain connectivity in terms of different measures [51, 62]. Finally, we mapped filtered 10 million streamlines onto the Glasser template with 360 Regions of Interest (ROIs) [8] to generated the structural connectivity. Final brain networks were constructed using fibers going through white matter and connecting Glasser ROIs. We then applied three edge-level measures, namely fractional anisotropy (FA), fiber length (FL) and fiber number (FN). In addition, we binarized the brain network and obtained seven network-level topological features characterizing the integrity, segregation, and resilience of brain networks [47] (see Table 3.1).

3.2 Reliability of Connectomic Features

Tractography-based networks are known to have an issue with regards to measurement reliability. To investigate the precision of connectomic features, we estimated test-retest reliability by comparing three DWI data sets acquired for the same individuals but at different time points. We found the intraclass correlation coefficients (ICC) for each brain connectomic feature to evaluate their reliability [9]. All connectomic features with an ICC value greater than or equal to 0.75 are deemed to have good/excellent reliability and are included in the subsequent heritability analysis [63].

3.3 Heritability Analysis

Heritability is defined as the proportion of phenotypic variance attributable to genetic variance. In this thesis, we used SOLAR-Eclipse [64], a software tool to estimate the heritability of all brain connectomic feature, including FA, FL, FN of $64,620$ edges and the seven network level measures given in Table 3.1). Network level measures are derived from the binarized brain network mentioned above, such that the weight of a link is set to 1 if it exists and deemed reliable, but 0 otherwise [47].

SOLAR-Eclipse is chosen over the traditional ACE model [65] due to its ability to evaluate covariate effects, significance of heritability, and the standard error for each phenotype trait [3]. Prior to conducting the heritability analysis, the data is transformed to have a zero-mean and unit-variance Gaussian distribution. This is done to ensure normality of all the measures. Since many previous studies have reported the effect of age (linear/nonlinear), gender and their interactions on structural brain connectivity [66–69], all heritability analyses were conducted with age at scan, age^2, sex, age$\times$sex and age$^2\times$sex as covariates. Output from SOLAR-Eclipse includes heritability measure (h^2), standard error, and the corresponding significance p value for each feature. In addition, we obtained the total variance explained by all covariate variables.

To determine the heritability measure (h^2), we need to utilize the SOLAR-Eclipse polygenic variance component model [64] for phenotype trait vector Y on N twin subjects, which is given by:

$$Y = X\beta + a + \epsilon, \tag{3.1}$$

where X is an $N \times 5$ array of age, age^2, sex, age$\times$sex and age$^2\times$sex covariates for each individual, a is an $N \times 1$ vector of unobserved additive genetic effect, and $N \times 1$ vector ϵ denotes residual errors. Here we denote Σ the trait covariance matrix of Y and assume data follows a multivariate normal distribution,

$$a + \epsilon \sim \mathcal{N}(0, \Sigma)$$

Hence, Y can be written as,

$$Y \sim \mathcal{N}(X\beta, \Sigma)$$

The covariance matrix Σ can be found from,

$$\Sigma = 2\sigma_A^2\Phi + \sigma_E^2 I, \tag{3.2}$$

where Φ is a kinship matrix contains the pairwise relationship between all N input twin individuals, I is known as identity matrix, σ_A^2 is the additive genetic variance

component and σ_E^2 the is environmental variance component. Hence, the narrow sense of additive genetic heritability is defined as,

$$h^2 = \frac{\sigma_A^2}{\sigma_A^2 + \sigma_E^2} \tag{3.3}$$

The maximum log likelihood of the original polygenic model (Eqs. 3.1 and 3.2) is given by:

$$\arg\max_\beta L(\beta) = log \prod_{i=1}^{N} \frac{1}{|\Sigma|^{1/2}\sqrt{2\pi}} e^{\left[-\frac{1}{2}(Y-X\beta)^T\Sigma^{-1}(Y-X\beta)\right]} \tag{3.4}$$

The log likelihood is then transformed as,

$$L(\beta, \epsilon, Y, X) = -\frac{1}{2}Nlog(2\pi) - \frac{1}{2}Nlog(|\Sigma|) - \frac{1}{2}(Y - X\beta)^T\Sigma^{-1}(Y - X\beta) \tag{3.5}$$

By introducing a transforming matrix S, the original model becomes an eigen-simplified polygenic model. Matrix S consists of the eigenvectors of Φ which are also the eigenvectors of Σ in Equation 3.2. Applying the transformed matrix to Equation 3.1 returns,

$$S^T Y = S^T X\beta + S^T a + S^T \epsilon. \tag{3.6}$$

Denoting the transformed versions of Y, X, a and ϵ by Y^*, X^*, and ϵ^*respectively, then,

$$Y^* = X^*\beta + \epsilon^* \tag{3.7}$$

Similarly, we denote Σ^* the trait covariance matrix of Y^* and assume data follows a multivariate normal distribution,

$$\epsilon^* \sim \mathcal{N}(0, \Sigma^*),\ Y^* \sim \mathcal{N}(X^*\beta, \Sigma^*)$$

Diagonalizing matrix 2Φ in Eqs. 3.2 to a matrix D_g, where D_g is a diagonal matrix comprising the eigenvalues of 2Φ, that is $D_g = diag\{\lambda_{gi} : i = 1, \cdots, N\}$:

$$Var(\epsilon^*) = \Sigma^* = \sigma_A^2 D_g + \sigma_E^2 I \tag{3.8}$$

After the transformation, the variables have been changed, the and variance has the representation:

$$\Sigma = S\Sigma^* S^T$$

The log likelihood takes on the exact same form except it is much easier to work with since Σ^*:

$$L\left(\beta^*, \sigma_A, \sigma_E; Y^*, X^*\right) = -\frac{1}{2} N log\left(2\pi\right) - \frac{1}{2}\sum_{i=1}^{N} log\left(\sigma_A^2 \lambda_{gi} + \sigma_E^2\right) - \frac{1}{2}\sum_{i=1}^{N} \frac{\left(Y_i^* - (X^*\beta)_i\right)^2}{\sigma_A^2 \lambda_{gi} + \sigma_E^2} \tag{3.9}$$

Solve above optimization problem benefits σ_A and σ_E and regression coefficient β. Substituting value of σ_A and σ_E in Eqs. 3.2 returns heritability estimation of input trait. The subsequent sections provide the results of all the experiments carried out.

3.4 Results for HCP cohort with 358 twin subjects

3.4.1 Reliability of brain connectomic features

We first determine the reliability of brain connectomic features for the HCP cohort comprising 358 twin subjects. Figures 3.1 (a), (b), and (c) depict scatter plots of edge-level reliability vs heritability as estimated by SOLAR-Eclipse. Each dot corresponds to one edge and the color indicates the significance of the heritability. With regards to the FA, FL and FN measures, 11.13%, 9.95%, and 45.54%, respectively, of all the edges show consistency across the three sessions, that is they had a good/excellent reliability score (ICC ≥ 0.75). In total, $43,051$ out of $193,860$ edge-level features passed the reliability test. All tested network level measures show very good reproducibility across sessions, having ICC values ranging from 0.85 to 0.92 (see Table 3.1). Since we focus on the features reproducible across three sessions, the heritability analysis was only performed on the DWI data from one session.

3.4.2 Heritability of edge-level measures

After excluding the edges that fail the reliability test, there are 5105 remaining edges whose FA show significantly high heritability after applying the stringent Bonferroni correction ($p \leq 0.05/(64,620 \times 3) = 2.58 \times 10^{-7}$) [70]. In the case of the FL and

FN measures, there were 2687 edges and 7311 edges that passed the significance test, respectively. From Figures 3.1(a), (b), and (c), here red dots indicate the heritability estimation p-val for this edge is around 10^{-4}, whereas the yellow dots show the not significant p-val around 10^{-2}. To visualize the reliable and significant heritable edges (black dots on top right), we further plot the distributions of these edges.

From Figures 3.1(d), (e), and (f), we observe that the heritability (h^2) of the FA measure is between 0.4 and 0.85. FL and FN measures show similar heritability distributions, except that there are fewer edges that have very high heritability ($h^2 \geq 0.8$).

Figures 3.1(g), (h), and (i) exhibit the "heatmaps" of the anatomical connection matrix with ICC$\geq$0.75 and $p \leq 2.58e-7$ for FA, FL, and FN measures respectively. Here red dots indicate the heritability estimation value for this edge is very high ($h^2 > 0.8$), whereas the yellow dots show relatively lower value (h^2 around 0.6). Glasser brain regions were reordered to form seven functional groups as defined in the Yeo parcellation [71] (see Figure 3.2). A subcortical part was added to complement the Yeo atlas. For all three edge-level measures, the majority of significantly heritable and reliable edges are located within the default mode network, the visual circuit, or the connections of default mode network with other circuits, such as Ventral Attention and Frontal-Parietal. The default mode network brain region was discovered accidentally while the increasing activity were detected in the passive control states, comparing to states people were consciously doing goal oriented tasks [72]. Edges connecting Visual and Somato-Motor circuits show the highest average heritability ($h^2 = 0.69$) in terms of the FA measure. Based on the FL and FN measures, edges with the highest average heritability were found to belong to the Limbic System ($h^2 = 0.64$ in the case of FL and $h^2 = 0.49$ in the case of FN).

Subsequently, for each type of measure, we further ranked the edges based on their heritability (h^2) and examined the brain regions connected by the top heritable edges. Figures 3.3 (a), (b), and (c) depict the "heatmaps" indicating the heritability of the top 0.5% edges based on the FA, FL, and FN measures respectively. Similarly, here red

dots indicate edges with the relatively high heritability estimation value ($h^2 > 0.8$), while yellow dots show relatively lower value (h^2 around 0.6) of heritability estimation. In the brain connectivity maps, shown in Figures 3.3(d), (e), and (f), we observed that many top heritable edges are within the frontal lobe, while several brain regions in occipital lobe (primary visual cortex) are categorized as hubs connected by some highly heritable edges based on the FA and FL measures. These fiber tracts belong to white matter regions inferior to the longitudinal fasciculus, whose regional FA value was previously identified to be highly heritable [3]. In addition, we found that the length of Cingulum tracts (vertical lines in the middle of the brain) are also largely controlled by genetic factors, with h^2 around 0.65. Its FA measure was also previously reported to be heritable with $h^2 = 0.81$ [3].

Based on FN, top heritable edges show a different spatial pattern and are more evenly distributed across the whole brain. Functional brain circuits that are mostly connected by these top heritable edges are Default Mode Network(DMN) and Fronto-Parietal(FP) as shown in Figures 3.3(g), (h), and (i).

Finally, we examined the expression patterns of those brain regions involved in the DMN circuit in the Allen Human Brain Atlas, including the medial prefrontal cortex, the angular gyrus, the precuneus, the posterior cingulate cortex, and the hippocampus. Interestingly, many of these brain regions which are connected by heritable edges show very similar gene expression patterns.

3.4.3 Heritability of network-level measures

For each individual, we extracted seven network-level topological features to evaluate the integrity, segregation, and resilience of brain network. These features are the assortativity coefficient, modularity, local efficiency, cluster efficiency, transitivity, characteristic path length, and global efficiency [47].

A brain network is initially binarized in such a way that the weight of the link is set to 1 when it exists and 0 otherwise. Thus, the FA brain structural connectivity

was used to extract the seven network-level topological features needed to quantify individual brain network with seven neurobilogical meaningful numbers. Denoting the number of links to a node as its "degree", the assortativity coefficient is defined to be correlation coefficient between the degrees of all $64,620$ pairs of connections. This is used as a measure of network *resilience*. Network *segregation* is quantified by the presence of modules or clusters, which is based on modularity (defined to be the number of non-overlapping modules), local efficiency (mean value of inverse distance of the shortest edge not passing through a target node i but connected other two nodes in a triangle divided by the square value of a degree for this target node) [47],

$$E_{loc} = \frac{1}{n}\sum_{i\in N}\frac{\sum_{j,h\in N, j\neq i} a_{ij}a_{jh}[d_{jh}\left(N_i\right)]^{-1}}{k_i\left(k_i-1\right)} \tag{3.10}$$

cluster efficiency (average fraction of the number of triangles in a target node divided by the square value of a degree for this node) [47],

$$C = \frac{1}{n}\sum_{i\in N}\frac{2triangle_i}{k_i\left(k_i-1\right)} \tag{3.11}$$

and its variant transitivity (normalized collectively) [47]:

$$T = \frac{\sum_{i\in N} 2triangle_i}{\sum_{i\in N} k_i\left(k_i-1\right)} \tag{3.12}$$

The shortest path length, also known as characteristic path length, which is measured by the average distance between the target node and all other nodes and its inverse global efficiency, which is a measure to evaluate disconnected network, are both used to characterize the network *integrity* [47].

Table 3.1 provides a summary of the estimated heritability of all topological features. The five covariates: age, age^2, sex, age$\times$sex and age$^2\times$sex, were found to account for approximately 15% of the variance of all topological features except for the assortativity coefficient and the characteristic path length. The covariates: sex and age$^2\times$ sex are the only factors that exhibit significant influence on the network topology heritability. Assortativity coefficient was found to have the highest reliability, but only 58% of variance can be attributed to the additive genetic effect. The

other six features are estimated to have similar heritability of approximately 0.75. These findings are consistent with previous studies. It was reported in [4] that the characteristic path length and the clustering coefficient of an anatomical brain network are highly heritable. The heritability estimation carried out in this work is slightly higher than reported in [4], possibly due to the selection of different brain parcellation schemes.

3.4.4 Top five significant heritable edge-level measures.

The variance explained by the five covariates for selected edges are listed in Table 3.2. Each pair of functional groups in the Yeo parcellation are shown for the top 5 most significant heritable connections. The top significant heritable edges have very high reliability (ICC ≥ 0.90) and their heritable estimation values for both FA and FL are above 0.8. With regards to edges related to FL, the variance is largely explained by the covariate "sex". In addition, the top heritable edge in terms of FN has a relatively high significant p-value for the covariate "sex" as well. Hence, gender effect on the heritability of brain connectivity is further discussed in the next several sections.

3.5 Results for HCP cohort with 154 male and 204 female twin subjects

As depicted in Fig. 3.4, gender effect indicates that females have more significant heritable edges in terms of feature Fractional Anisotropy. Based on Fig. 3.7, the number of significant heritable edges in the female cohort is double that in male cohorts. Further, the number of edges found in the female cohort are triple those in the male cohort. Although the collapsed connectivity matrix corresponding to the functional group in the Yeo parcellation has similar patterns for both male and female brain connectivity, yet it is challenging to interpret such difference solely based on gender, given that the sample size is different between both female and male groups. It is noticeable that the sample size strongly influences the output since there are more

subjects in the cohort of female twins than in a cohort of male twins. In addition, the average h^2 values for edges connecting with function groups in Yeo parcellation are slightly larger in the cohort of male twins. To better understand why this we examine the effect of sample size. The original cohort is further divided into two groups. One comprised 1/3 of the subjects of the original twin group, while the other one consisted of the rest of subjects. The heritability estimation of both groups was conducted and is discussed in the next section.

3.5.1 Results for HCP cohort with one third group and two thirds group

As mentioned previously the subjects were divided into two groups: one group consisting of only 1/3 of all the subjects, while the second group consisted of the rest, that is 2/3 of all subjects. Female to male ratio and MZ to DZ ratio are all reserved to remove the bias from the sample structure. This resulted in one group having $N = 118$ twins while the other had $N = 240$ twins. This was repeated for a total of five times. From Fig.3.13 - Fig. 3.30 are comparisons across FA, FL and FN features between small twin group and large twin group. It is observed that similar values for all three edge-level features were obtained for the two groups, respectively.

Furthermore, comparison of the top 0.5% edges in the two groups reveals that the top significant heritable connections are usually detected first. Comparing brain maps it is observed that connections pattern are similar across the three edge-level features. Within the group made up of one third of the twins, the average h^2 value for detected edges was 0.2 higher than the h^2 value detected in the cohort comprising two thirds of twins. All the evidence indicate that the result varies based on the selection of subjects. However, the top significant heritable edges have similar connection pattern since they are detected first. To further investigate the effect of gender, those differences between males and females in terms of brain connectivity, two cohorts made up of equivalent number of subjects (N=154) are constructed with same MZ:DZ ratio. The results are discussed in the subsequent section.

3.6 Difference between HCP cohort with 154 male and 154 female twin subjects

In this study, the subjects were grouped into two cohorts, one consisting of only $N = 154$ male subjects while the other was comprised of $N = 154$ female subjects. To obtain the FA, FL, and FN measures, the masks created for the corresponding reliability test with original cohort were applied to filter out edges with lower reliability score (that is ICC < 0.75).

As shown in Figure3.31, there were 2053 edges found for the female cohort and a slightly higher number of 2644 edges for male cohort whose FA exhibit significantly high heritability after applying the stringent Bonferroni correction. If the edges detected in both female and male cohorts are excluded then there remain 593 edges and 1184 edges that pass the significance threshold, respectively. The number of the significant heritable edges left in the male cohort are approximately double those in the female cohort. However, Figure3.31 shows that there are slightly more edges for female cohort, in particular 948 than the 644 edges found for male cohort whose FL are significantly high heritable. In turn, the significant heritable edges left in female cohort are double those in the male cohort. With regards to the FN measure, significant heritable edges have similar distributions in both female and male cohorts. In all three histogram figures, the heritability (h^2) of FA, FL, and FN are all between 0.55 and 0.9. However there are much fewer edges with very high heritability ($h^2 \geq 0.8$), based on the FL and FN measures, in the male cohort in comparison to the female cohort.

Figures 3.32, 3.35, and 3.38(a)(b) provide "heatmaps" of the anatomical connection matrix for the FA, FL, and FN measures, that are significantly reliable (ICC$\geq$0.75 and $p \leq 2.58 \times 10^{-7}$) after the common edges between the female and male cohorts have been excluded. Similarly, Figures 3.32, 3.35, and 3.38(c) exhibit the "heatmaps" showing differences between the female and male cohorts in regards to the significant heritable and reliable anatomical connections existing in both groups. Here again,

Glasser brain regions were reordered to form seven functional groups as defined in Yeo parcellation [71]. Again, in the first and second column, here red dots/edges/blocks indicate edges with the relatively high heritability estimation value ($h^2 > 0.8$) , while yellow dots/edges/blocks show relatively lower value (h^2 around 0.6) of heritability estimation. While in the third column, the red dots/edges/blocks indicate the heritability estimation value (h^2) in female group are 0.2 higher those edges in male group, whereas green dots/edges/blocks show inverse result.

3.6.1 Influence of the Fractional Anisotropy Measure

The figures indicate that, based on the FA measure, the majority of significantly heritable and reliable edges in the cohort of female twins are located within Default Mode Network, connect the Default Mode Network with other circuits such as the Ventral Attention, the Frontal-Parietal, and the Somato-Motor circuits, or connect the Dorsal Attention and the Somato-Motor circuits. In contrast, the majority of significantly heritable and reliable edges in the cohort of male twins mainly exist within the Visual circuits, connect the Default Mode Network with Ventral Attention circuit, or connect the Dorsal Attention and Somato-Motor circuits. The common connections for both female and male groups are largely found between the Default Mode Network and other circuits.

In general, the average h^2 value for female only twins group was found to be 0.696, whereas it was 0.723 for the male only twins group. Further, considering only connections with highest average heritability (these had more than 40 edges), these were found to be connecting the Dorsal Attention and Somato-Motor circuits in the female only cohort (with $h^2 = 0.69$), whereas they were between the Dorsal Attention and Ventral Attention circuits in the male only cohort (with $h^2 = 0.71$).

In the brain connectivity map, shown in Figures 3.32(d-f), the significant heritable edges belonging to the female only twins group are located within the temporal lobe. Moreover, the FA measures for Cingulum tracts (vertical lines in the middle of brain)

are found to be influenced by genetic factors, with h^2 around 0.65, as was previously found in the heritability estimation based on Fiber Length (FL) for the entire cohort ($N = 358$). In comparison, the edges detected only in male twins group are mainly located within the temporal lobe and within the limbic lobe, with h^2 around 0.70. Among these, around 80 edges are identified as highly heritable ($h^2 \geq 0.8$), hence are marked as red connections. For the male only group, these fiber tracts belong to white matter region inferior longitudinal fasciculus, whose regional FA value was previously identified to be highly heritable [3].

Following [73] and focusing on the right hemisphere reveals that for the cohort of female twins, there are relatively more heritable edges on the right hemisphere. In fact [73] shows gender difference in DMN and DA networks in response to reward and punishment, indicating that there is relative effect of the networks in DMN (internal) and DA (external) to attention. Women exhibited greater activation of limbic and prefrontal structures, while men portrayed greater activation of parietal areas such as the superior parietal lobule and left precuneus [74]. These results suggested that women may have neural processing biases toward stimuli representing reward and punishment [73]. Our findings give the pathway of these circuits and further investigation within these connections would provide more genetic influences on the brain structures.

3.6.2 Impact of Fiber Length

Similar to FA, FL measures indicate that the majority of significantly heritable and reliable edges existing in the cohort of female twins are located in the edges connecting the Default Mode Network with other circuits, such as the Ventral Attention and Frontal-Parietal. In contrast, the majority of significantly heritable and reliable edges in the cohort of male twins mainly connected in the same regions as female cohort, only the existing edge numbers are less than female cohort. The common connections for both female and male groups are largely found within Default Mode Network,

between Default Mode Network and Frontal-Parietal. For the common connections for both female and male groups, the edges heritable value h^2 in female group are overall higher than male group.

In general, the average h^2 value for female only twins group was found to be 0.712, whereas it was 0.704 for the male only twins group. Further, considering only connections with more than 20 edges, these were found to be connecting the Default Mode Network and Fronto-Parietal circuits in the female only cohort (with $h^2 = 0.69$), whereas they are within the Default Mode Network in the male only cohort (with $h^2 = 0.67$).

3.6.3 Influence of the Fiber Number Measure

Similar to the findings based on the FA and FL measures, the FN measures indicate that the majority of significantly heritable and reliable edges existing in the cohort of male twins are located within the Visual circuits, connect the Default Mode Network with other circuits, such as the Ventral Attention, Frontal-Parietal, and Somato-Motor circuits. In contrast, the majority of significantly heritable and reliable edges in the cohort of female twins mainly exist within the Default Mode Network, or connecting the Default Mode Network with Dorsal Attention circuit and Fronto-Parietal. The common connections for both female and male groups are very sparse hence is no meaningful information.

In general, the average h^2 value for female only twins group was found to be 0.665, whereas it was 0.667 for the male only twins group. Further, considering only connections with more than 40 edges, these were found to be within the Default Mode Network in the female only cohort (with $h^2 = 0.68$), and are similarly within the Default Mode Network in the male only cohort (with $h^2 = 0.68$).

Table 3.1.
Heritability of topological features derived from brain networks.

Topological Features	ICC	h^2	Std. Error	P-value	Variance (Covariates)
Assortativity Coefficient	0.92	0.59	0.06	3.50×10^{-13}	0.04
Local Efficiency	0.89	0.76	0.04	1.36×10^{-24}	0.18
Modularity	0.87	0.70	0.05	3.02×10^{-19}	0.11
Transitivity	0.89	0.77	0.04	3.90×10^{-24}	0.16
Cluster Coefficient	0.89	0.76	0.04	1.37×10^{-24}	0.17
Global Efficiency	0.87	0.75	0.04	4.88×10^{-23}	0.16
Characteristic Path Length	0.85	0.72	0.04	5.71×10^{-23}	0.02

Table 3.2.
Top 5 Significant heritability edges in edge-level brain connectivity measures.

Data Type	ROI1	ROI2	Intro Class Correlation	$h^2 \pm SE(p)$	Covariates					Variance explained (%)
					Age(p)	Age^2(p)	Sex(p)	$Age \times Sex(p)$	$Age^2 \times Sex$(p)	
Fiber Mean Fractional Anisotropy	DMN	FP	0.9582	$0.85 \pm 0.00(10^{-31})$	0.84	0.27	0.95	0.46	0.80	2.60
	DMN	DMN	0.9723	$0.84 \pm 0.00(10^{-31})$	0.22	0.23	0.61	0.96	0.83	6.23
	DMN	DMN	0.9445	$0.84 \pm 0.02(10^{-29})$	0.85	0.07	0.58	0.89	0.35	5.67
	VA	FP	0.9527	$0.83 \pm 0.00(10^{-31})$	0.82	0.21	0.46	0.38	0.83	2.41
	DMN	FP	0.9507	$0.83 \pm 0.00(10^{-31})$	0.22	-	0.12	0.34	0.85	6.22
Mean of Fiber Length	DMN	DMN	0.9852	$0.83 \pm 0.02(10^{-36})$	0.20	0.76	1.40×10^{-8}	0.77	0.73	25.68
	DMN	FP	0.9680	$0.83 \pm 0.00(10^{-34})$	0.33	-	5.55×10^{-12}	0.93	-	24.47
	DMN	L	0.9788	$0.83 \pm 0.02(10^{-33})$	0.39	0.83	1.12×10^{-11}	0.83	0.72	34.23
	VIS	VIS	0.9359	$0.82 \pm 0.00(10^{-34})$	0.06	-	-	0.17	5.70×10^{-3}	7.50
	DMN	DMN	0.9764	$0.82 \pm 0.00(10^{-34})$	0.16	0.71	1.72×10^{-12}	0.62	-	26.16
Fiber Number	VA	VA	0.9494	$0.73 \pm 0.00(10^{-22})$	0.84	0.86	8.32×10^{-3}	0.72	-	4.70
	SM	DA	0.9378	$0.71 \pm 0.04(10^{-21})$	0.82	0.60	0.57	0.89	0.61	0.76
	VIS	VIS	0.9688	$0.71 \pm 0.00(10^{-21})$	0.56	0.57	0.47	0.79	0.92	0.81
	SM	DA	0.9478	$0.70 \pm 0.04(10^{-19})$	0.53	0.41	0.99	0.81	0.47	0.47
	DMN	SM	0.9060	$0.69 \pm 0.00(10^{-20})$	0.80	0.25	0.04	0.86	0.56	2.64

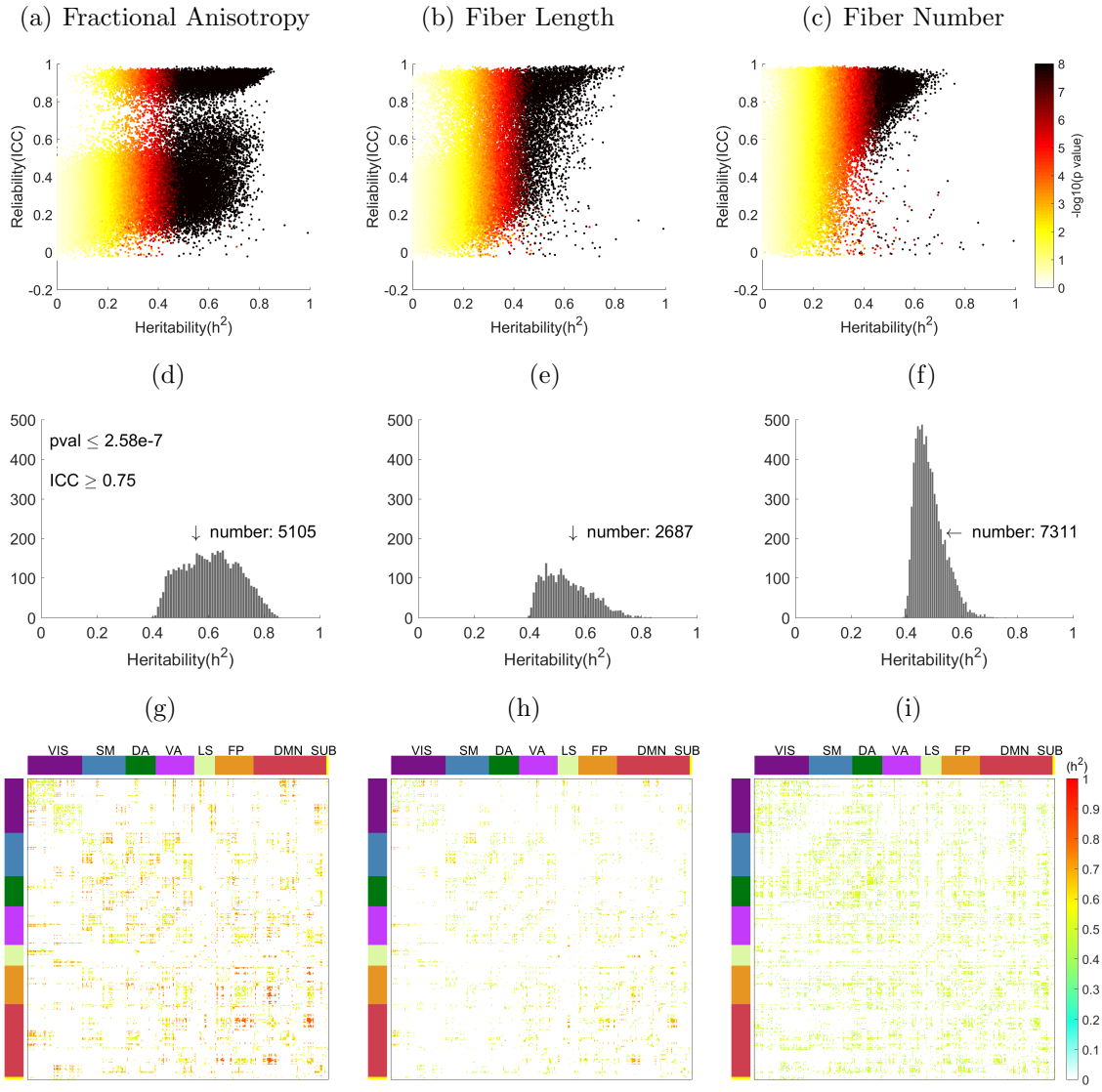

Fig. 3.1. Heritability distribution of all significant and reliable edges for FA, FL and FN features. (a) (b) (c) Scatter plots of reliability against heritability. Dot color indicates log-transformed p-values. (d) (e) (f) Histogram for reliable edges. (g) (h) (i) Heatmap of anatomical connection matrix. Rows and columns are reordered to form seven functional groups corresponding to Yeo parcellation. Top and side color panels indicate the corresponding Yeo parcellation of each ROI. The last subcortical (SUB) group is added to complement the Yeo atlas.

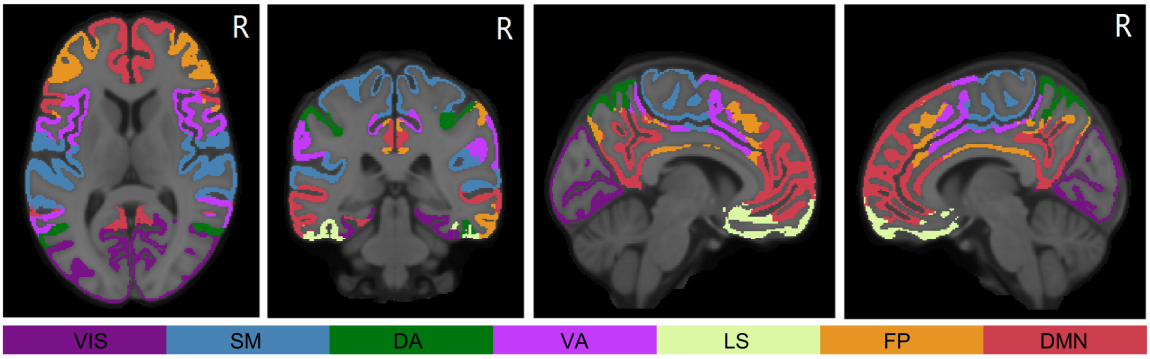

Fig. 3.2. Brain map of Yeo parcellation in MNI space. From left to right: axial view, coronal view, sagittal view (Left) and sagittal view (Right). The bottom color panel indicates the color scheme of different regions: Visual (VIS), Somato-Motor (SM), Dorsal Attention (DA), Ventral Attention (VA), Limbic system (LS), Fronto-Parietal (FP) and Default Mode Network (DMN).

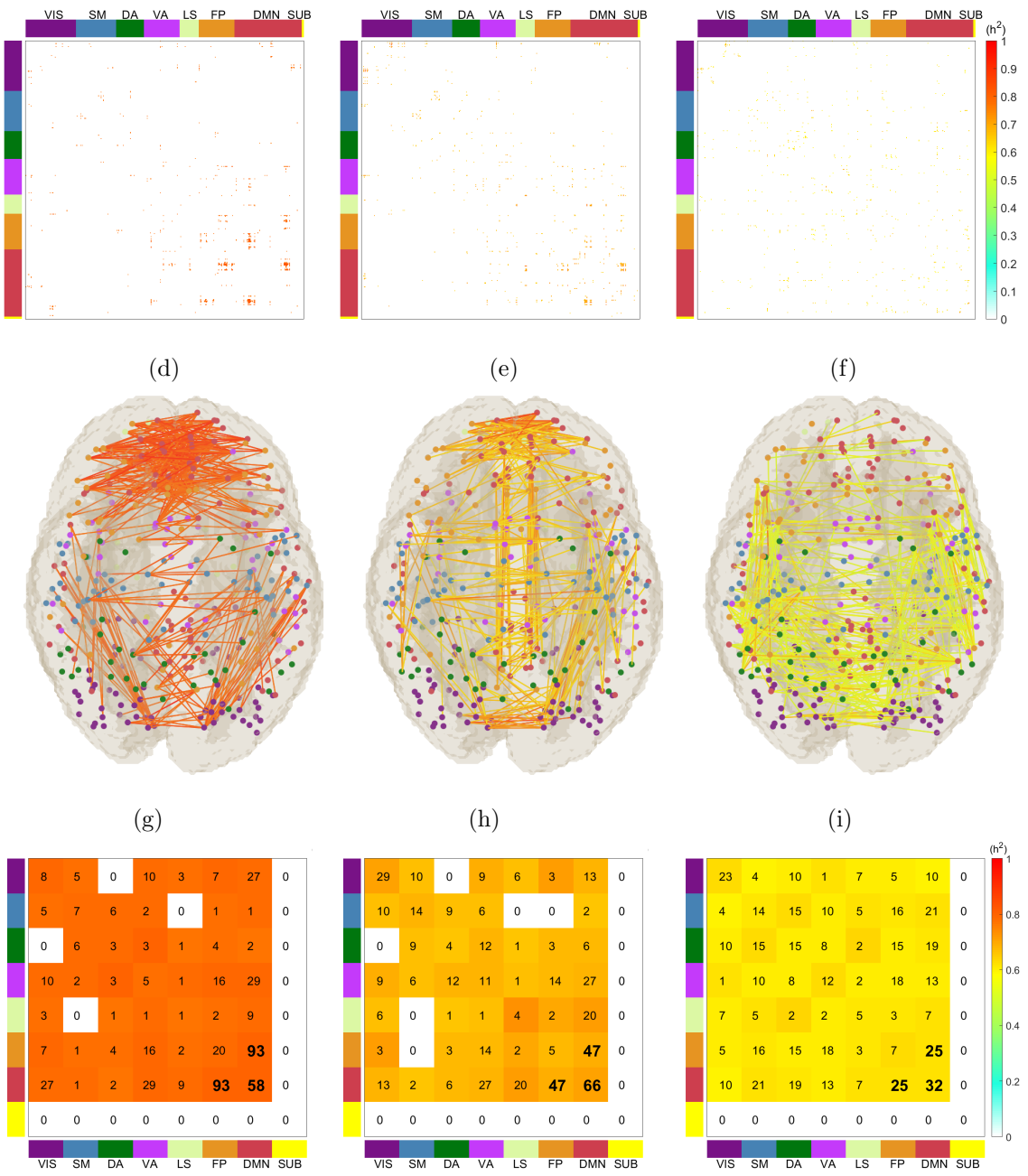

Fig. 3.3. Heritability of top 0.5% edges ranked by h^2 for FA, FL and FN features. (a) (b) (c) Heatmap of anatomical connection matrix. (d) (e) (f) Heritability of edge-level measures in the brain map. Node color indicates different Yeo functional groups. (g) (h) (i) Heatmap showing total number and average h^2 value of edges connecting each pair of functional groups in Yeo parcellation. Top and side color panels indicate the corresponding Yeo parcellation of each ROI. The last subcortical (SUB) group is added to complement the Yeo atlas.

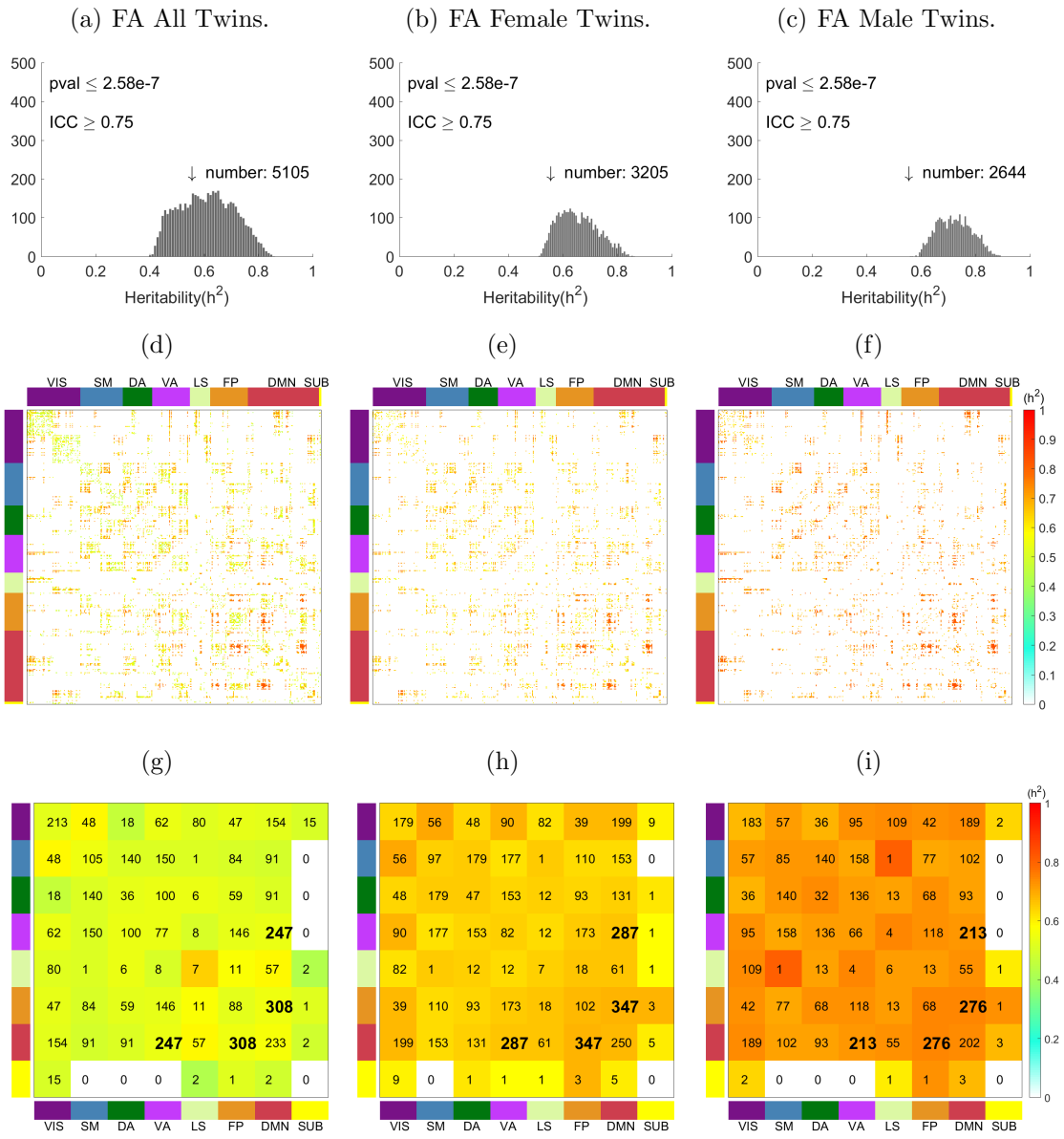

Fig. 3.4. Heritability distribution of all significant and reliable edges for all twins, female twins and male twins within the Fractional Anisotropy feature. (a) (b) (c) Histogram for reliable edges. (d) (e) (f) Heatmap of anatomical connection matrix. Rows and columns are reordered to form seven functional groups corresponding to Yeo parcellation. Top and side color panels indicate the corresponding Yeo parcellation of each ROI. The last subcortical (SUB) group is added to complement the Yeo atlas. (g) (h) (i) Heatmap showing total number corresponding to number in histogram above and average h^2 value of edges connecting each pair of functional groups in Yeo parcellation. Bottom and side color panels indicate the corresponding Yeo parcellation of each ROI.

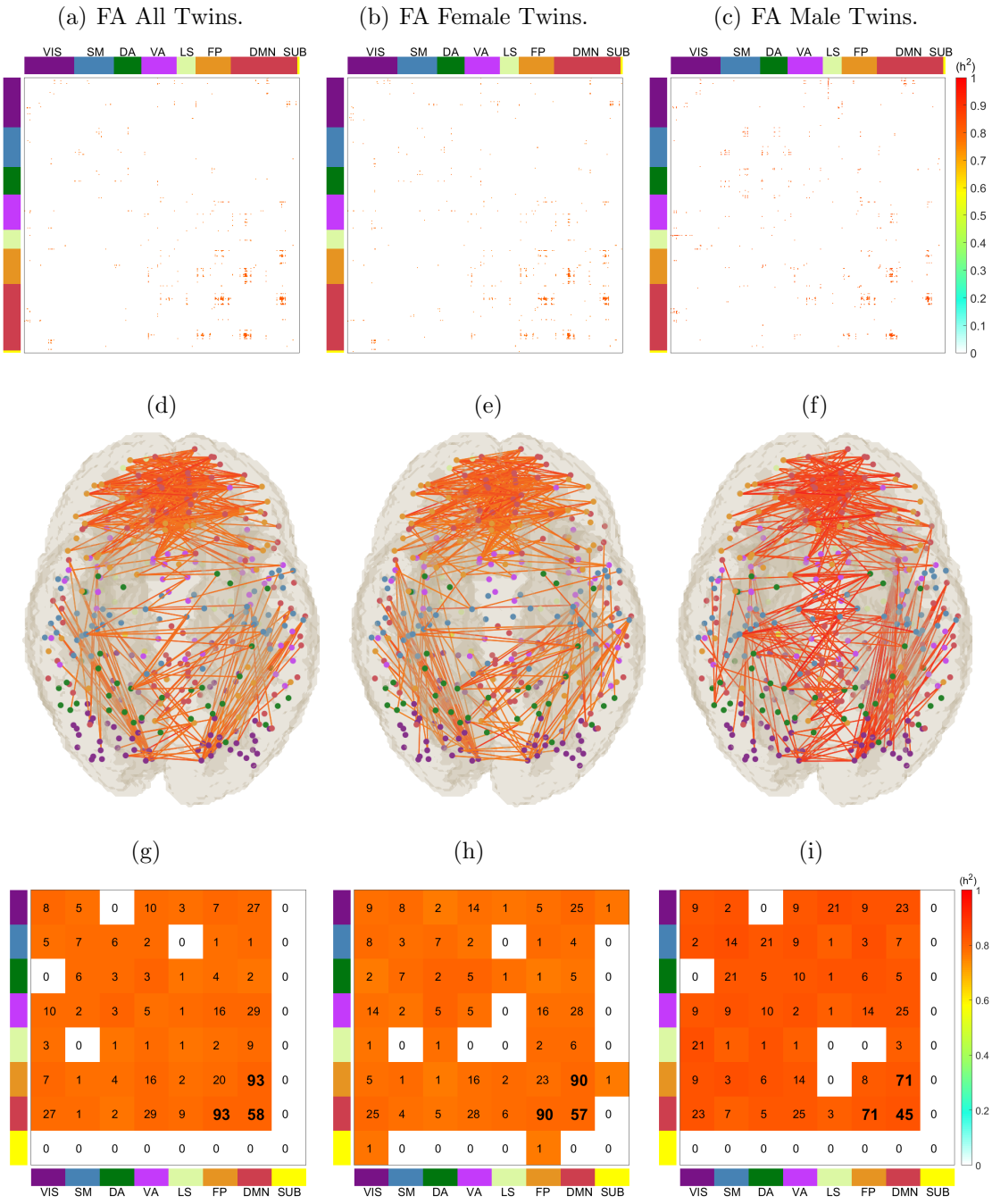

Fig. 3.5. Heritability of top 0.5% edges ranked by h^2. (a)-(c) Heatmap of anatomical connection matrix. (d)-(f) Heritability of edge-level measures in the brain map. Node color indicates different Yeo functional groups. (g)-(i) Heatmap showing total number and average h^2 value of edges connecting each pair of functional groups in Yeo parcellation. Top and side color panels indicate the corresponding Yeo parcellation of each ROI. The last subcortical (SUB) group is added to complement the Yeo atlas.

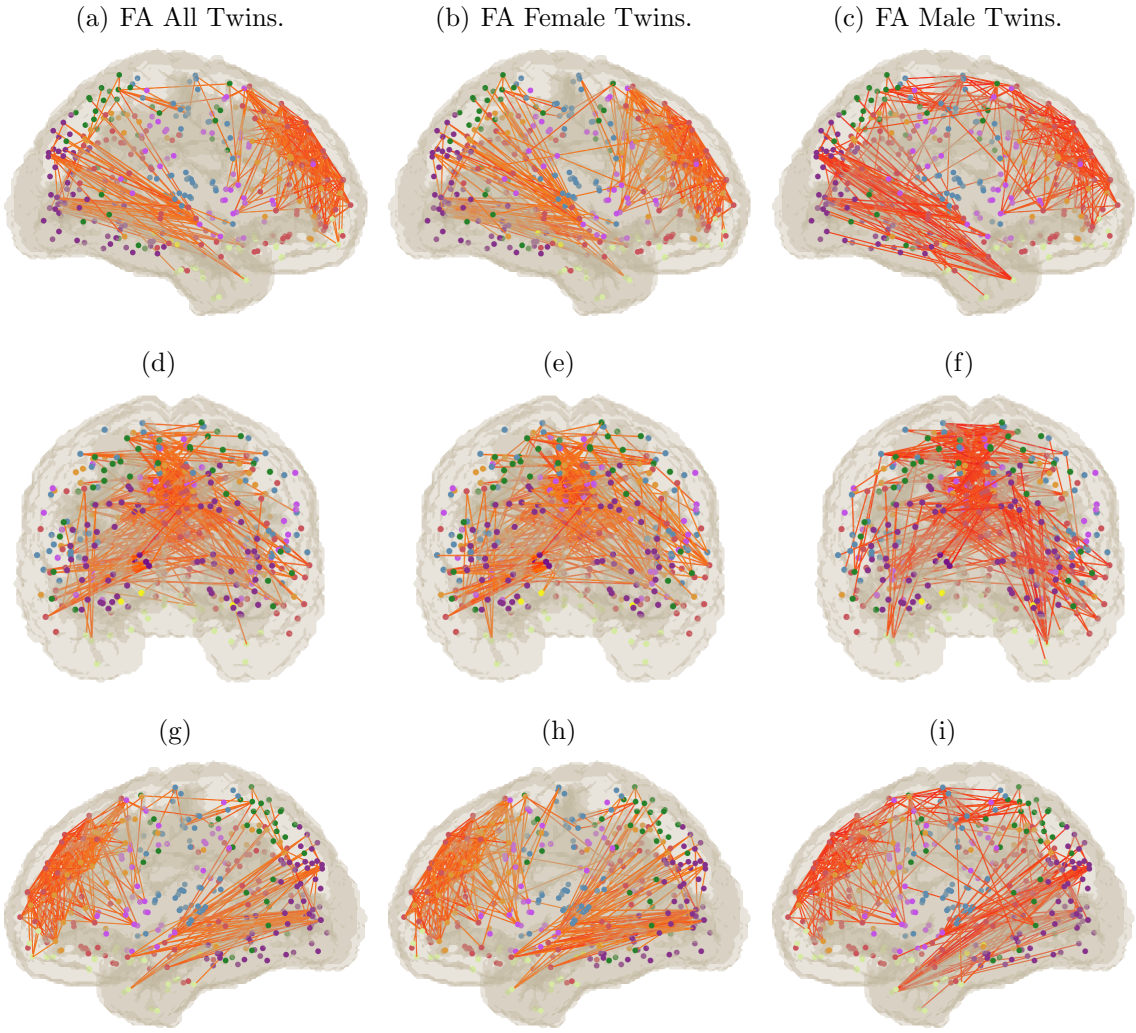

Fig. 3.6. Heritability of top 0.5% edges ranked by h^2.Node color indicates different Yeo functional groups. (a)-(c) Heritability of edge-level fractional anisotropy measures in the brain map of Left View. (d)-(f) The brain map of heritable fractional anisotropy edges in the Front View accordingly. (g)-(i) Edges with significant heritable fractional anisotropy in the brain map of Right View.

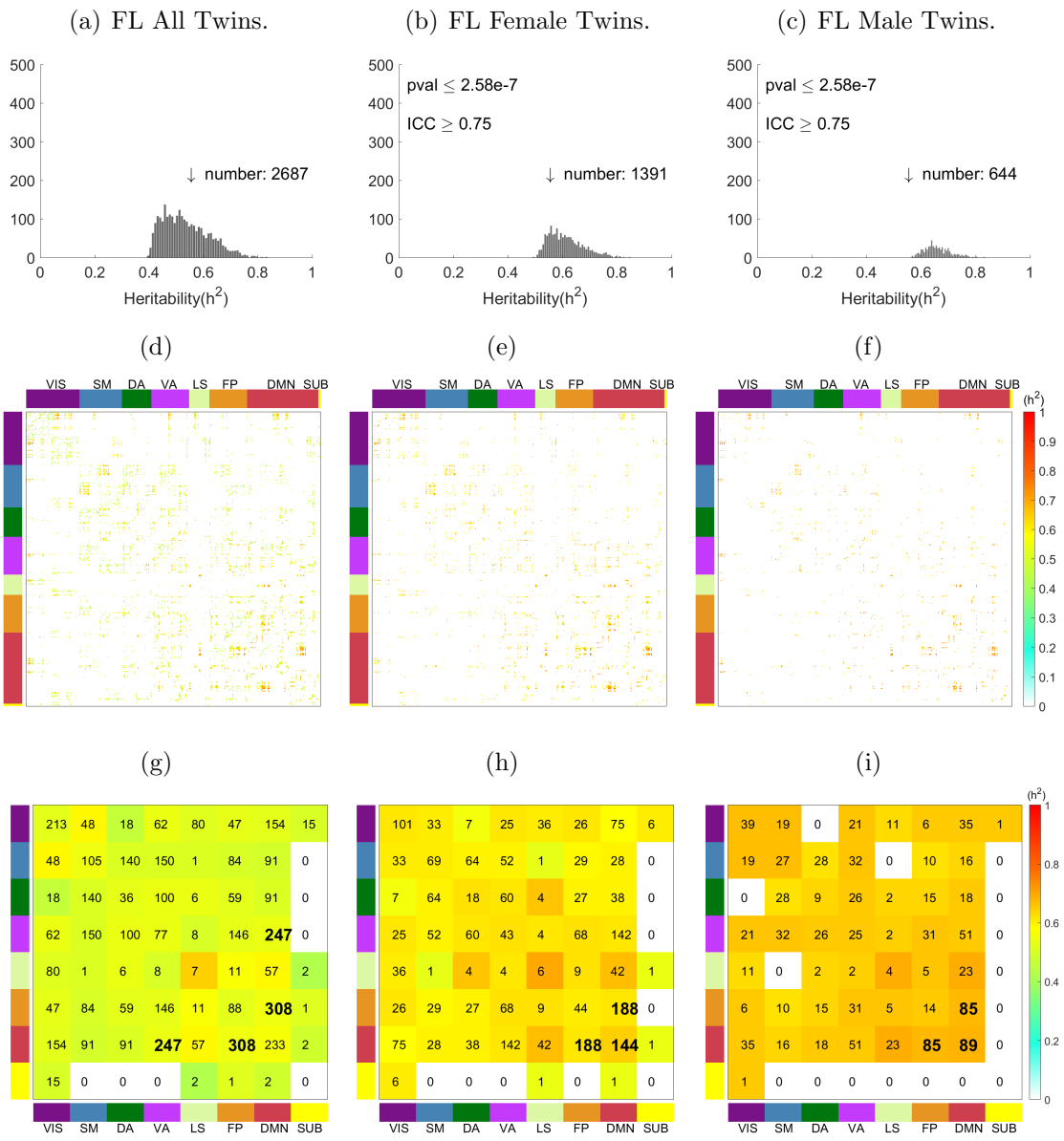

Fig. 3.7. Heritability distribution of all significant and reliable edges for all twins, female twins and male twins within the Fiber Length feature. (a) (b) (c) Histogram for reliable edges. (d) (e) (f) Heatmap of anatomical connection matrix. Rows and columns are reordered to form seven functional groups corresponding to Yeo parcellation. Top and side color panels indicate the corresponding Yeo parcellation of each ROI. The last subcortical (SUB) group is added to complement the Yeo atlas. (g) (h) (i) Heatmap showing total number and average h^2 value of edges connecting each pair of functional groups in Yeo parcellation. Bottom and side color panels indicate the corresponding Yeo parcellation of each ROI.

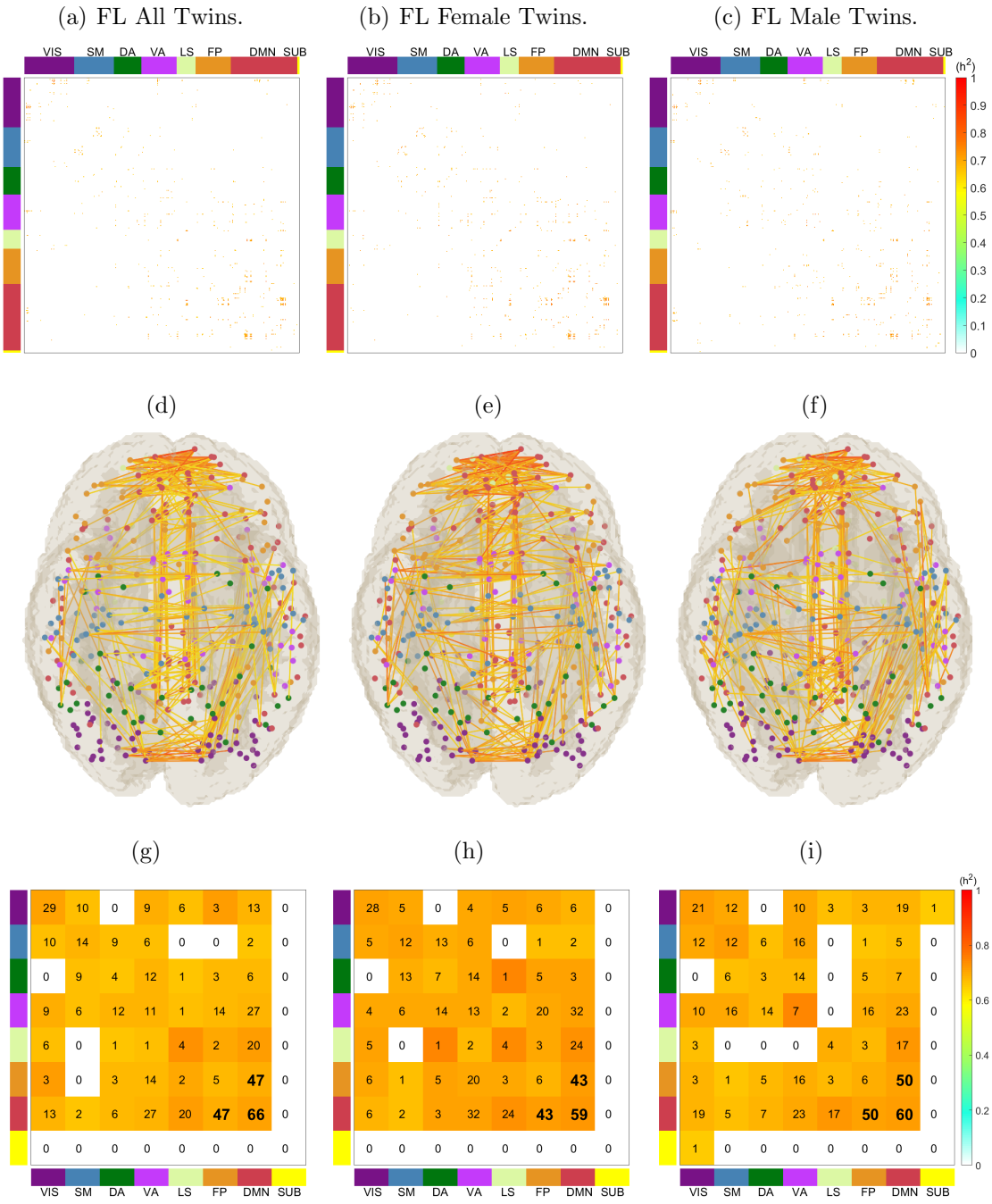

Fig. 3.8. Heritability of top 0.5% edges ranked by h^2. (a)-(c) Heatmap of anatomical connection matrix. (d)-(f) Heritability of edge-level measures in the brain map. Node color indicates different Yeo functional groups. (g)-(i) Heatmap showing total number and average h^2 value of edges connecting each pair of functional groups in Yeo parcellation. Top and side color panels indicate the corresponding Yeo parcellation of each ROI. The last subcortical (SUB) group is added to complement the Yeo atlas.

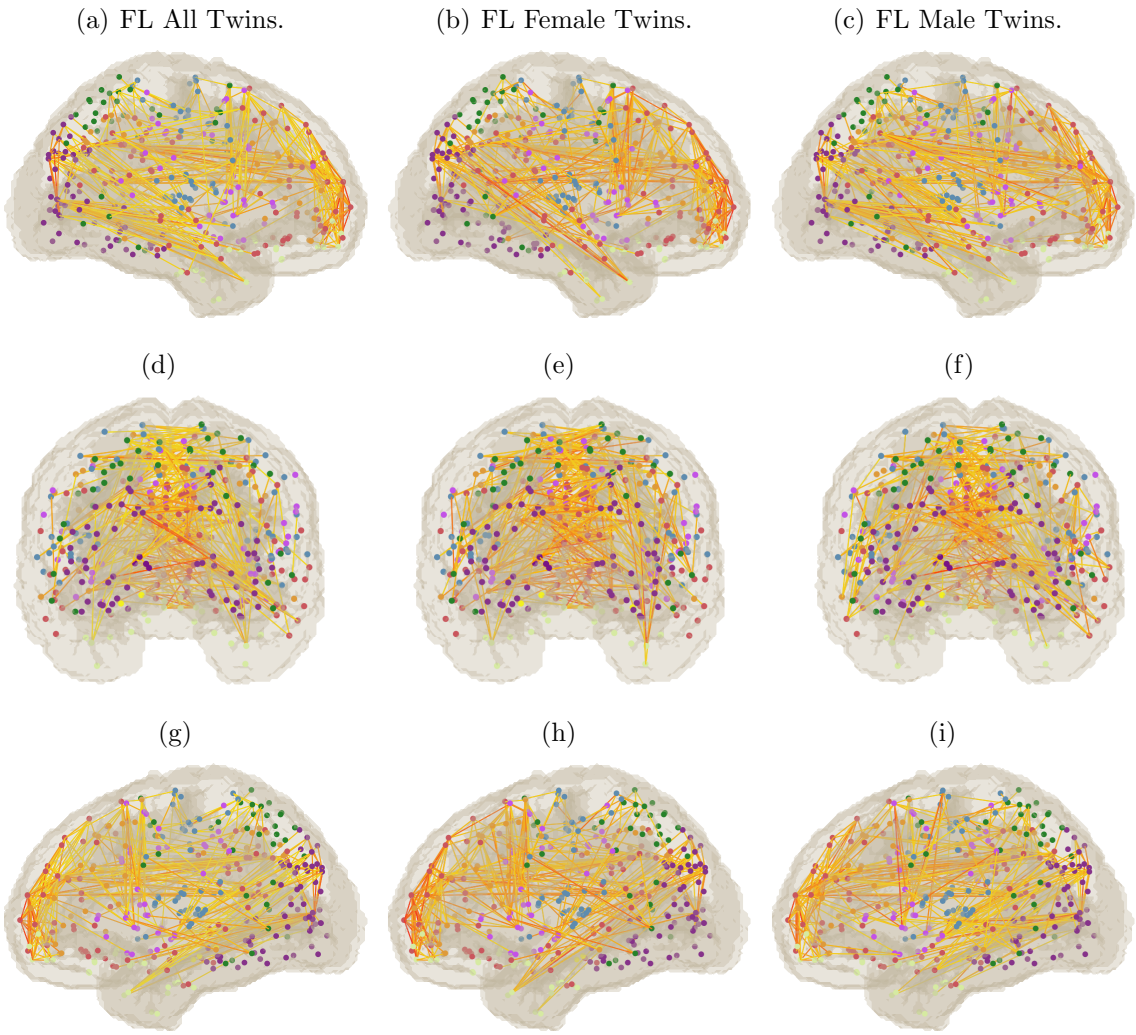

Fig. 3.9. Heritability of top 0.5% edges ranked by h^2.Node color indicates different Yeo functional groups. (a)-(c) Heritability of edge-level measures in the brain map of Left View. (d)-(f) Heritability of edge-level measures in the brain map of Front View accordingly. (g)-(i) Heritability of edge-level measures in the brain map of Right View.

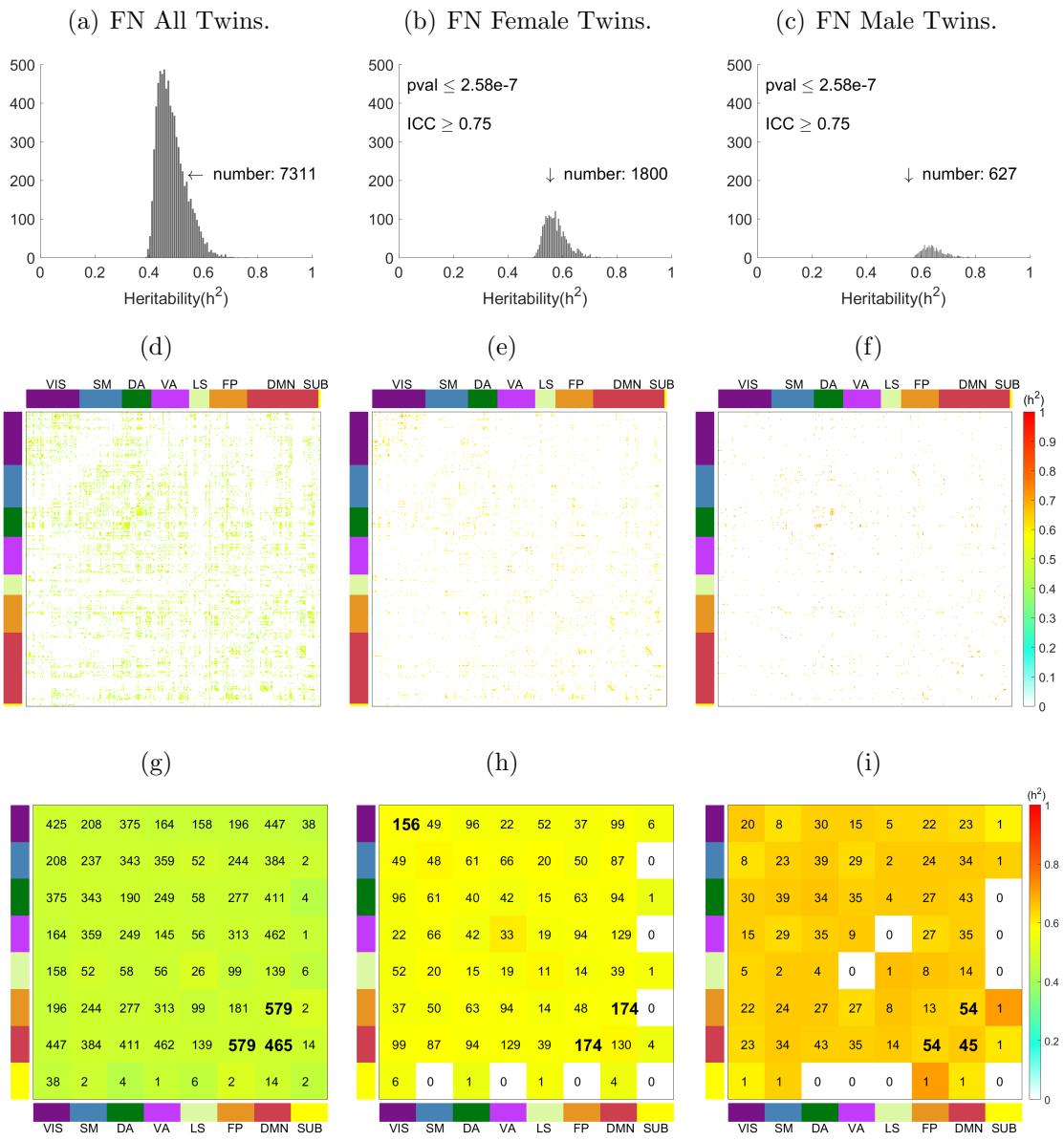

Fig. 3.10. Heritability distribution of all significant and reliable edges for all twins, female twins and male twins within the Fiber Number feature. (a) (b) (c) Histogram for reliable edges. (d) (e) (f) Heatmap of anatomical connection matrix. Rows and columns are reordered to form seven functional groups corresponding to Yeo parcellation. Top and side color panels indicate the corresponding Yeo parcellation of each ROI. The last subcortical (SUB) group is added to complement the Yeo atlas. (g) (h) (i) Heatmap showing total number and average h^2 value of edges connecting each pair of functional groups in Yeo parcellation. Bottom and side color panels indicate the corresponding Yeo parcellation of each ROI.

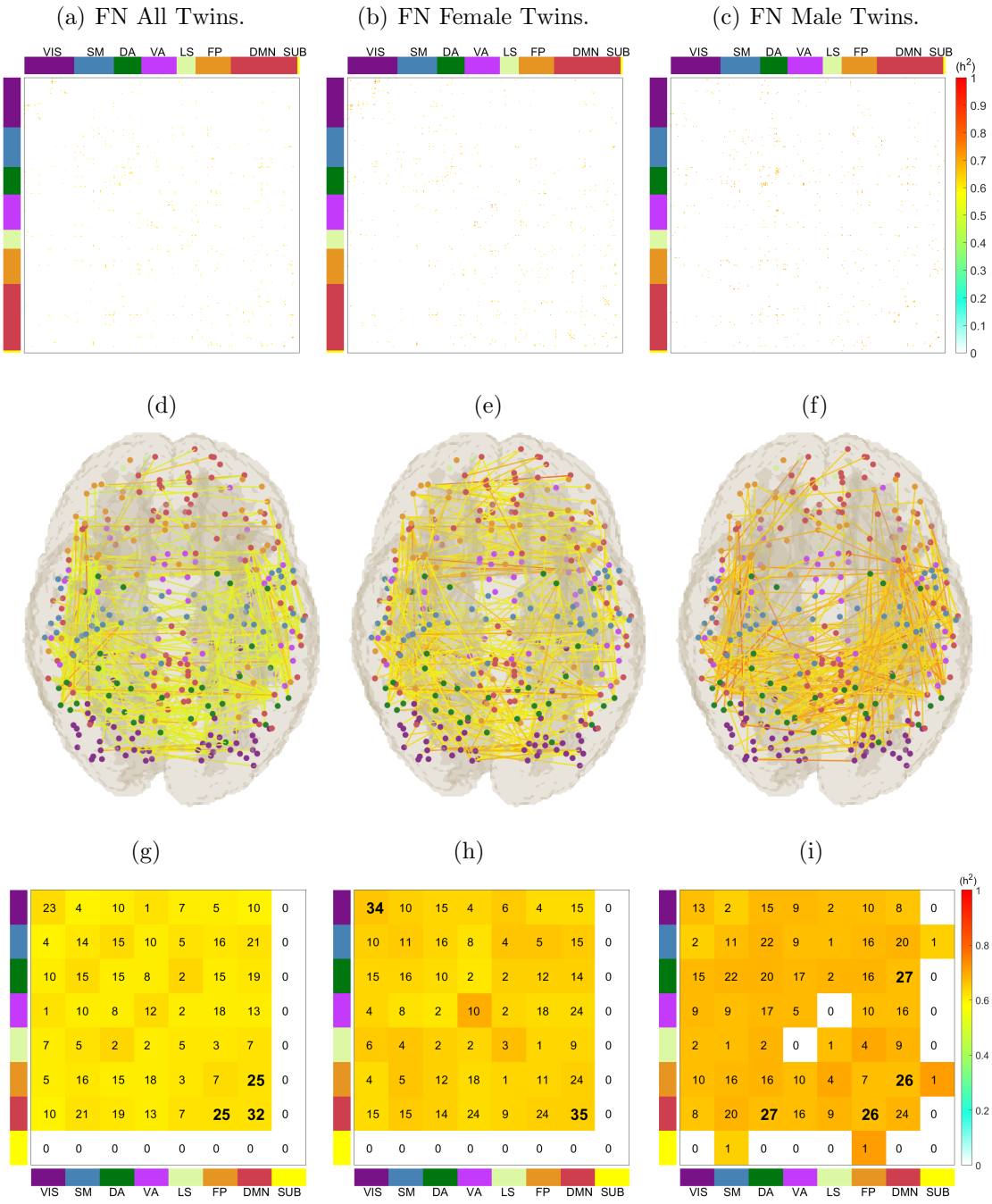

Fig. 3.11. Heritability of top 0.5% edges ranked by h^2. (a)-(c) Heatmap of anatomical connection matrix. (d)-(f) Heritability of edge-level measures in the brain map. Node color indicates different Yeo functional groups. (g)-(i) Heatmap showing total number and average h^2 value of edges connecting each pair of functional groups in Yeo parcellation. Top and side color panels indicate the corresponding Yeo parcellation of each ROI. The last subcortical (SUB) group is added to complement the Yeo atlas.

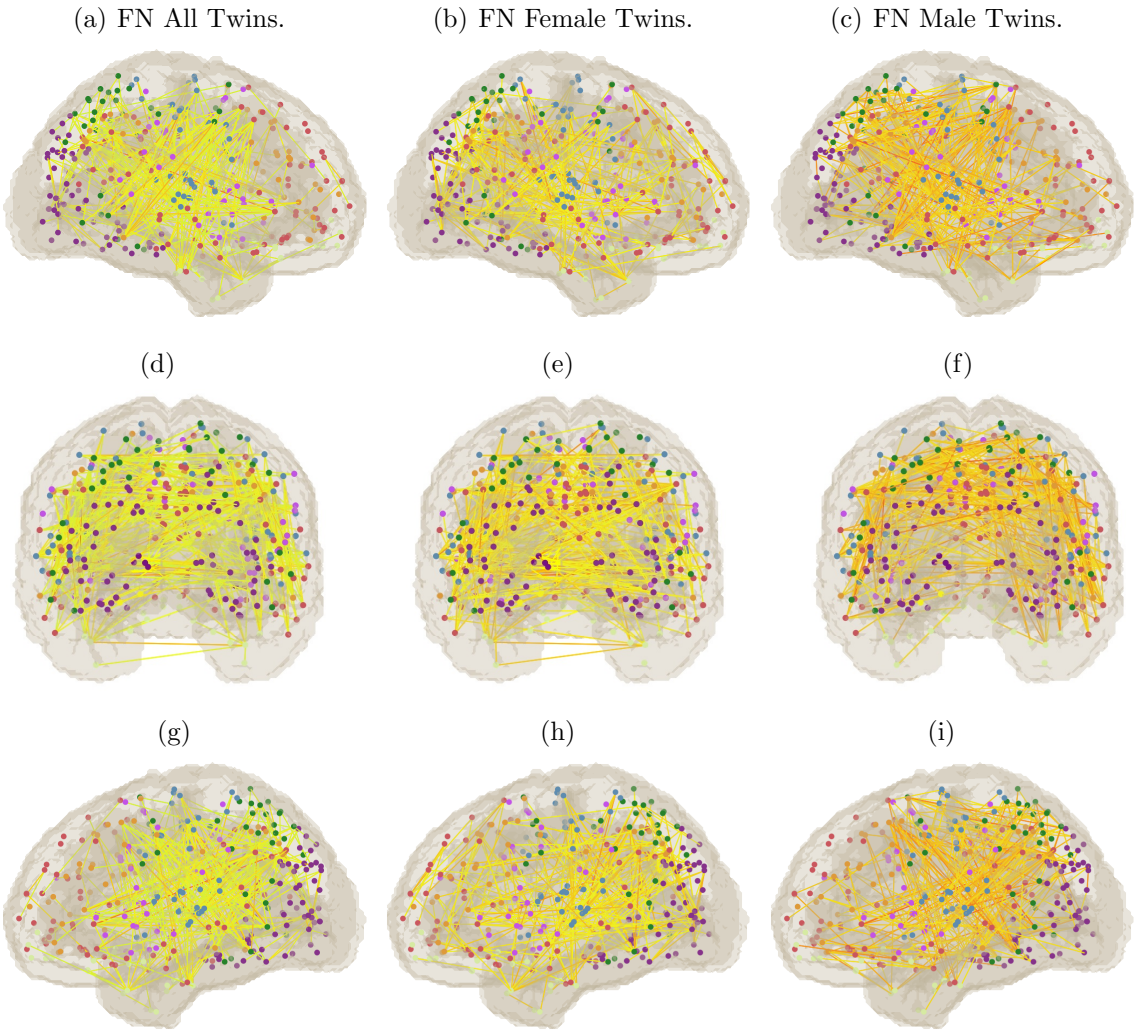

Fig. 3.12. Heritability of top 0.5% edges ranked by h^2.Node color indicates different Yeo functional groups. (a)-(c) Heritability of edge-level measures in the brain map of Left View. (d)-(f) Heritability of edge-level measures in the brain map of Front View accordingly. (g)-(i) Heritability of edge-level measures in the brain map of Right View.

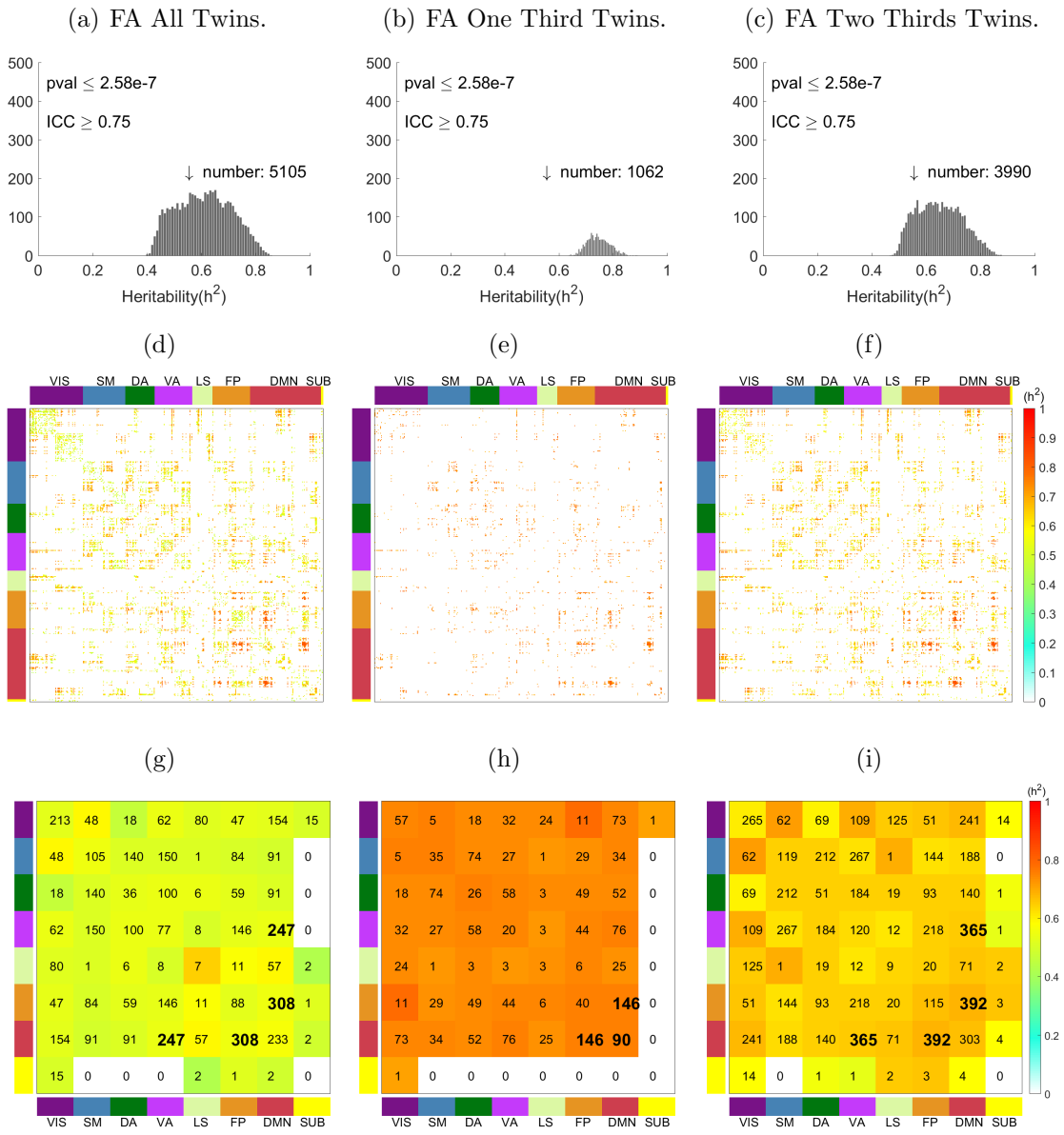

Fig. 3.13. Heritability distribution of all significant and reliable edges for all twins, one third twins and two thirds twins within the Fractional Anisotropy feature. (a) (b) (c) Histogram for reliable edges. (d) (e) (f) Heatmap of anatomical connection matrix. Rows and columns are reordered to form seven functional groups corresponding to Yeo parcellation. Top and side color panels indicate the corresponding Yeo parcellation of each ROI. The last subcortical (SUB) group is added to complement the Yeo atlas. (g) (h) (i) Heatmap showing total number and average h^2 value of edges connecting each pair of functional groups in Yeo parcellation. Bottom and side color panels indicate the corresponding Yeo parcellation of each ROI.

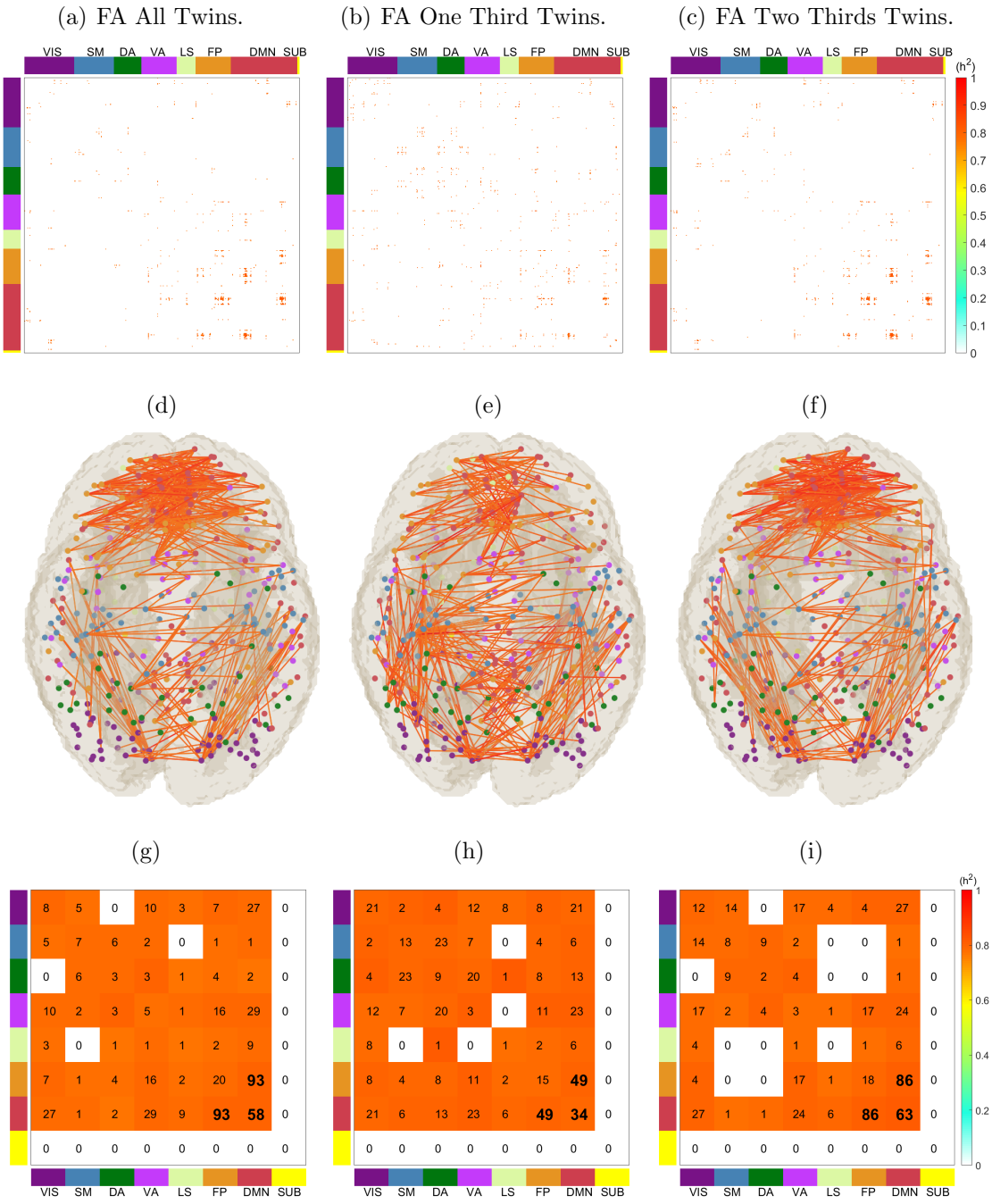

Fig. 3.14. Heritability of top 0.5% edges ranked by h^2. (a)-(c) Heatmap of anatomical connection matrix. (d)-(f) Heritability of edge-level measures in the brain map. Node color indicates different Yeo functional groups. (g)-(i) Heatmap showing total number and average h^2 value of edges connecting each pair of functional groups in Yeo parcellation. Top and side color panels indicate the corresponding Yeo parcellation of each ROI. The last subcortical (SUB) group is added to complement the Yeo atlas.

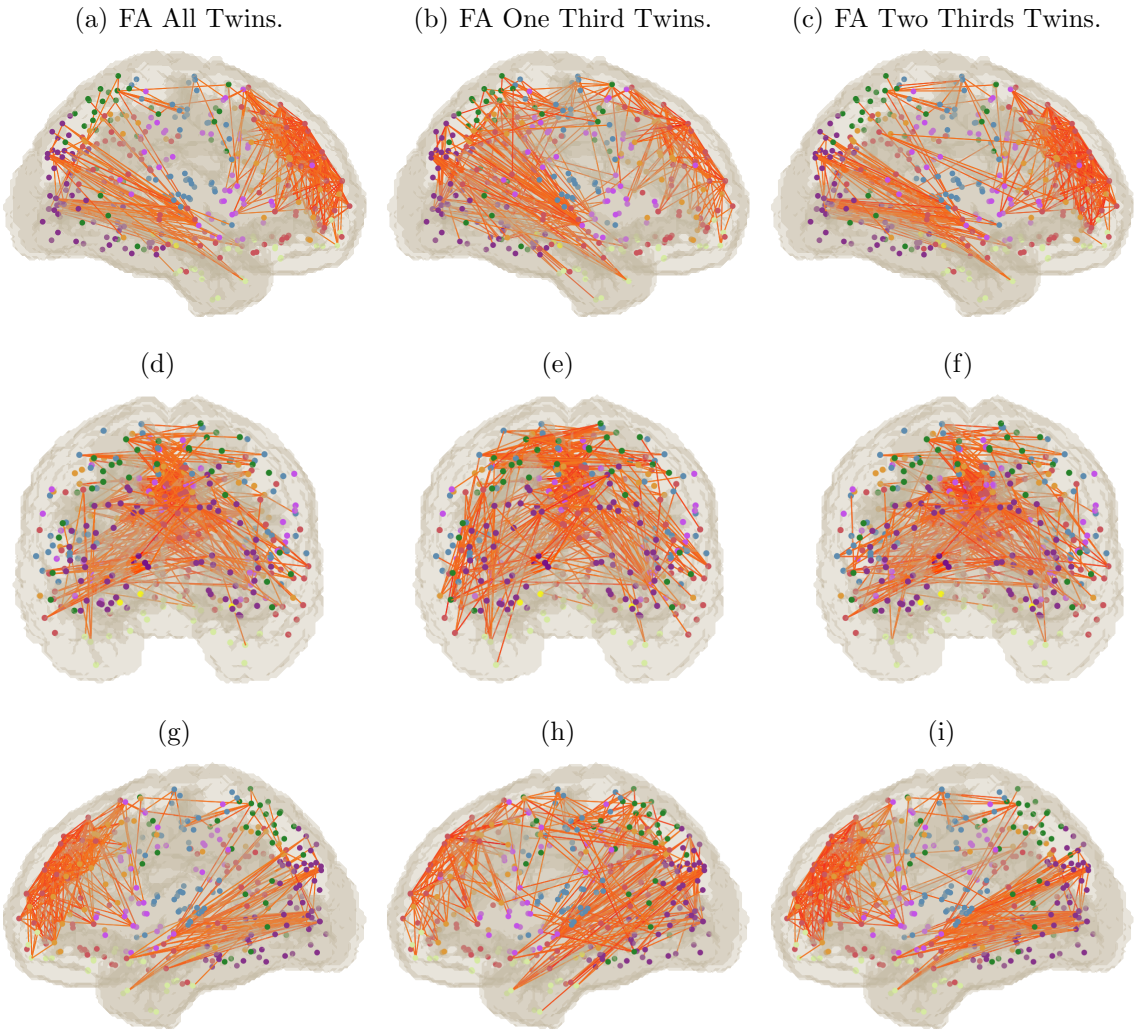

Fig. 3.15. Heritability of top 0.5% edges ranked by h^2.Node color indicates different Yeo functional groups. (a)-(c) Heritability of edge-level measures in the brain map of Left View. (d)-(f) Heritability of edge-level measures in the brain map of Front View accordingly. (g)-(i) Heritability of edge-level measures in the brain map of Right View.

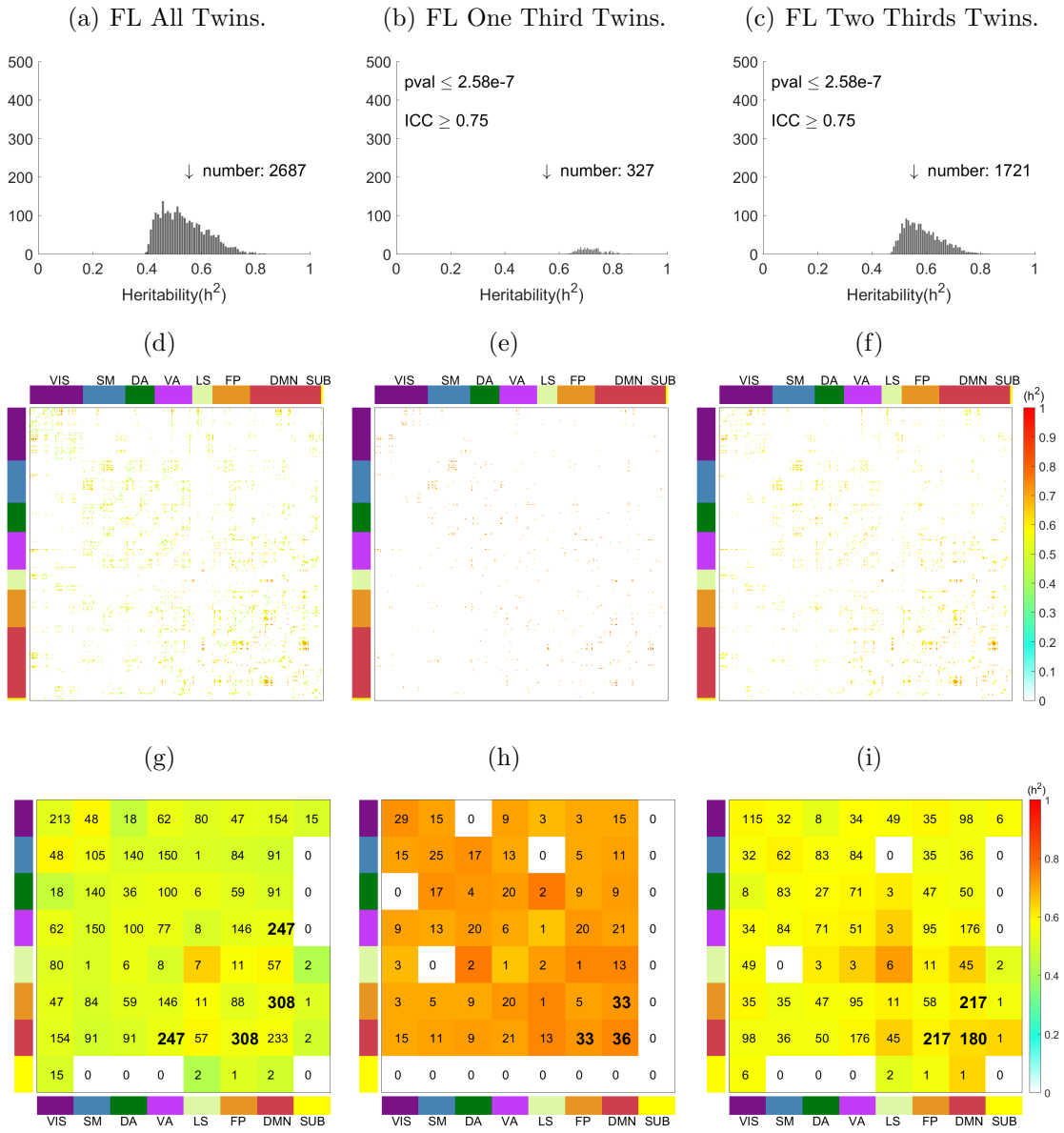

Fig. 3.16. Heritability distribution of all significant and reliable edges for all twins, one third twins and two thirds twins within the Fiber Length feature. (a) (b) (c) Histogram for reliable edges. (d) (e) (f) Heatmap of anatomical connection matrix. Rows and columns are reordered to form seven functional groups corresponding to Yeo parcellation. Top and side color panels indicate the corresponding Yeo parcellation of each ROI. The last subcortical (SUB) group is added to complement the Yeo atlas. (g) (h) (i) Heatmap showing total number and average h^2 value of edges connecting each pair of functional groups in Yeo parcellation. Bottom and side color panels indicate the corresponding Yeo parcellation of each ROI.

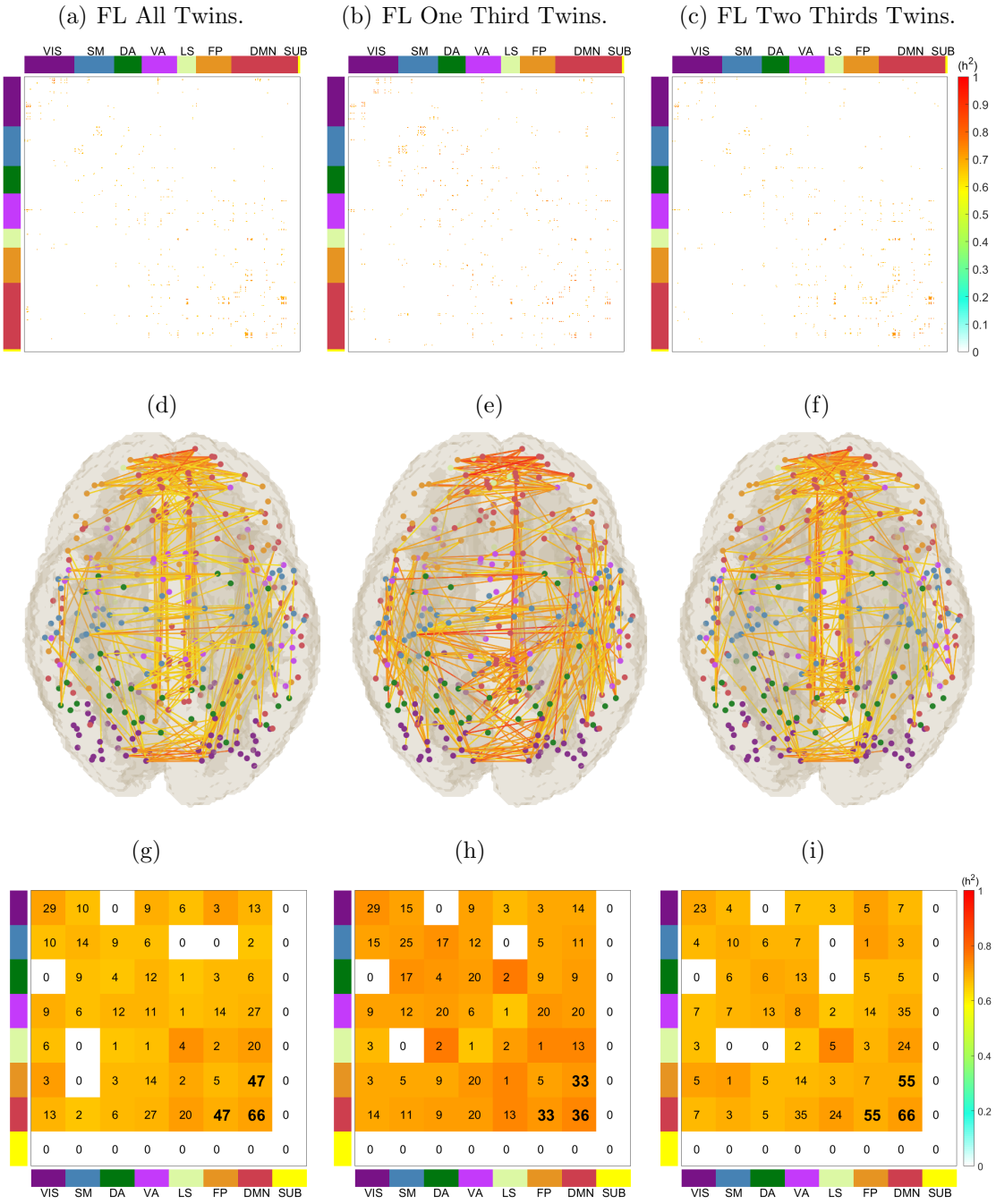

Fig. 3.17. Heritability of top 0.5% edges ranked by h^2. (a)-(c) Heatmap of anatomical connection matrix. (d)-(f) Heritability of edge-level measures in the brain map. Node color indicates different Yeo functional groups. (g)-(i) Heatmap showing total number and average h^2 value of edges connecting each pair of functional groups in Yeo parcellation. Top and side color panels indicate the corresponding Yeo parcellation of each ROI. The last subcortical (SUB) group is added to complement the Yeo atlas.

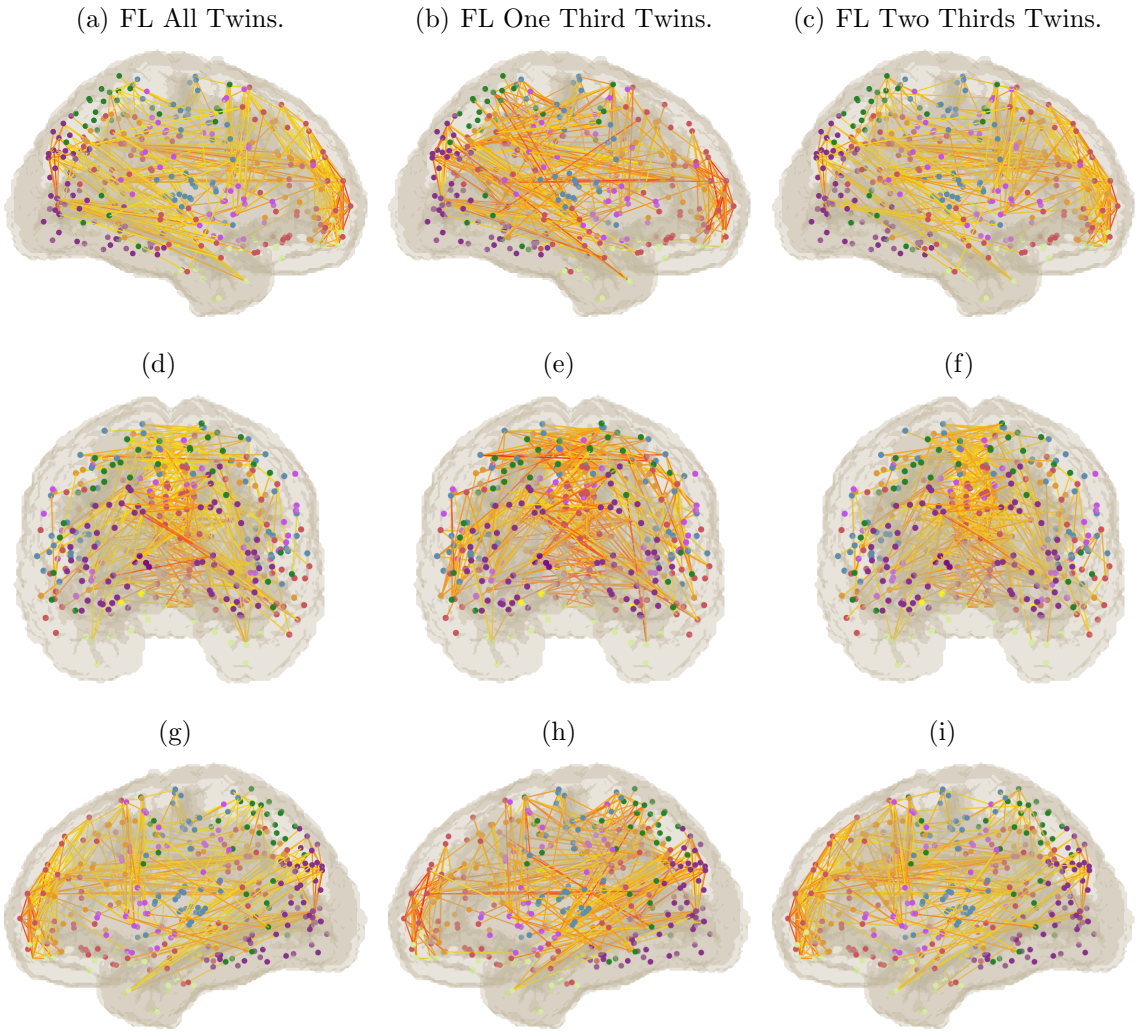

Fig. 3.18. Heritability of top 0.5% edges ranked by h^2.Node color indicates different Yeo functional groups. (a)-(c) Heritability of edge-level measures in the brain map of Left View. (d)-(f) Heritability of edge-level measures in the brain map of Front View accordingly. (g)-(i) Heritability of edge-level measures in the brain map of Right View.

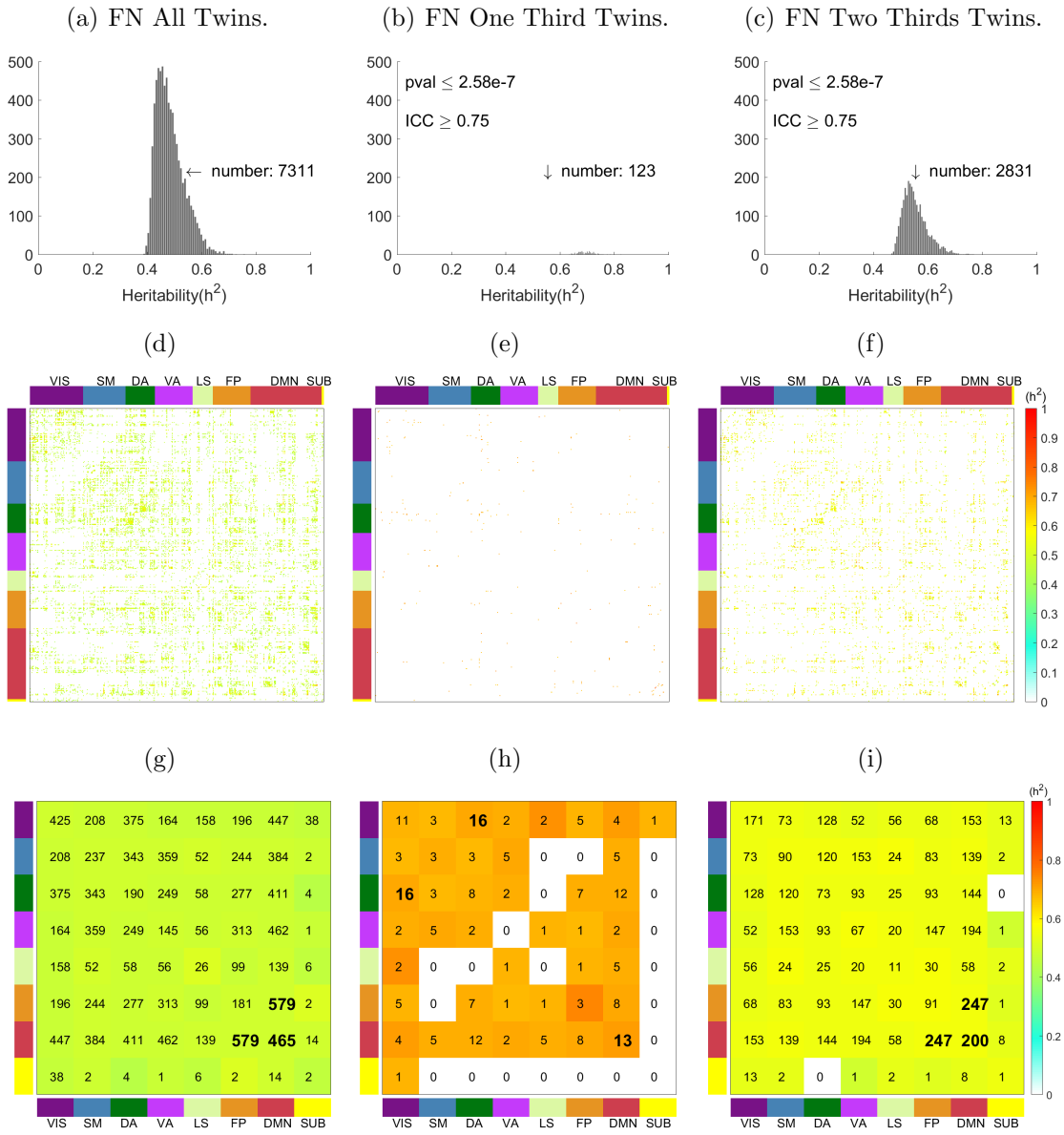

Fig. 3.19. Heritability distribution of all significant and reliable edges for all twins, one third twins and two thirds twins within the Fiber Number feature. (a) (b) (c) Histogram for reliable edges. (d) (e) (f) Heatmap of anatomical connection matrix. Rows and columns are reordered to form seven functional groups corresponding to Yeo parcellation. Top and side color panels indicate the corresponding Yeo parcellation of each ROI. The last subcortical (SUB) group is added to complement the Yeo atlas. (g) (h) (i) Heatmap showing total number and average h^2 value of edges connecting each pair of functional groups in Yeo parcellation. Bottom and side color panels indicate the corresponding Yeo parcellation of each ROI.

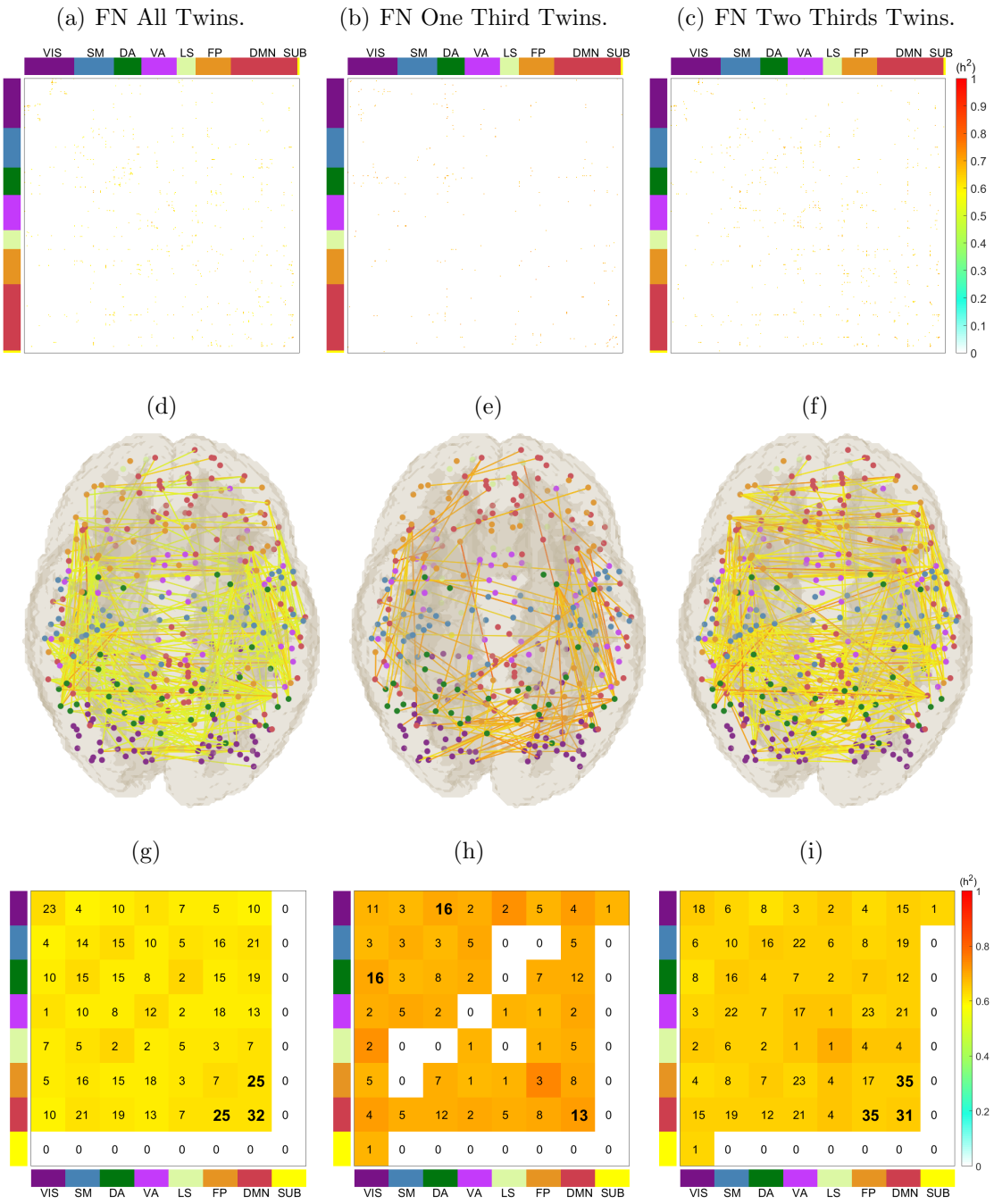

Fig. 3.20. Heritability of top 0.5% edges ranked by h^2. (a)-(c) Heatmap of anatomical connection matrix. (d)-(f) Heritability of edge-level measures in the brain map. Node color indicates different Yeo functional groups. (g)-(i) Heatmap showing total number and average h^2 value of edges connecting each pair of functional groups in Yeo parcellation. Top and side color panels indicate the corresponding Yeo parcellation of each ROI. The last subcortical (SUB) group is added to complement the Yeo atlas.

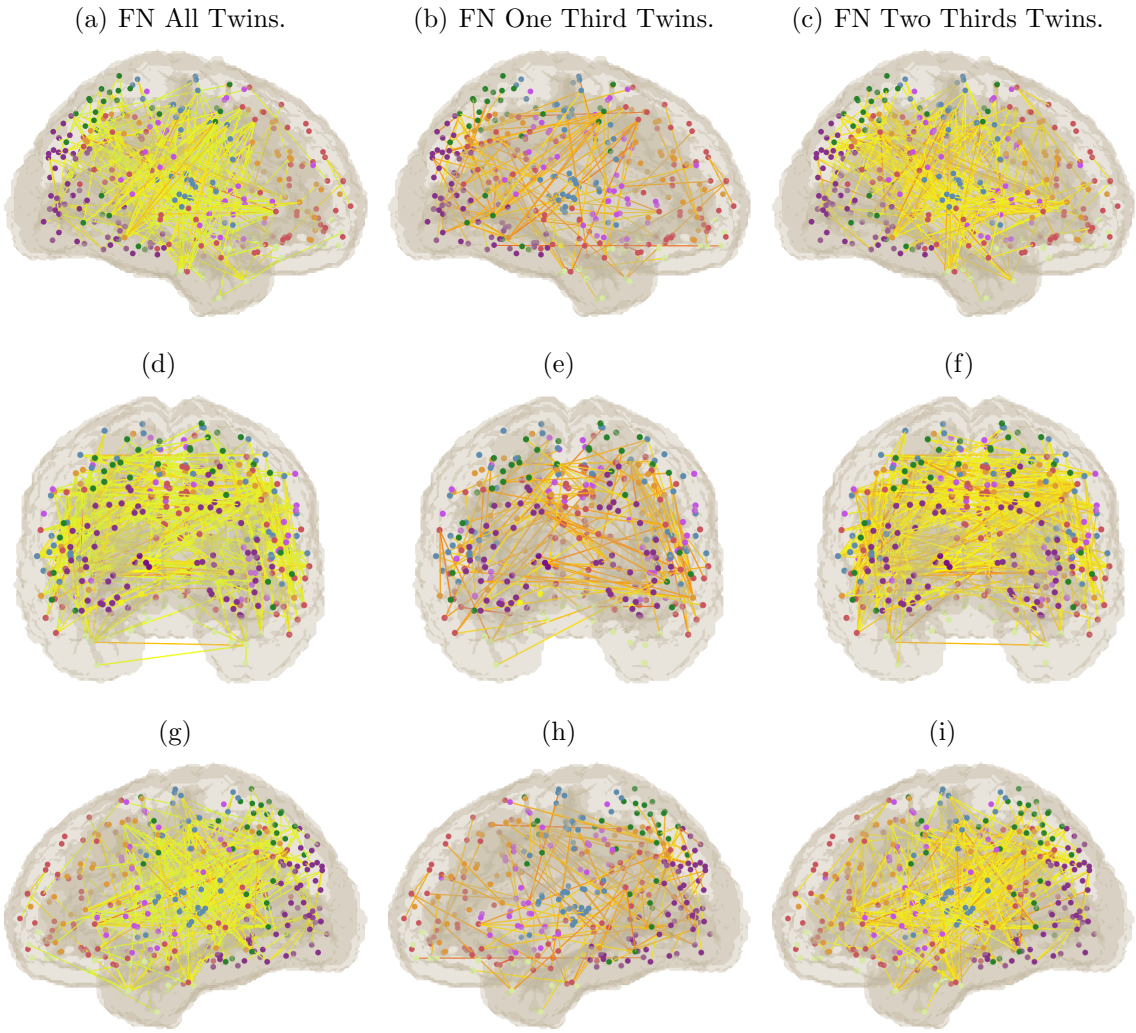

Fig. 3.21. Heritability of top 0.5% edges ranked by h^2.Node color indicates different Yeo functional groups. (a)-(c) Heritability of edge-level measures in the brain map of Left View. (d)-(f) Heritability of edge-level measures in the brain map of Front View accordingly. (g)-(i) Heritability of edge-level measures in the brain map of Right View.

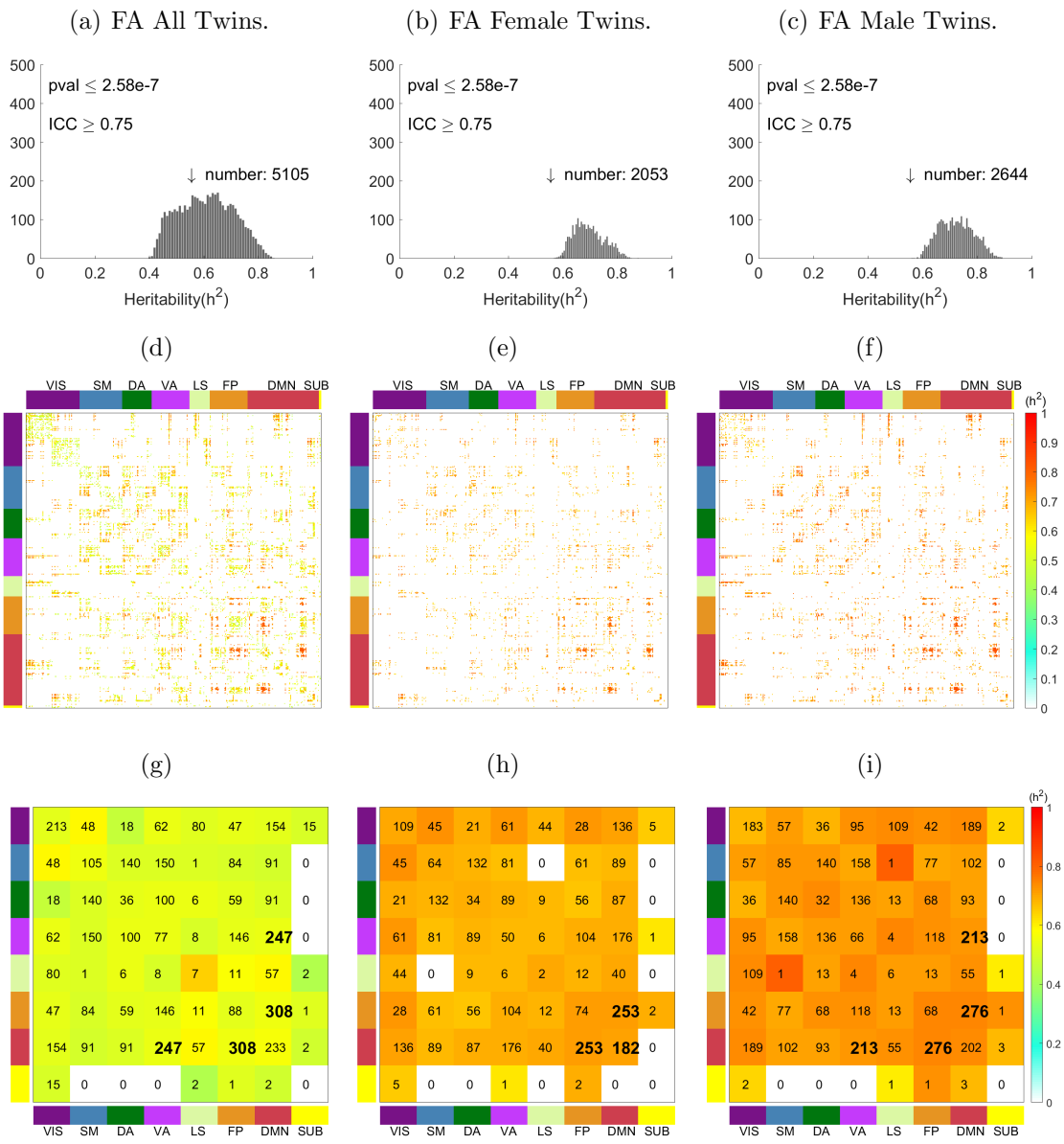

Fig. 3.22. Heritability distribution of all significant and reliable edges for all twins, female twins and male twins within the Fractional Anisotropy feature. (a) (b) (c) Histogram for reliable edges. (d) (e) (f) Heatmap of anatomical connection matrix. Rows and columns are reordered to form seven functional groups corresponding to Yeo parcellation. Top and side color panels indicate the corresponding Yeo parcellation of each ROI. The last subcortical (SUB) group is added to complement the Yeo atlas. (g) (h) (i) Heatmap showing total number and average h^2 value of edges connecting each pair of functional groups in Yeo parcellation. Bottom and side color panels indicate the corresponding Yeo parcellation of each ROI.

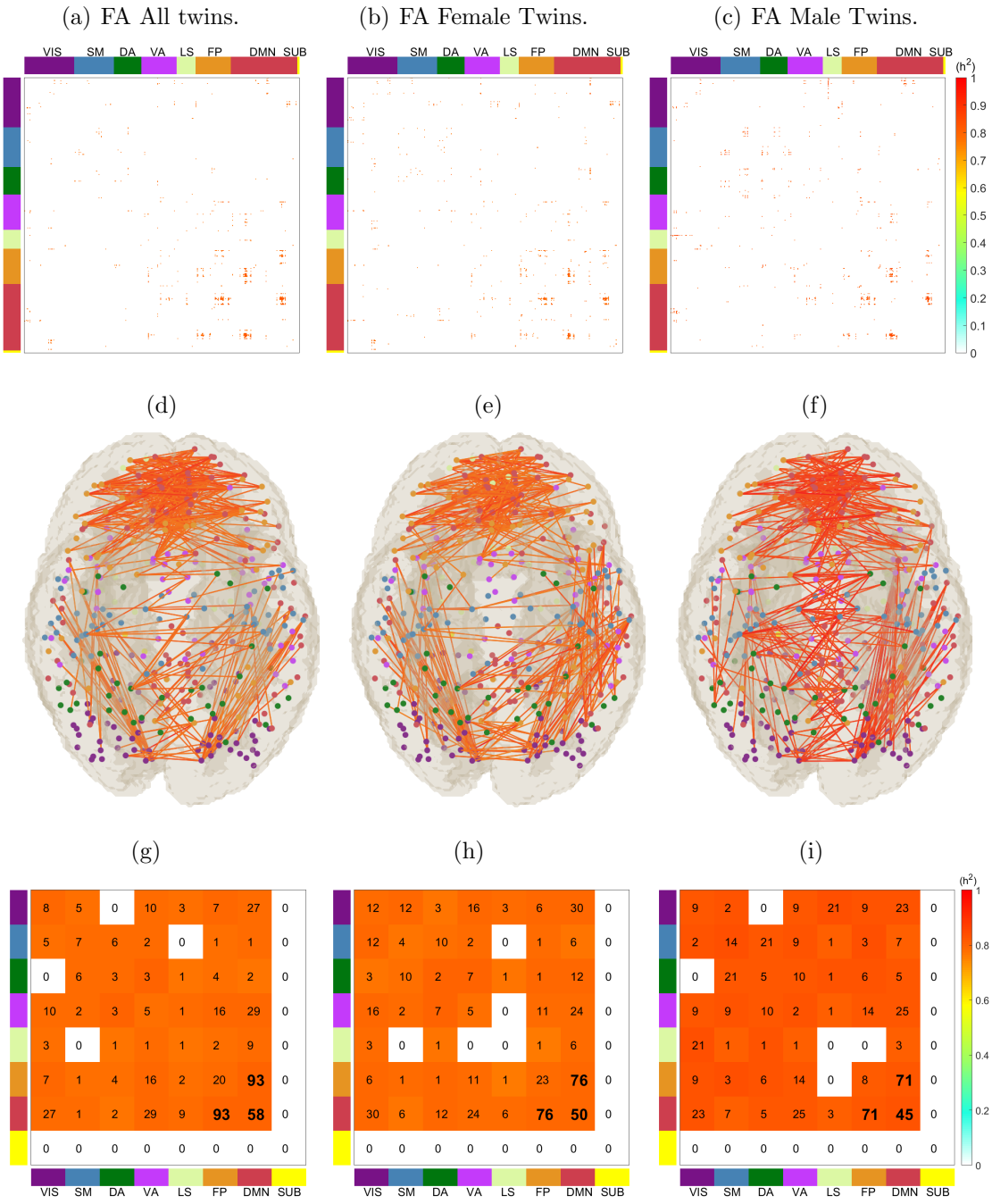

Fig. 3.23. Heritability of top 0.5% edges ranked by h^2. (a)-(c) Heatmap of anatomical connection matrix. (d)-(f) Heritability of edge-level measures in the brain map. Node color indicates different Yeo functional groups. (g)-(i) Heatmap showing total number and average h^2 value of edges connecting each pair of functional groups in Yeo parcellation. Top and side color panels indicate the corresponding Yeo parcellation of each ROI. The last subcortical (SUB) group is added to complement the Yeo atlas.

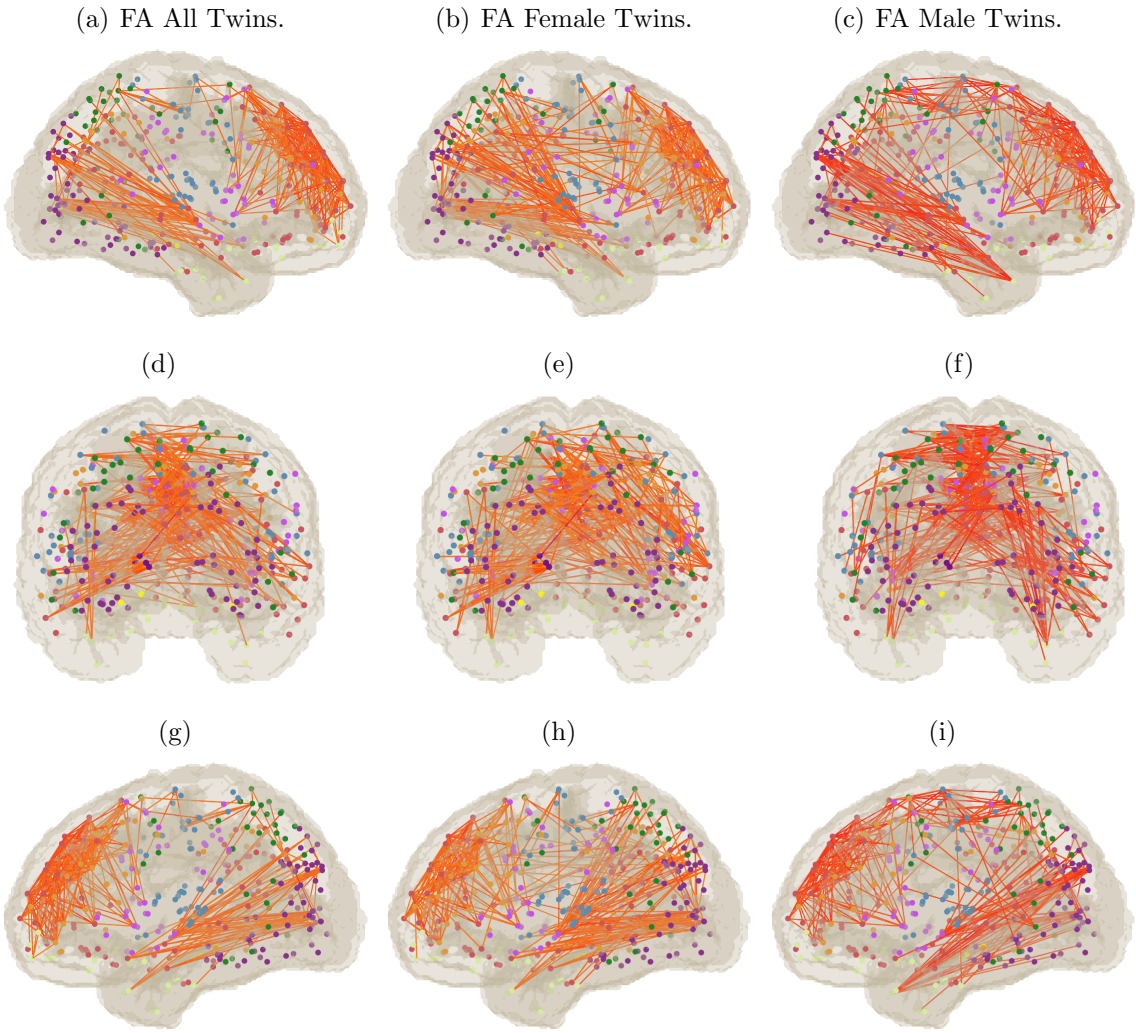

Fig. 3.24. Heritability of top 0.5% edges ranked by h^2.Node color indicates different Yeo functional groups. (a)-(c) Heritability of edge-level measures in the brain map of Left View. (d)-(f) Heritability of edge-level measures in the brain map of Front View accordingly. (g)-(i) Heritability of edge-level measures in the brain map of Right View.

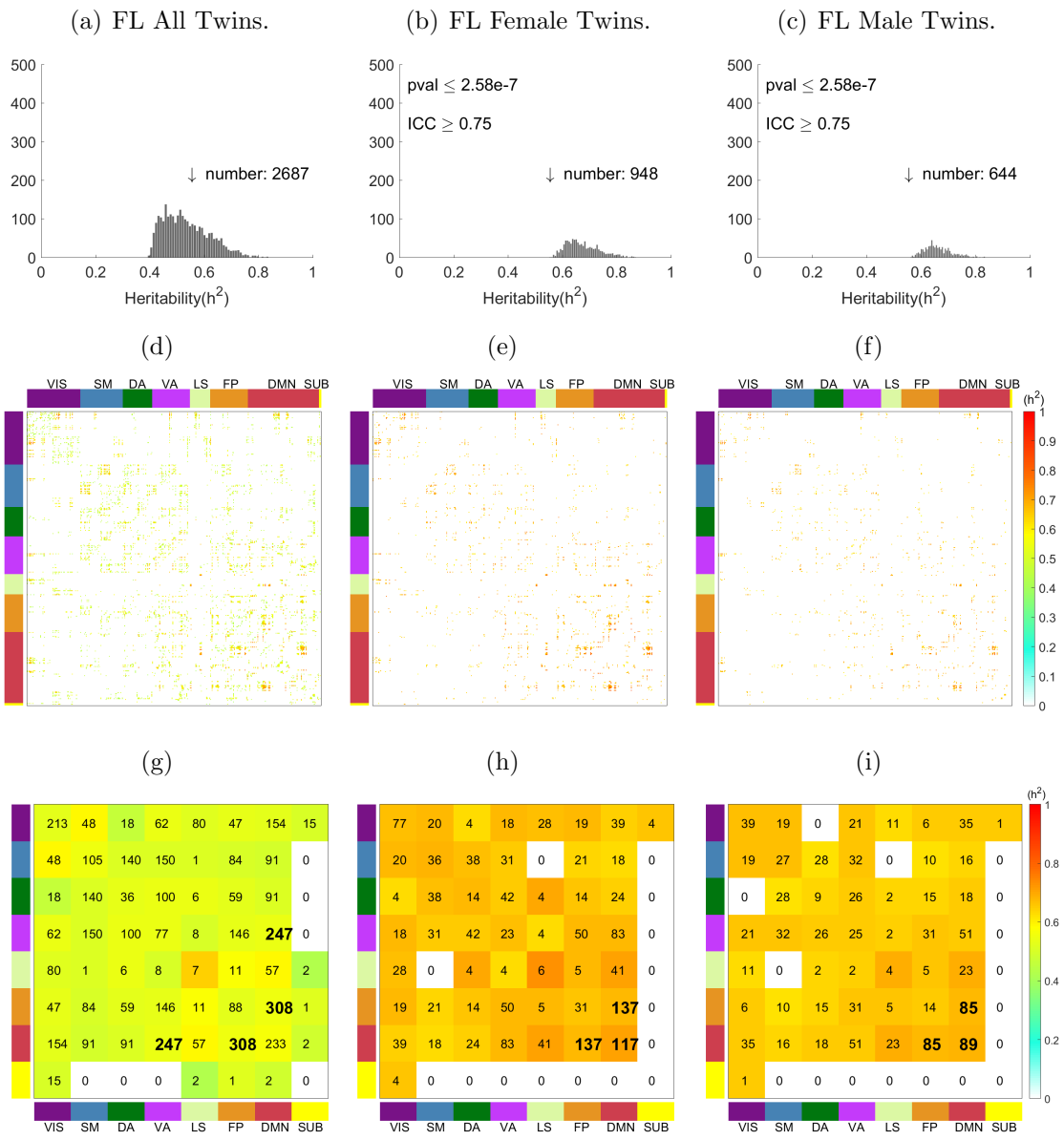

Fig. 3.25. Heritability distribution of all significant and reliable edges for all twins, female twins and male twins within the Fiber Length feature. (a) (b) (c) Histogram for reliable edges. (d) (e) (f) Heatmap of anatomical connection matrix. Rows and columns are reordered to form seven functional groups corresponding to Yeo parcellation. Top and side color panels indicate the corresponding Yeo parcellation of each ROI. The last subcortical (SUB) group is added to complement the Yeo atlas. (g) (h) (i) Heatmap showing total number and average h^2 value of edges connecting each pair of functional groups in Yeo parcellation. Bottom and side color panels indicate the corresponding Yeo parcellation of each ROI.

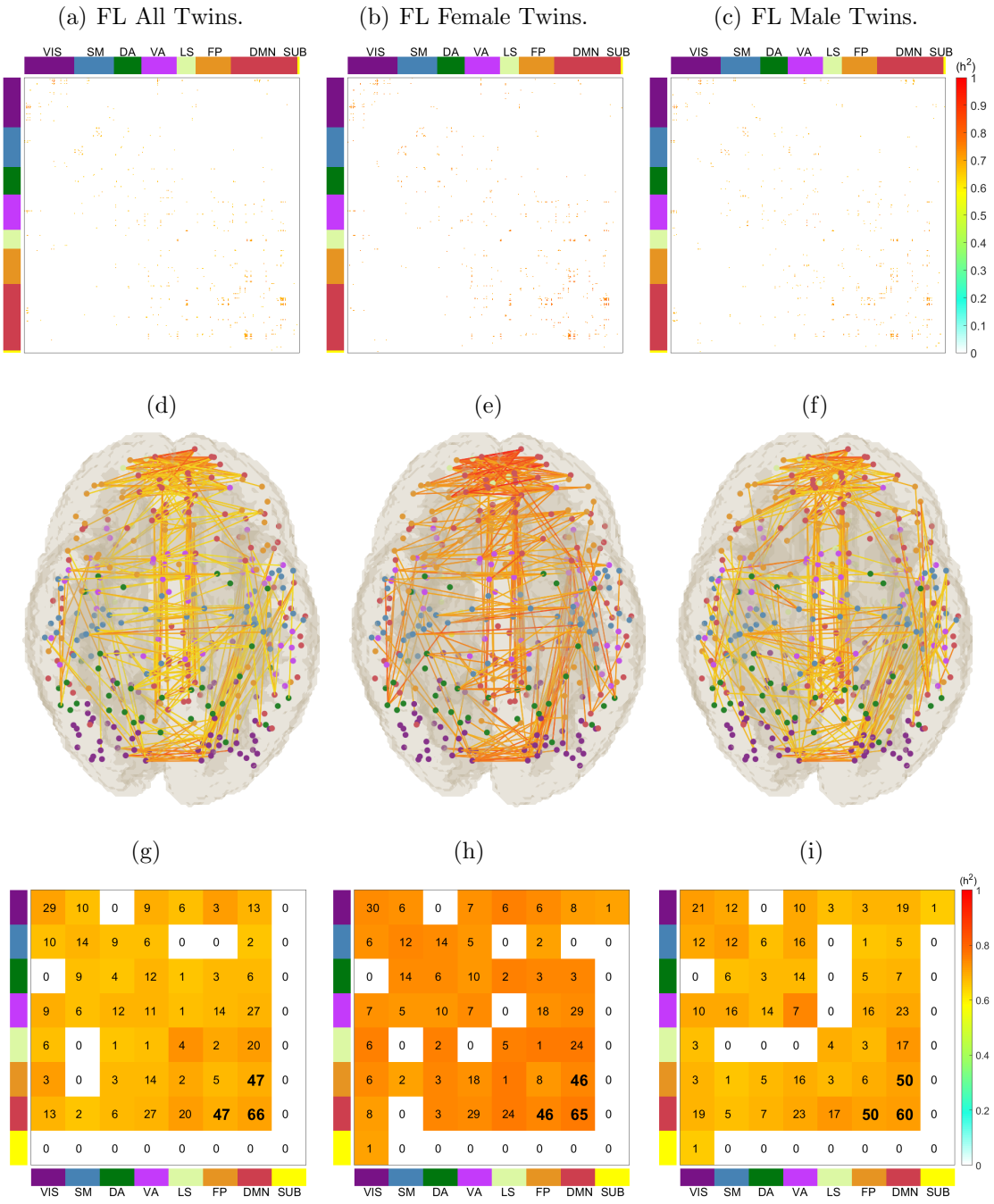

Fig. 3.26. Heritability of top 0.5% edges ranked by h^2. (a)-(c) Heatmap of anatomical connection matrix. (d)-(f) Heritability of edge-level measures in the brain map. Node color indicates different Yeo functional groups. (g)-(i) Heatmap showing total number and average h^2 value of edges connecting each pair of functional groups in Yeo parcellation. Top and side color panels indicate the corresponding Yeo parcellation of each ROI. The last subcortical (SUB) group is added to complement the Yeo atlas.

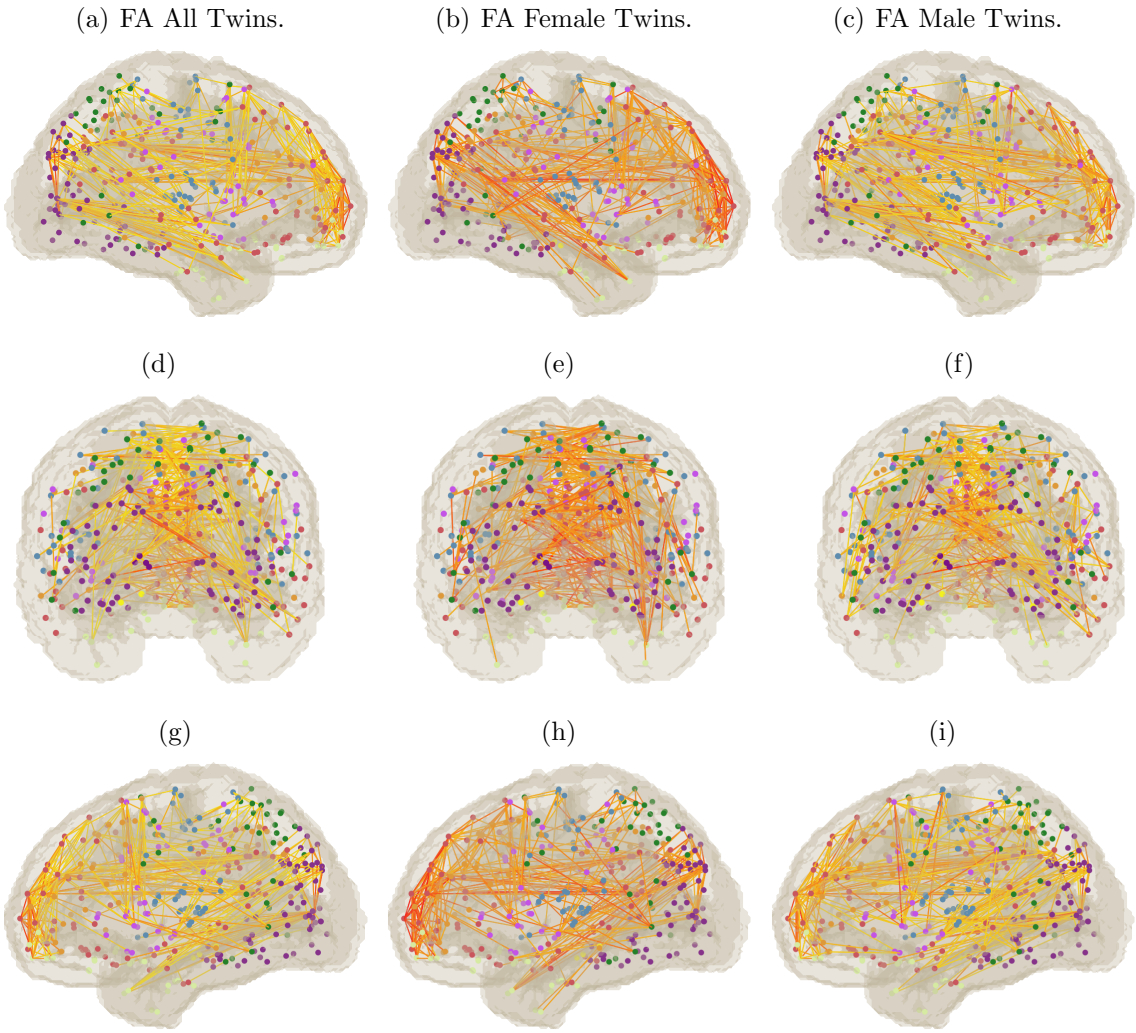

Fig. 3.27. Heritability of top 0.5% edges ranked by h^2.Node color indicates different Yeo functional groups. (a)-(c) Heritability of edge-level measures in the brain map of Left View. (d)-(f) Heritability of edge-level measures in the brain map of Front View accordingly. (g)-(i) Heritability of edge-level measures in the brain map of Right View.

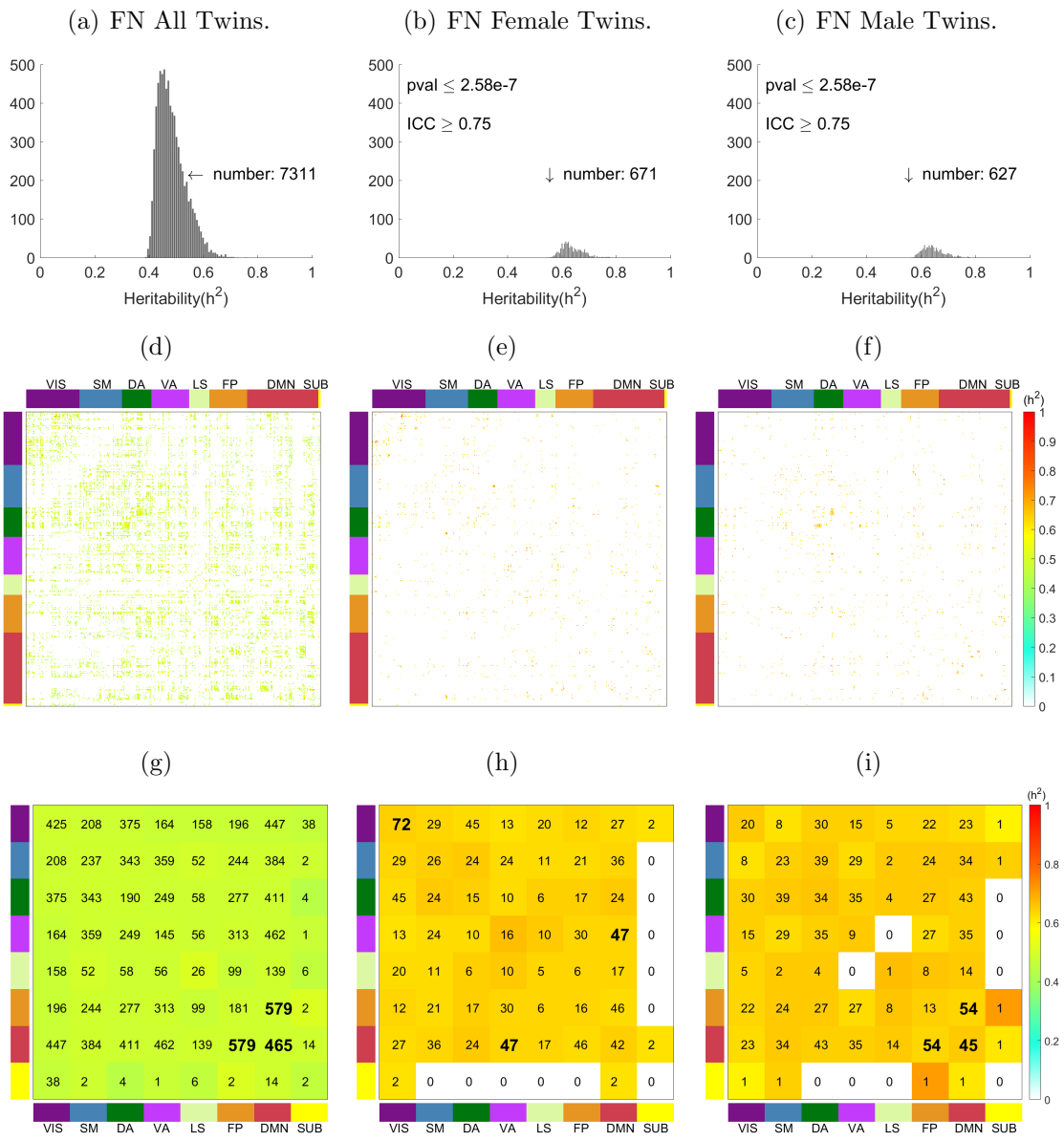

Fig. 3.28. Heritability distribution of all significant and reliable edges for all twins, female twins and male twins within the Fiber Number feature. (a) (b) (c) Histogram for reliable edges. (d) (e) (f) Heatmap of anatomical connection matrix. Rows and columns are reordered to form seven functional groups corresponding to Yeo parcellation. Top and side color panels indicate the corresponding Yeo parcellation of each ROI. The last subcortical (SUB) group is added to complement the Yeo atlas. (g) (h) (i) Heatmap showing total number and average h^2 value of edges connecting each pair of functional groups in Yeo parcellation. Bottom and side color panels indicate the corresponding Yeo parcellation of each ROI.

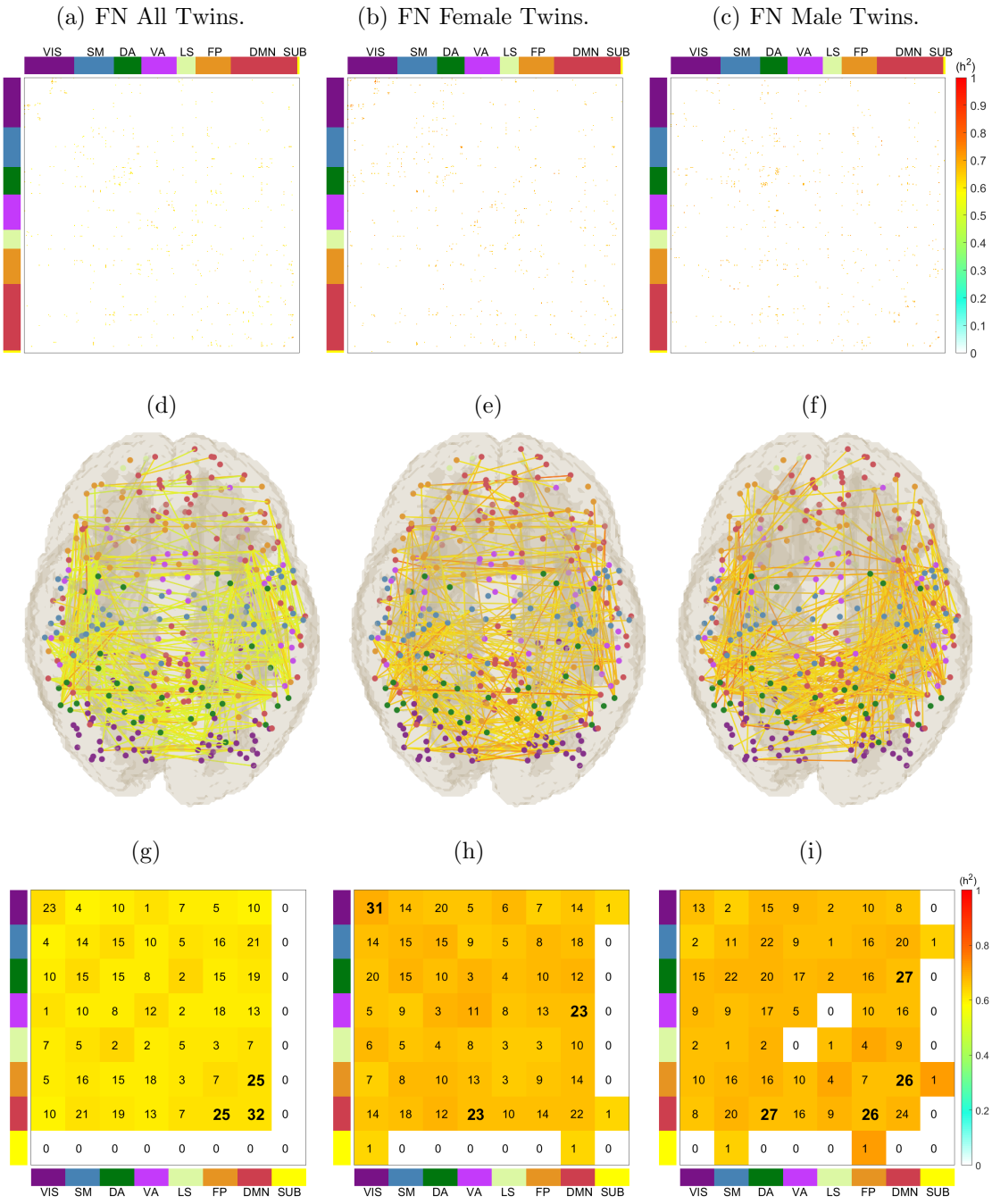

Fig. 3.29. Heritability of top 0.5% edges ranked by h^2. (a)-(c) Heatmap of anatomical connection matrix. (d)-(f) Heritability of edge-level measures in the brain map. Node color indicates different Yeo functional groups. (g)-(i) Heatmap showing total number and average h^2 value of edges connecting each pair of functional groups in Yeo parcellation. Top and side color panels indicate the corresponding Yeo parcellation of each ROI. The last subcortical (SUB) group is added to complement the Yeo atlas.

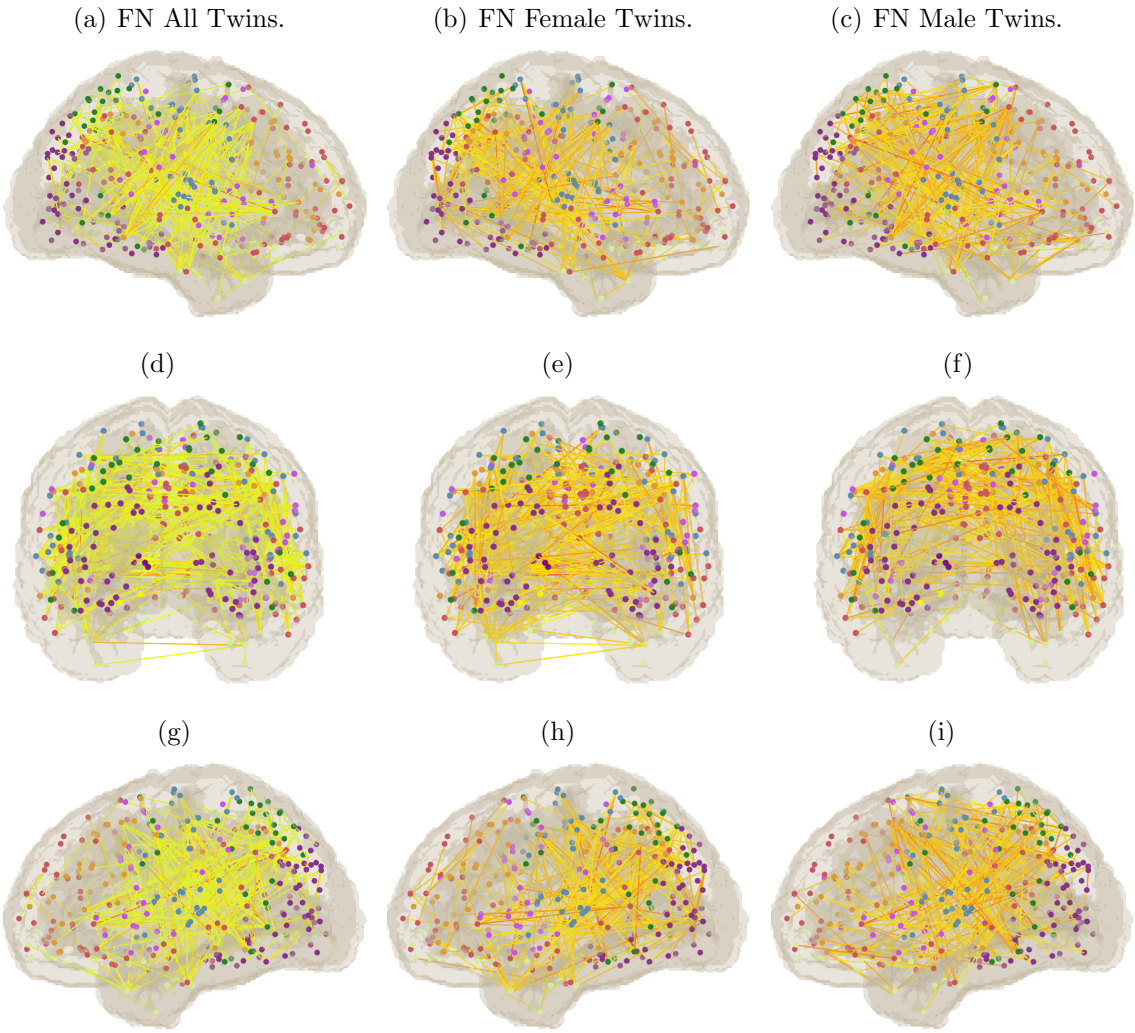

Fig. 3.30. Heritability of top 0.5% edges ranked by h^2.Node color indicates different Yeo functional groups. (a)-(c) Heritability of edge-level measures in the brain map of Left View. (d)-(f) Heritability of edge-level measures in the brain map of Front View accordingly. (g)-(i) Heritability of edge-level measures in the brain map of Right View.

(a) FA Female Twins.

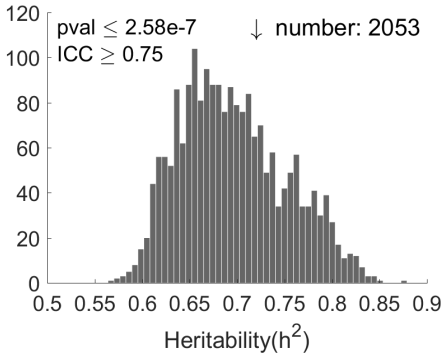

(b) FA Male Twins.

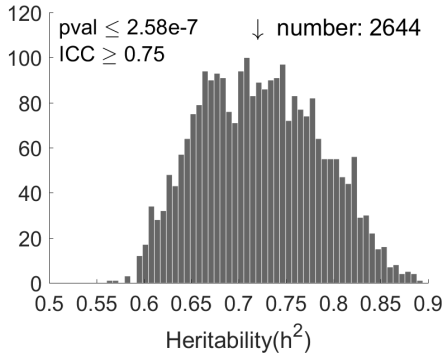

(c) FA Female Non-overlapped.

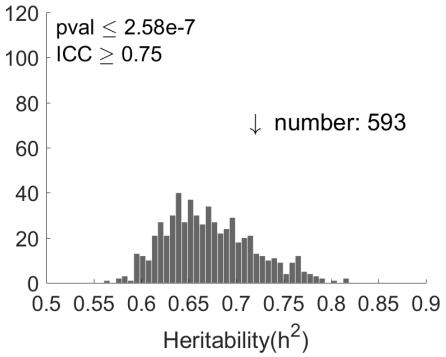

(d) FA Male Non-overlapped

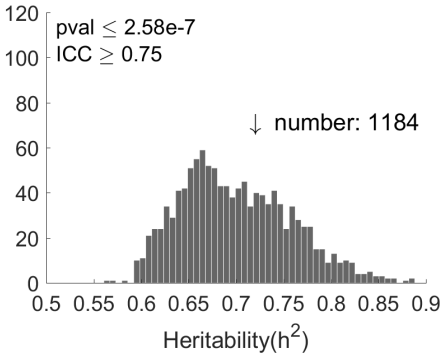

Fig. 3.31. Heritability distribution of all significant and reliable edges for 154 female twins and 154 male twins within the Fractional Anisotropy feature in the scale of 120. (a) (b) Histogram for all reliable edges. (c) (d) Histogram for non-overlapped reliable edges.

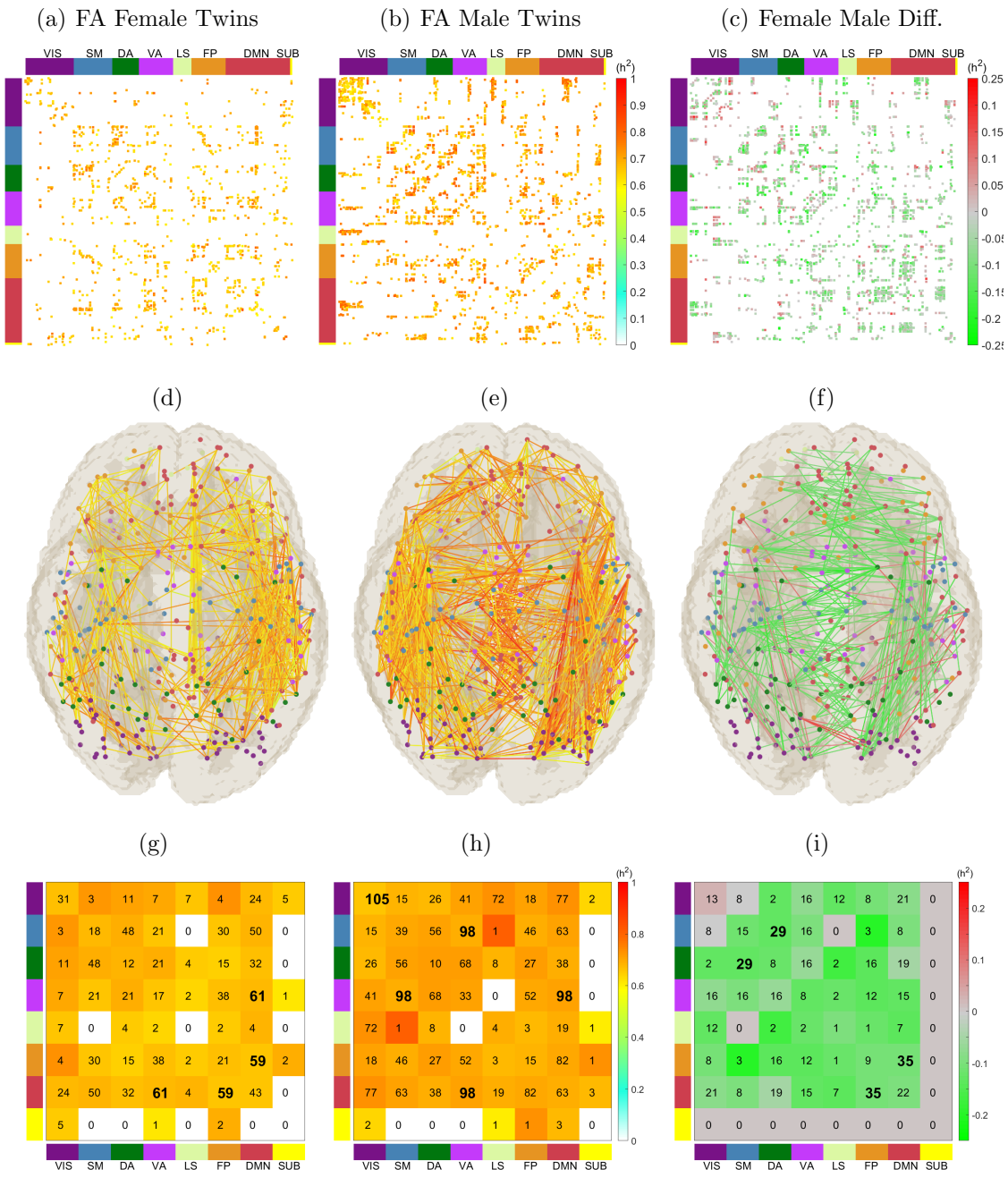

Fig. 3.32. Heritability of non-overlapped reliable edges for female and male twins (first and second column), and heritability of top 324 edges ranked by abstract value of h^2 difference between female and male twins group (third column), within the Fractional Anisotropy feature. (a)-(c) Heatmap of anatomical connection matrix. (d)-(f) Heritability of edge-level measures in the brain map. Node color indicates different Yeo functional groups. (g)-(i) Heatmap showing total number and average h^2 value of edges connecting each pair of functional groups in Yeo parcellation. Top and side color panels indicate the corresponding Yeo parcellation of each ROI. The last subcortical (SUB) group is added to complement the Yeo atlas.

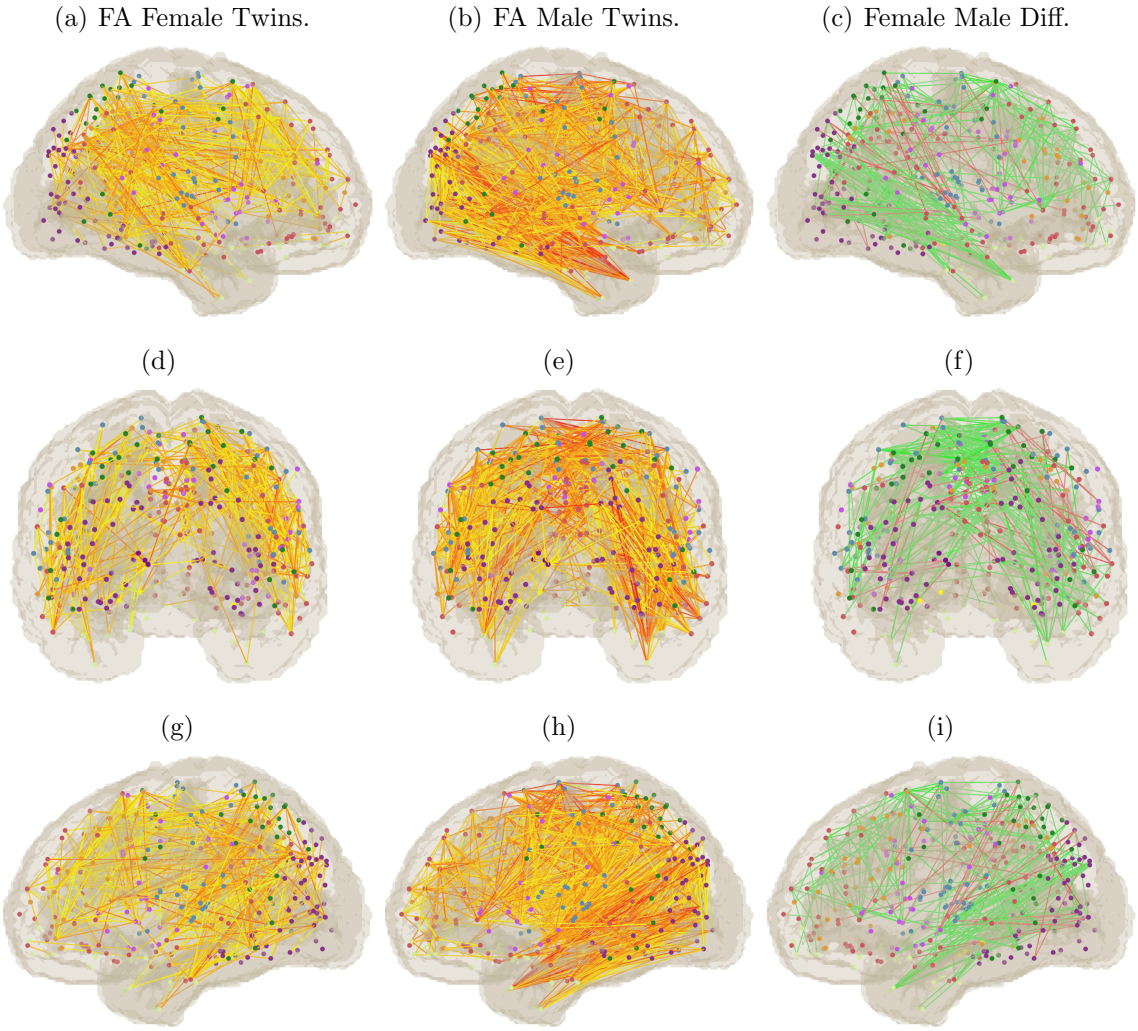

Fig. 3.33. Heritability brain map of non-overlapped reliable edges for female and male twins (first and second column), and heritability brain map of top 324 edges ranked by abstract value of h^2 difference between female and male twins group (third column). (a)-(c) Heritability of edge-level measures in the brain map of Left View. (d)-(f) Heritability of edge-level measures in the brain map of Front View accordingly. (g)-(i) Heritability of edge-level measures in the brain map of Right View.

(a) FL Female Twins.

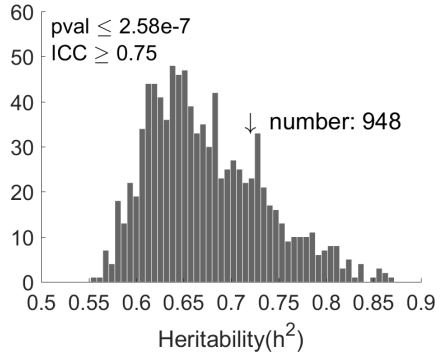

(b) FL Male Twins.

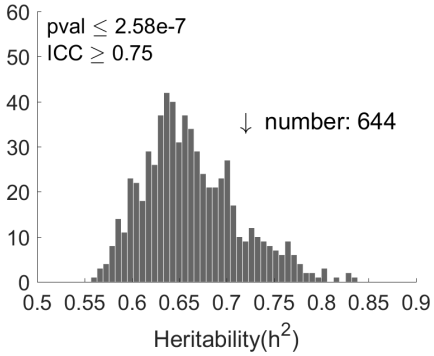

(c) FL Female Non-overlapped.

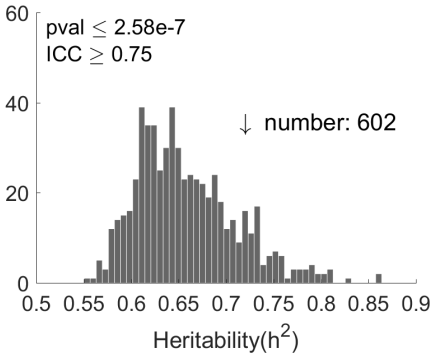

(d) FL Female Male Diff.

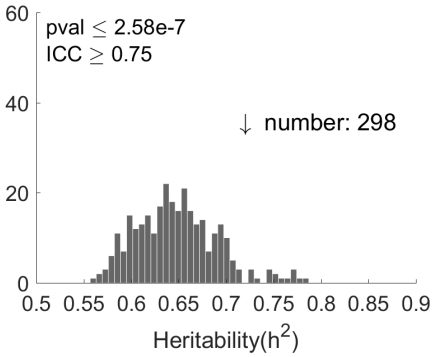

Fig. 3.34. Heritability distribution of all significant and reliable edges for 154 female twins and 154 male twins within the Fiber Length feature in the scale of 60. (a) (b) Histogram for all reliable edges. (c) (d) Histogram for non-overlapped reliable edges.

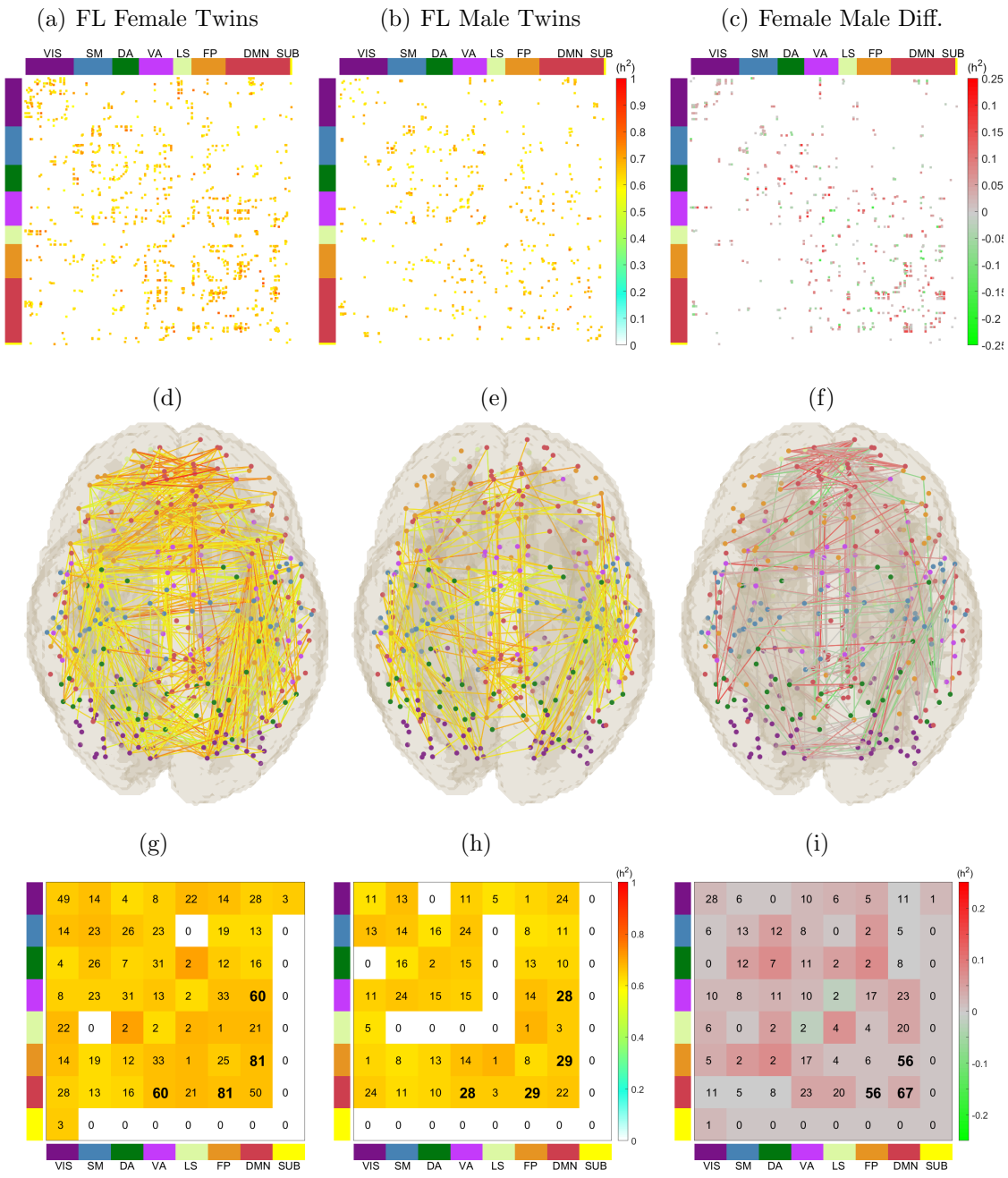

Fig. 3.35. Heritability of non-overlapped reliable edges for female and male twins (first and second column), and heritability of top 324 edges ranked by abstract value of h^2 difference between female and male twins group (third column), within the Fiber Length feature. (a)-(c) Heatmap of anatomical connection matrix. (d)-(f) Heritability of edge-level measures in the brain map. Node color indicates different Yeo functional groups. (g)-(i) Heatmap showing total number and average h^2 value of edges connecting each pair of functional groups in Yeo parcellation. Top and side color panels indicate the corresponding Yeo parcellation of each ROI. The last subcortical (SUB) group is added to complement the Yeo atlas.

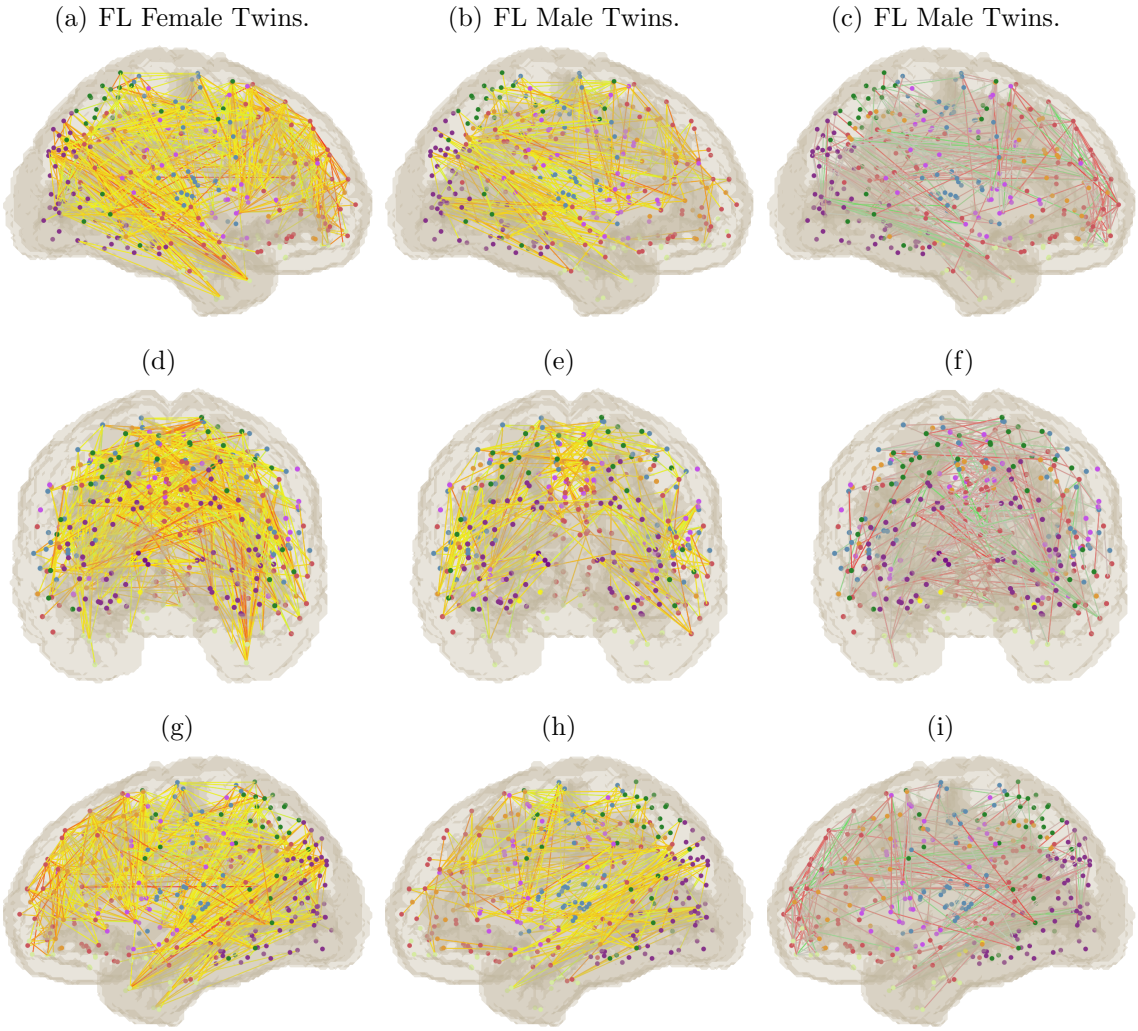

Fig. 3.36. Heritability brain map of non-overlapped reliable edges for female and male twins (first and second column), and heritability brain map of top 324 edges ranked by abstract value of h^2 difference between female and male twins group (third column). (a)-(c) Heritability of edge-level measures in the brain map of Left View. (d)-(f) Heritability of edge-level measures in the brain map of Front View accordingly. (g)-(i) Heritability of edge-level measures in the brain map of Right View.

(a) FN Female Twins.

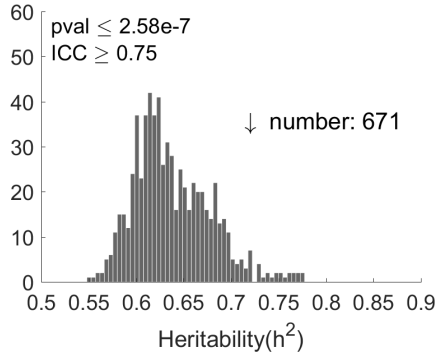

(b) FN Male Twins.

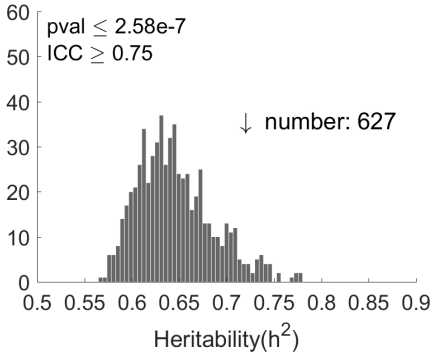

(c) FN Female Non-overlapped.

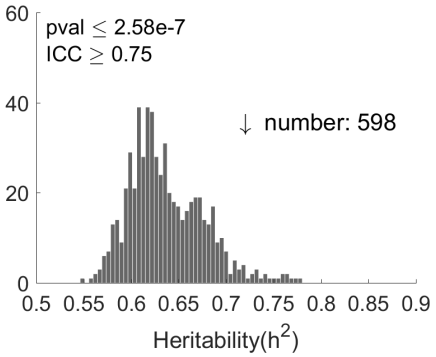

(d) FN Male Non-overlapped

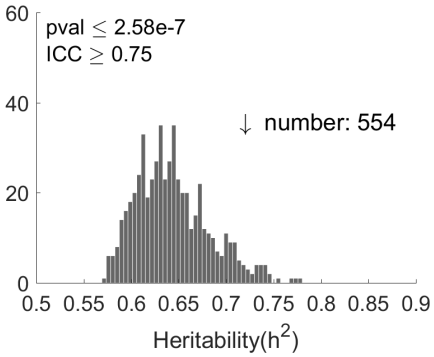

Fig. 3.37. Heritability distribution of all significant and reliable edges for 154 female twins and 154 male twins within the Fiber Number feature in the scale of 60. (a) (b) Histogram for all reliable edges. (c) (d) Histogram for non-overlapped reliable edges.

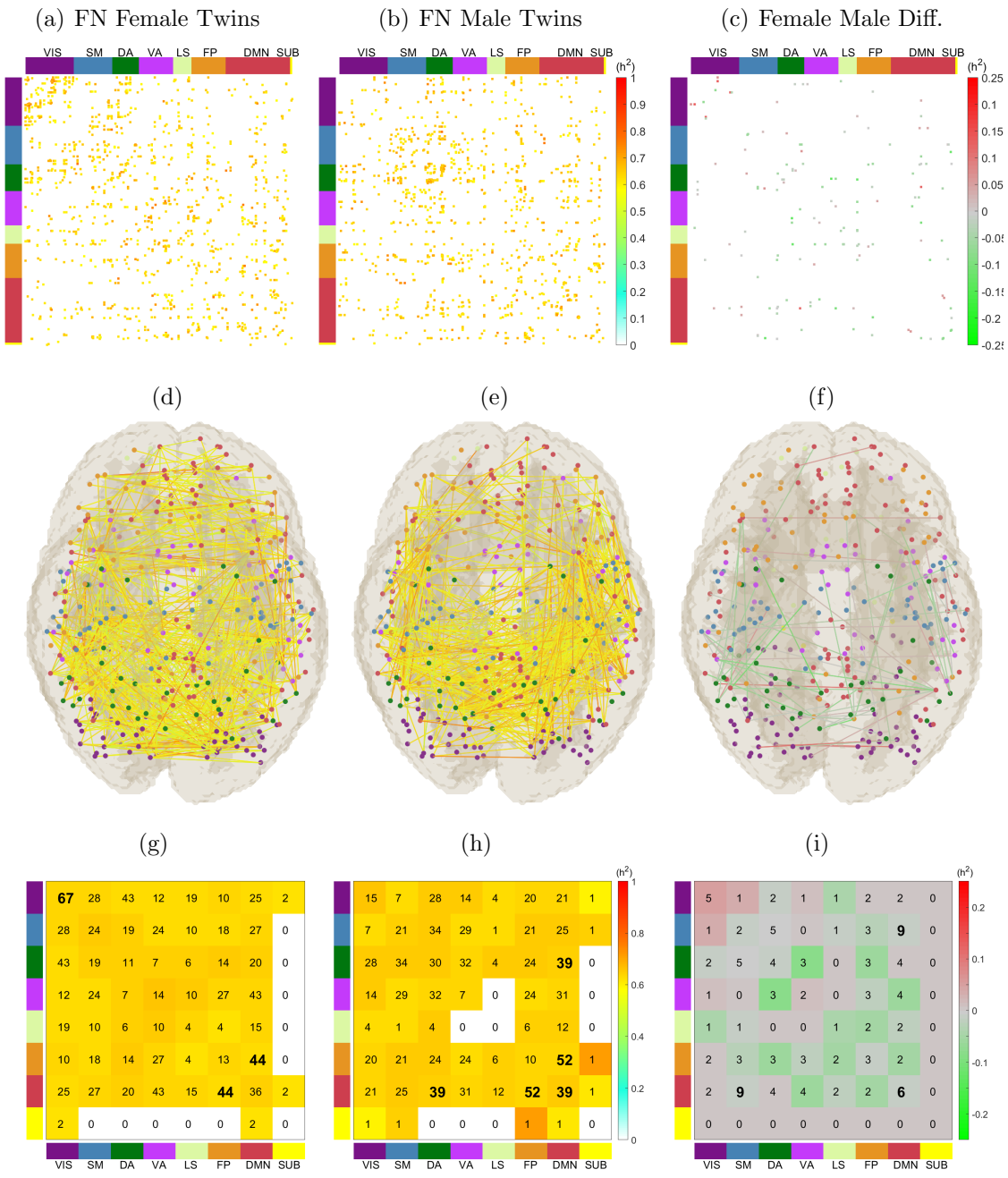

Fig. 3.38. Heritability of non-overlapped reliable edges for female and male twins (first and second column), and heritability of all 73 edges showing difference value of h^2 between female and male twins group (third column), within the Fiber Number feature. (d)-(f) Heritability of edge-level measures in the brain map. Node color indicates different Yeo functional groups. (g)-(i) Heatmap showing total number and average h^2 value of edges connecting each pair of functional groups in Yeo parcellation. Top and side color panels indicate the corresponding Yeo parcellation of each ROI. The last subcortical (SUB) group is added to complement the Yeo atlas.

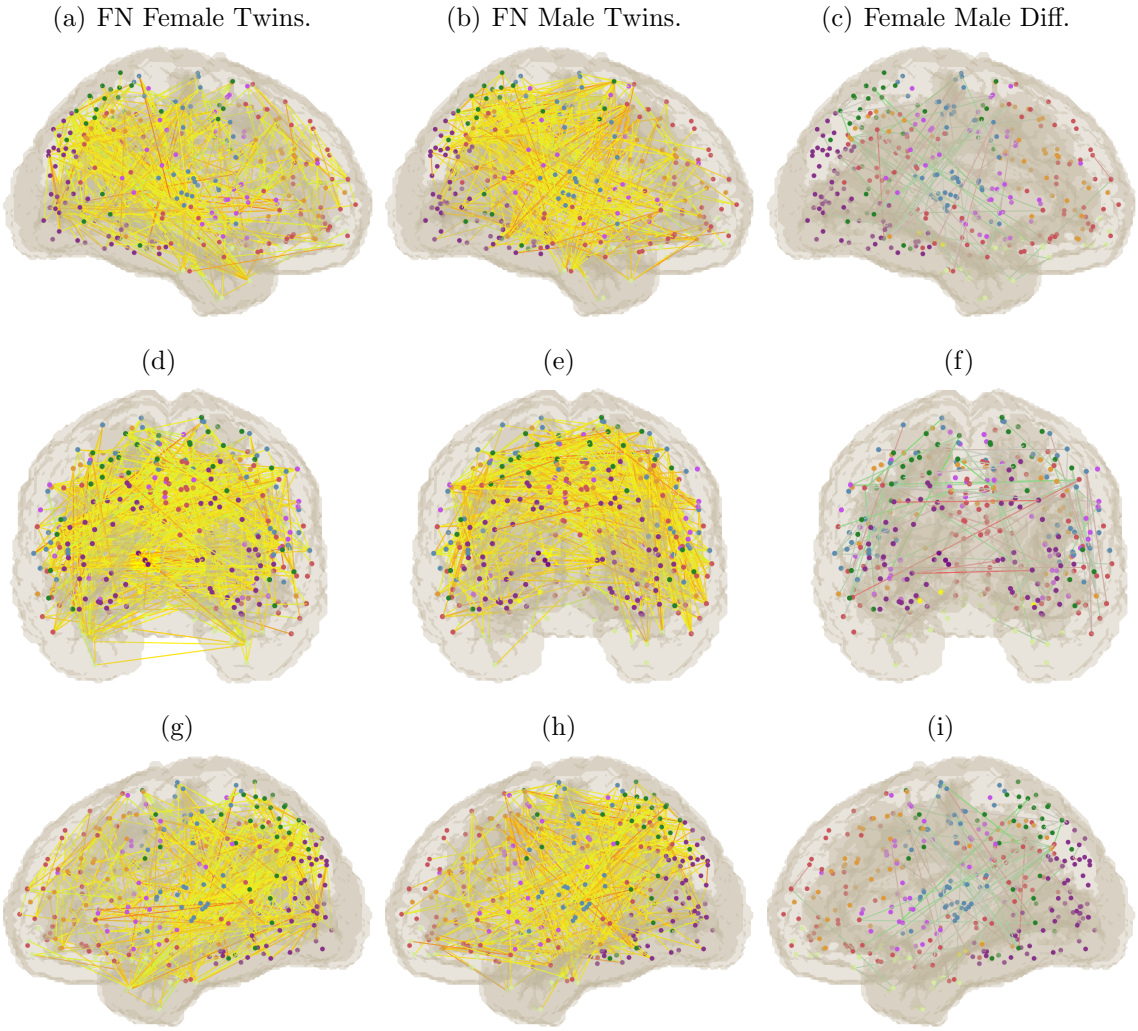

Fig. 3.39. Heritability brain map of non-overlapped reliable edges for female and male twins (first and second column), and heritability brain map of all 73 edges showing difference value of h^2 between female and male twins group (third column), within the Fiber Number feature. (a)-(c) Heritability of edge-level measures in the brain map of Left View. (d)-(f) Heritability of edge-level measures in the brain map of Front View accordingly. (g)-(i) Heritability of edge-level measures in the brain map of Right View.

4. CONCLUSIONS AND FUTURE WORK

4.1 Conclusions

In this thesis a comprehensive heritability analysis for both edge-level and network-level brain connectomic features was performed. Unlike previous studies that largely focused on tracts (white matter regions of interest), brain region volumes (gray and white matter volumes, cerebellar volumes) [75], or a few network topology measures, a new brain parcellation was used in this thesis to construct brain networks (connectome) with improved anatomical precision. Seven network-level features were tested and found to reliable and significantly heritable. To the best of our knowledge, this work is the first heritability study focusing on anatomical networks of human brain (i.e. connectome). Results indicate the degree to which the genetic factors may influence the structural coordination between/within functional brain circuits. Many edges/tracts were found to be highly heritable, particularly those connecting the default mode network circuit or visual circuit. This is consistent with other findings that have indicated that regions in the default mode network have very similar gene expression patterns.

In addition, female and male differences, with regards to brain connectivity, were investigated and their genetic variance explained. Further, the heritable circuit of the edges connecting pairs of functional groups in Yeo parcellation were investigated in both female and male group. Many edges/tracts were found to have an overall higher heritable h^2 value in the male group than the female group, in terms of fractional anisotropy, especially the connections between the Somato-Motor and Dosal Attention, or between the Fronto-Parietal and Default Mode Network. Conversely, many edges showing with significant fiber lengths were found to have overall less heritable h^2 value in the male group than the female group, especially those connecting

within the Default Mode Network, or between the Fronto-Parietal and Default Mode Network. These findings might be helpful to reveal gender difference on the basis of functional MRI in response to particular tests or tasks. In addition, these findings will enhance our understanding of how the structural connected pathways influence the functional connected circuits.

4.2 Future Work

Future work comprising the statistical analysis of gender differences and their corresponding biological/anatomical meanings needs to be preformed, since the work done herein did not conclude if anatomical connectivity differences between genders are statistically significant. In addition, one more covariate, the intracranial volume (ICV), needs to be included in heritability estimation, since ICV has obvious effect on fiber length for each individual.

Another study to be performed in future, across functional atlases (e.g. Shen Atals [45]), is an investigation of how distinct brain templates affect brain network heritability. Similarly, a comparison can be conducted across anatomical brain templates (such as the AAL Atlas [41] and the JHu Atlas [43]) with the aim of revealing alterations in brain structural connectivity for potential risk of neurodegenerative disease. The genetic variation in terms of brain connectivity can then be applied in future Genome-wide association study of Alzheimer's Disease.

REFERENCES

REFERENCES

[1] T. M. Nir, N. Jahanshad, J. E. Villalon-Reina, A. W. Toga, C. R. Jack, M. W. Weiner, P. M. Thompson, A. D. N. I. (ADNI, and others), "Effectiveness of regional DTI measures in distinguishing alzheimer's disease, MCI, and normal aging," *NeuroImage: Clinical*, vol. 3, pp. 180–195, 2013.

[2] P. J. Basser and C. Pierpaoli, "Microstructural and physiological features of tissues elucidated by quantitative-diffusion-tensor MRI," *Journal of Magnetic Resonance, Series B*, vol. 111, no. 3, pp. 209–219, 1996.

[3] P. Kochunov, N. Jahanshad, D. Marcus, A. Winkler, E. Sprooten, T. E. Nichols, S. N. Wright, L. E. Hong, B. Patel, T. Behrens, S. Jbabdi, J. Andersson, C. Lenglet, E. Yacoub, S. Moeller, E. Auerbach, K. Ugurbil, S. N. Sotiropoulos, R. M. Brouwer, B. Landman, H. Lemaitre, A. den Braber, M. P. Zwiers, S. Ritchie, K. van Hulzen, L. Almasy, J. Curran, G. I. deZubicaray, R. Duggirala, P. Fox, N. G. Martin, K. L. McMahon, B. Mitchell, R. L. Olvera, C. Peterson, J. Starr, J. Sussmann, J. Wardlaw, M. Wright, D. I. Boomsma, R. Kahn, E. J. de Geus, D. E. Williamson, A. Hariri, D. van 't Ent, M. E. Bastin, A. McIntosh, I. J. Deary, H. E. Hulshoff Pol, J. Blangero, P. M. Thompson, D. C. Glahn, and D. C. Van Essen, "Heritability of fractional anisotropy in human white matter: a comparison of human connectome project and ENIGMA-DTI data," *Neuroimage*, vol. 111, pp. 300–11, 2015.

[4] M. M. Bohlken, R. C. Mandl, R. M. Brouwer, M. P. van den Heuvel, A. M. Hedman, R. S. Kahn, and H. E. Hulshoff Pol, "Heritability of structural brain network topology: a DTI study of 156 twins," *Hum Brain Mapp*, vol. 35, no. 10, pp. 5295–305, 2014.

[5] Y. Jin, Y. Shi, S. H. Joshi, N. Jahanshad, L. Zhan, G. I. de Zubicaray, K. L. McMahon, N. G. Martin, M. J. Wright, A. W. Toga, and P. M. Thompson, "Heritability of white matter fiber tract shapes: A HARDI study of 198 twins," *Multimodal Brain Image Anal (2011)*, vol. 2011, pp. 35–43, 2011.

[6] K. K. Shen, S. Rose, J. Fripp, K. L. McMahon, G. I. de Zubicaray, N. G. Martin, P. M. Thompson, M. J. Wright, and O. Salvado, "Investigating brain connectivity heritability in a twin study using diffusion imaging data," *Neuroimage*, vol. 100, pp. 628–41, 2014.

[7] D. C. Van Essen, S. M. Smith, D. M. Barch, T. E. Behrens, E. Yacoub, K. Ugurbil, W. H. Consortium *et al.*, "The WU-Minn human connectome project: an overview," *Neuroimage*, vol. 80, pp. 62–79, 2013.

[8] M. F. Glasser, T. S. Coalson, E. C. Robinson, C. D. Hacker, J. Harwell, E. Yacoub, K. Ugurbil, J. Andersson, C. F. Beckmann, M. Jenkinson *et al.*, "A multimodal parcellation of human cerebral cortex," *Nature*, vol. 536, no. 7615, pp. 171–178, 2016.

[9] K. O. McGraw and S. P. Wong, "Forming inferences about some intraclass correlation coefficients." *Psychological methods*, vol. 1, no. 1, p. 30, 1996.

[10] F. A. Azevedo, L. R. Carvalho, L. T. Grinberg, J. M. Farfel, R. E. Ferretti, R. E. Leite, R. Lent, S. Herculano-Houzel *et al.*, "Equal numbers of neuronal and nonneuronal cells make the human brain an isometrically scaled-up primate brain," *Journal of Comparative Neurology*, vol. 513, no. 5, pp. 532–541, 2009.

[11] V. Braitenberg and A. Schüz, *Anatomy of the cortex: statistics and geometry*. Springer Science & Business Media, 2013, vol. 18.

[12] O. Sporns, G. Tononi, and R. Kötter, "The human connectome: a structural description of the human brain," *PLoS Computational Biology*, vol. 1, no. 4, p. e42, 2005.

[13] P. Hagmann, "From diffusion MRI to brain connectomics," PhD Dissertation, University of Lausanne, Switzerland, 2005.

[14] D. S. Bassett and E. Bullmore, "Small-world brain networks," *The Neuroscientist*, vol. 12, no. 6, pp. 512–523, 2006.

[15] M. Kaiser and C. C. Hilgetag, "Nonoptimal component placement, but short processing paths, due to long-distance projections in neural systems," *PLoS Computational Biology*, vol. 2, no. 7, p. e95, 2006.

[16] O. Sporns and J. D. Zwi, "The small world of the cerebral cortex," *Neuroinformatics*, vol. 2, no. 2, pp. 145–162, 2004.

[17] S. Achard, R. Salvador, B. Whitcher, J. Suckling, and E. Bullmore, "A resilient, low-frequency, small-world human brain functional network with highly connected association cortical hubs," *Journal of Neuroscience*, vol. 26, no. 1, pp. 63–72, 2006.

[18] Q. Wen and D. B. Chklovskii, "Segregation of the brain into gray and white matter: a design minimizing conduction delays," *PLoS Computational Biology*, vol. 1, no. 7, p. e78, 2005.

[19] S. Achard and E. Bullmore, "Efficiency and cost of economical brain functional networks," *PLoS Computational Biology*, vol. 3, no. 2, p. e17, 2007.

[20] E. Bullmore and O. Sporns, "Complex brain networks: graph theoretical analysis of structural and functional systems," *Nature Reviews Neuroscience*, vol. 10, no. 3, p. 186, 2009.

[21] T. E. Bullmore and O. Sporns, "The economy of brain network organization," *Nature Reviews Neuroscience*, vol. 13, no. 5, p. 336, 2012.

[22] J. G. White, E. Southgate, J. N. Thomson, and S. Brenner, "The structure of the nervous system of the nematode caenorhabditis elegans," *Philos Trans R Soc Lond B Biol Sci*, vol. 314, no. 1165, pp. 1–340, 1986.

[23] D. J. Felleman and D. E. Van, "Distributed hierarchical processing in the primate cerebral cortex." *Cerebral Cortex (New York, NY: 1991)*, vol. 1, no. 1, pp. 1–47, 1991.

[24] M. P. Young, "Objective analysis of the topological organization of the primate cortical visual system," *Nature*, vol. 358, no. 6382, p. 152, 1992.

[25] M. Young, "The organization of neural systems in the primate cerebral cortex," *Proceedings of the Royal Society of London B*, vol. 252, no. 1333, pp. 13–18, 1993.

[26] F. Crick and E. Jones, "Backwardness of human neuroanatomy." *Nature*, vol. 361, no. 6408, pp. 109–110, 1993.

[27] D. Le Bihan, J.-F. Mangin, C. Poupon, C. A. Clark, S. Pappata, N. Molko, and H. Chabriat, "Diffusion tensor imaging: concepts and applications," *Journal of Magnetic Resonance Imaging*, vol. 13, no. 4, pp. 534–546, 2001.

[28] S. Mori and J. Zhang, "Principles of diffusion tensor imaging and its applications to basic neuroscience research," *Neuron*, vol. 51, no. 5, pp. 527–539, 2006.

[29] C. Pierpaoli, P. Jezzard, P. J. Basser, A. Barnett, and G. Di Chiro, "Diffusion tensor MR imaging of the human brain." *Radiology*, vol. 201, no. 3, pp. 637–648, 1996.

[30] M. Doran, J. V. Hajnal, N. B. Van, M. D. King, I. R. Young, and G. M. Bydder, "Normal and abnormal white matter tracts shown by mr imaging using directional diffusion weighted sequences." *Journal of Computer Assisted Tomography*, vol. 14, no. 6, pp. 865–873, 1990.

[31] M. E. Moseley, Y. Cohen, J. Kucharczyk, J. Mintorovitch, H. Asgari, M. Wendland, J. Tsuruda, and D. Norman, "Diffusion-weighted mr imaging of anisotropic water diffusion in cat central nervous system." *Radiology*, vol. 176, no. 2, pp. 439–445, 1990.

[32] D. Le Bihan, E. Breton, D. Lallemand, P. Grenier, E. Cabanis, and M. Laval-Jeantet, "MR imaging of intravoxel incoherent motions: application to diffusion and perfusion in neurologic disorders." *Radiology*, vol. 161, no. 2, pp. 401–407, 1986.

[33] S. Pajevic and C. Pierpaoli, "Color schemes to represent the orientation of anisotropic tissues from diffusion tensor data: application to white matter fiber tract mapping in the human brain," *Magnetic Resonance in Medicine: An Official Journal of the International Society for Magnetic Resonance in Medicine*, vol. 42, no. 3, pp. 526–540, 1999.

[34] J. D. Schmahmann, D. N. Pandya, R. Wang, G. Dai, H. E. D'arceuil, A. J. de Crespigny, and V. J. Wedeen, "Association fibre pathways of the brain: parallel observations from diffusion spectrum imaging and autoradiography," *Brain*, vol. 130, no. 3, pp. 630–653, 2007.

[35] C. Honey, O. Sporns, L. Cammoun, X. Gigandet, J.-P. Thiran, R. Meuli, and P. Hagmann, "Predicting human resting-state functional connectivity from structural connectivity," *Proceedings of the National Academy of Sciences*, vol. 106, no. 6, pp. 2035–2040, 2009.

[36] C. Zhou, L. Zemanová, G. Zamora, C. C. Hilgetag, and J. Kurths, "Hierarchical organization unveiled by functional connectivity in complex brain networks," *Physical Review Letters*, vol. 97, no. 23, p. 238103, 2006.

[37] E. Ravasz and A.-L. Barabási, "Hierarchical organization in complex networks," *Physical Review E*, vol. 67, no. 2, p. 026112, 2003.

[38] D. S. Bassett, E. Bullmore, B. A. Verchinski, V. S. Mattay, D. R. Weinberger, and A. Meyer-Lindenberg, "Hierarchical organization of human cortical networks in health and schizophrenia," *Journal of Neuroscience*, vol. 28, no. 37, pp. 9239–9248, 2008.

[39] R. Guillery, "Brodmann's localisation in the cerebral cortex. translated and edited by laurence j. garey.(pp. xviii+ 300; illustrated;£ 28 hardback; isbn 1 86094 176 1.) london: Imperial college press. 1999." *Journal of Anatomy*, vol. 196, no. 3, pp. 493–496, 2000.

[40] R. S. Desikan, F. Ségonne, B. Fischl, B. T. Quinn, B. C. Dickerson, D. Blacker, R. L. Buckner, A. M. Dale, R. P. Maguire, B. T. Hyman *et al.*, "An automated labeling system for subdividing the human cerebral cortex on mri scans into gyral based regions of interest," *Neuroimage*, vol. 31, no. 3, pp. 968–980, 2006.

[41] N. Tzourio-Mazoyer, B. Landeau, D. Papathanassiou, F. Crivello, O. Etard, N. Delcroix, B. Mazoyer, and M. Joliot, "Automated anatomical labeling of activations in spm using a macroscopic anatomical parcellation of the mni mri single-subject brain," *Neuroimage*, vol. 15, no. 1, pp. 273–289, 2002.

[42] D. W. Shattuck, M. Mirza, V. Adisetiyo, C. Hojatkashani, G. Salamon, K. L. Narr, R. A. Poldrack, R. M. Bilder, and A. W. Toga, "Construction of a 3d probabilistic atlas of human cortical structures," *Neuroimage*, vol. 39, no. 3, pp. 1064–1080, 2008.

[43] K. Oishi, A. Faria, and S. Mori, "Jhu-mni-ss atlas," *Google Scholar*, 2010.

[44] B. Thomas Yeo, F. M. Krienen, J. Sepulcre, M. R. Sabuncu, D. Lashkari, M. Hollinshead, J. L. Roffman, J. W. Smoller, L. Zöllei, J. R. Polimeni *et al.*, "The organization of the human cerebral cortex estimated by intrinsic functional connectivity," *Journal of Neurophysiology*, vol. 106, no. 3, pp. 1125–1165, 2011.

[45] X. Shen, F. Tokoglu, X. Papademetris, and R. T. Constable, "Groupwise whole-brain parcellation from resting-state fMRI data for network node identification," *Neuroimage*, vol. 82, pp. 403–415, 2013.

[46] G. Gong, Y. He, L. Concha, C. Lebel, D. W. Gross, A. C. Evans, and C. Beaulieu, "Mapping anatomical connectivity patterns of human cerebral cortex using in vivo diffusion tensor imaging tractography," *Cerebral Cortex*, vol. 19, no. 3, pp. 524–536, 2008.

[47] M. Rubinov and O. Sporns, "Complex network measures of brain connectivity: uses and interpretations," *Neuroimage*, vol. 52, no. 3, pp. 1059–1069, 2010.

[48] U. Wieshmann, M. Symms, G. Parker, C. Clark, L. Lemieux, G. Barker, and S. Shorvon, "Diffusion tensor imaging demonstrates deviation of fibres in normal appearing white matter adjacent to a brain tumour," *Journal of Neurology, Neurosurgery & Psychiatry*, vol. 68, no. 4, pp. 501–503, 2000.

[49] S. Wakana, H. Jiang, L. M. Nagae-Poetscher, P. C. Van Zijl, and S. Mori, "Fiber tract–based atlas of human white matter anatomy," *Radiology*, vol. 230, no. 1, pp. 77–87, 2004.

[50] P. J. Basser, S. Pajevic, C. Pierpaoli, J. Duda, and A. Aldroubi, "In vivo fiber tractography using dt-mri data," *Magnetic Resonance in Medicine*, vol. 44, no. 4, pp. 625–632, 2000.

[51] R. E. Smith, J.-D. Tournier, F. Calamante, and A. Connelly, "Sift: spherical-deconvolution informed filtering of tractograms," *Neuroimage*, vol. 67, pp. 298–312, 2013.

[52] K. Supekar, V. Menon, D. Rubin, M. Musen, and M. D. Greicius, "Network analysis of intrinsic functional brain connectivity in alzheimer's disease," *PLoS Computational Biology*, vol. 4, no. 6, p. e1000100, 2008.

[53] R. Belmaker and G. Agam, "Major depressive disorder," *New England Journal of Medicine*, vol. 358, no. 1, pp. 55–68, 2008.

[54] M. Catani and D. H. ffytche, "The rises and falls of disconnection syndromes," *Brain*, vol. 128, no. 10, pp. 2224–2239, 2005.

[55] A. A. Fingelkurts, A. A. Fingelkurts, H. Rytsälä, K. Suominen, E. Isometsä, and S. Kähkönen, "Impaired functional connectivity at eeg alpha and theta frequency bands in major depression," *Human Brain Mapping*, vol. 28, no. 3, pp. 247–261, 2007.

[56] S. L. Bressler and V. Menon, "Large-scale brain networks in cognition: emerging methods and principles," *Trends in Cognitive Sciences*, vol. 14, no. 6, pp. 277–290, 2010.

[57] J. Tournier, F. Calamante, A. Connelly *et al.*, "Mrtrix: diffusion tractography in crossing fiber regions," *International Journal of Imaging Systems and Technology*, vol. 22, no. 1, pp. 53–66, 2012.

[58] R. E. Smith, J.-D. Tournier, F. Calamante, and A. Connelly, "Anatomically-constrained tractography: improved diffusion MRI streamlines tractography through effective use of anatomical information," *Neuroimage*, vol. 62, no. 3, pp. 1924–1938, 2012.

[59] P. Callaghan, C. Eccles, and Y. Xia, "Nmr microscopy of dynamic displacements: k-space and q-space imaging," *Journal of Physics E: Scientific Instruments*, vol. 21, no. 8, p. 820, 1988.

[60] B. Jeurissen, J.-D. Tournier, T. Dhollander, A. Connelly, and J. Sijbers, "Multi-tissue constrained spherical deconvolution for improved analysis of multi-shell diffusion mri data," *NeuroImage*, vol. 103, pp. 411–426, 2014.

[61] D. Christiaens, M. Reisert, T. Dhollander, S. Sunaert, P. Suetens, and F. Maes, "Global tractography of multi-shell diffusion-weighted imaging data using a multi-tissue model," *Neuroimage*, vol. 123, pp. 89–101, 2015.

[62] R. E. Smith, J.-D. Tournier, F. Calamante, and A. Connelly, "Sift2: Enabling dense quantitative assessment of brain white matter connectivity using streamlines tractography," *Neuroimage*, vol. 119, pp. 338–351, 2015.

[63] T. K. Koo and M. Y. Li, "A guideline of selecting and reporting intraclass correlation coefficients for reliability research," *Journal of Chiropractic Medicine*, vol. 15, no. 2, pp. 155–163, 2016.

[64] H. Ganjgahi, A. M. Winkler, D. C. Glahn, J. Blangero, P. Kochunov, and T. E. Nichols, "Fast and powerful heritability inference for family-based neuroimaging studies," *NeuroImage*, vol. 115, pp. 256–268, 2015.

[65] A. Thapar, "Methodology for genetic studies of twins and families," *Journal of medical genetics*, vol. 30, no. 9, p. 800, 1993.

[66] A. Z. Burzynska, C. Preuschhof, L. Bäckman, L. Nyberg, S.-C. Li, U. Lindenberger, and H. R. Heekeren, "Age-related differences in white matter microstructure: region-specific patterns of diffusivity," *Neuroimage*, vol. 49, no. 3, pp. 2104–2112, 2010.

[67] T. Zhao, M. Cao, H. Niu, X.-N. Zuo, A. Evans, Y. He, Q. Dong, and N. Shu, "Age-related changes in the topological organization of the white matter structural connectome across the human lifespan," *Human Brain Mapping*, vol. 36, no. 10, pp. 3777–3792, 2015.

[68] G. Gong, Y. He, and A. C. Evans, "Brain connectivity: gender makes a difference," *The Neuroscientist*, vol. 17, no. 5, pp. 575–591, 2011.

[69] M. P. Lopez-Larson, J. S. Anderson, M. A. Ferguson, and D. Yurgelun-Todd, "Local brain connectivity and associations with gender and age," *Developmental Cognitive Neuroscience*, vol. 1, no. 2, pp. 187–197, 2011.

[70] C. Bonferroni, "Teoria statistica delle classi e calcolo delle probabilita," *Pubblicazioni del R Istituto Superiore di Scienze Economiche e Commericiali di Firenze*, vol. 8, pp. 3–62, 1936.

[71] B. T. Yeo, F. M. Krienen, J. Sepulcre, M. R. Sabuncu, D. Lashkari, M. Hollinshead, J. L. Roffman, J. W. Smoller, L. Zöllei, J. R. Polimeni *et al.*, "The organization of the human cerebral cortex estimated by intrinsic functional connectivity," *Journal of Neurophysiology*, vol. 106, no. 3, pp. 1125–1165, 2011.

[72] R. L. Buckner, J. R. Andrews-Hanna, and D. L. Schacter, "The brain's default network," *Annals of the New York Academy of Sciences*, vol. 1124, no. 1, pp. 1–38, 2008.

[73] K. M. Dumais, S. Chernyak, L. D. Nickerson, and A. C. Janes, "Sex differences in default mode and dorsal attention network engagement," *PLoS One*, vol. 13, no. 6, p. e0199049, 2018.

[74] A. C. Hill, A. R. Laird, and J. L. Robinson, "Gender differences in working memory networks: A brainmap meta-analysis," *Biological Psychology*, vol. 102, pp. 18–29, 2014.

[75] J. S. Peper, R. M. Brouwer, D. I. Boomsma, R. S. Kahn, and H. E. Hulshoff Pol, "Genetic influences on human brain structure: a review of brain imaging studies in twins," *Human Brain Mapping*, vol. 28, no. 6, pp. 464–473, 2007.